**Universidade do Porto**

Faculdade de Engenharia da Universidade do Porto

Instituto Ciências Biomédicas Abel Salazar

Instituto de Engenharia Biomédica

Instituto de Patologia e Imunologia Molecular da Universidade do Porto

# Establishment of a 3D model of EMT/MET-induction using molecularly-designed ECM-like hydrogels

**Sara Jorge Moreira da Rocha**

Masters in Bioengineering – Molecular Biotechnology

Porto, September 2014

# Establishment of a 3D model of EMT/MET-induction using molecularly-designed ECM-like hydrogels

Sara Jorge Moreira da Rocha

**FEUP** – Faculdade de Engenharia da Universidade do Porto

**ICBAS-UP** – Instituto de Ciências Biomédicas de Abel Salazar

**Thesis for Masters in Bioengineering**

Supervision:

Cristina Barrias, Ph.D.

Assistant Investigator, **INEB**

Co-supervision:

Patrícia Oliveira, Ph.D.

Post-Doctoral Investigator, **IPATIMUP**

Sílvia Bidarra, Ph.D.

Post-Doctoral Investigator, **INEB**

**INEB –** Instituto de Engenharia Biomédica, Universidade do Porto

**IPATIMUP –** Instituto de Patologia e Imunologia Molecular da Universidade do Porto

Porto, September 2014

*The most common way people give up their power*

*is by thinking they don't have any.*

Alice Walker

# ABSTRACT

Epithelial to mesenchymal transition (EMT) is a biologic process that allows a polarized epithelial cell to undergo biochemical changes that enable it to assume a mesenchymal cell phenotype. Therefore, EMT has been associated with a concomitant decrease of epithelial markers (e.g. E-cadherin) and increase of mesenchymal markers (e.g. Vimentin and α-SMA), as well as enhanced migratory and invasion capacity, resistance to apoptosis and increased production of extracellular matrix (ECM) components. EMT-cells may undergo a reverse process, mesenchymal to epithelial transition (MET), through which they are able to recover the epithelial phenotype. In some cases, EMT reversion may not be fully accomplished, giving rise to a metastable phenotype characterized by a simultaneous expression of epithelial and mesenchymal features. EMT has been shown to occur both under physiological settings, namely embryogenesis and wound healing, and in pathological situations, such as fibrosis. Several reports suggested that EMT/MET may also have a role during cancer progression and metastasis establishment. To elucidate this hypothesis, different EMT models have been implemented using traditional two-dimensional (2D) systems. However, such models lack the influence of a proper three-dimensional (3D) ECM-like structure that could better mimic the *in vivo* microenvironment, a major regulator of the EMT/MET program. Therefore, improved *in vitro* systems that better mimic the tumour microenvironment are needed in order to closely reproduce the EMT transcriptional program that occurs *in vivo*.

The central aim of this Master Thesis was the establishment of a 3D *in vitro* model of TGF-β1-driven EMT/MET induction in EpH4 epithelial cells cultured on an artificial alginate-based matrix with tuneable properties. In addition, we aimed to further characterize the 2D *in vitro* model of TGF-β1-driven EMT/MET induction previously established in the group, by assessing the stemness features of the EpH4 cells in different stages of the process, as well as their ability to produce matrix metalloproteinases (MMPs).

Our results demonstrated that the 2D EMT-derived cells have enhanced stem-like features (resulting from the enrichment in a $CD29^{+}/CD44^{+}$ subpopulation) and produce increased levels of MMP9. Regarding the 3D EMT/MET model, our findings showed a TGF-β1-mediated EMT program characterized by E-cadherin impairment and increased mesenchymal markers, both at RNA and protein level (e.g. Vimentin and α-SMA). Moreover, the removal of TGF-β1 stimulus enabled the establishment of a metastable phenotype with concomitant E-cadherin presence at cell membrane and α-SMA expression in the cell cytoplasm.

In conclusion, we created a 3D *in vitro* TGF-β1-mediated EMT/MET system that makes use of RGD-modified alginate hydrogels that provide a well-defined and tuneable environment. The insights gained with this Master Thesis, may ultimate be useful for the establishment of a high-throughput system for the study of cancer progression and metastasis.

# RESUMO

A transição epitelial-mesenquimal (EMT) trata-se de um processo biológico através do qual células epiteliais polarizadas sofrem modificações bioquímicas que lhes permitem adquirir um fenótipo mesenquimal. O processo de EMT encontra-se associado a uma concomitante diminuição de marcadores epiteliais (p. ex. Caderina-E) e aumento de marcadores mesenquimais (p. ex. Vimentina e α-SMA), bem como aumento da capacidade de migração e invasão, resistência à apoptose e maior produção de componentes da matriz extracelular (ECM). Células derivadas da transição epitelial-mesenquimal podem sofrer um processo de reversão, transição mesenquimal-epitelial (MET), através do qual recuperam um fenótipo epitelial. Por vezes, esta reversão não é completamente alcançada, originando um fenótipo metastável no qual se verifica uma expressão simultânea de características epiteliais e mesenquimais. A ocorrência da transição EMT tem vindo a ser demonstrada tanto em condições fisiológicas, nomeadamente durante a embriogénese e a cicatrização, como em situações patológicas, tal como a fibrose. Vários estudos sugerem que as transições EMT/MET podem também encontrar-se envolvidas na progressão de cancro e desenvolvimento de metástases. De forma a averiguar tal hipótese, vários modelos de EMT têm vindo a ser implementados usando os clássicos sistemas dimensionais (2D). Todavia, estes modelos não contemplam a influência de uma estrutura tridimensional (3D) semelhante à matriz extracelular, o que permitiria uma melhor mimetização do microambiente *in vivo*, um importante moderador do programa EMT/MET. Desta forma, é necessário desenvolver sistemas *in vitro* melhorados, que simulem o microambiente tumoral de forma mais adequada, permitindo assim o estabelecimento de programas de EMT que fidedignamente representam a transição que ocorre *in vivo*.

O principal objetivo desta Tese de Mestrado foi estabelecer um modelo 3D *in vitro* de indução de EMT/MET mediada por TGF-β1, em células EpH4 cultivadas em matrizes artificiais de alginato, com propriedades ajustáveis. Paralelamente, tínhamos como objetivo caracterizar o modelo 2D *in vitro* de indução de EMT/MET também mediada por TGF-β1, previamente estabelecido no grupo, através da caracterização das propriedades estaminais das células EpH4 nos diferentes estadios do processo, bem como da sua capacidade de produção de metaloproteases da matriz (MMPs).

Os nossos resultados demonstraram que as células derivadas do processo de EMT no sistema 2D apresentam aumento das características associadas a células estaminais (resultantes de um enriquecimento da subpopulação $CD29^{+}/CD44^{+}$) e da produção de MMP9. Relativamente ao

modelo EMT/MET em 3D, as nossas descobertas mostram que o programa de EMT mediado por TGF-β1 é caracterizado por uma deficiente função de Caderina-E e aumento de marcadores mesenquimais tanto ao nível de expressão de ARN como de proteína (p. ex. Vimentina e α-SMA). Adicionalmente, com a remoção do estímulo de TGF-β1 foi alcançado um fenótipo metastável com presença simultânea de Cadherina-E, na membrana celular, e de α-SMA, no citoplasma.

Concluindo, foi possível criar um sistema 3D *in vitro* de EMT/MET mediado por TGF-β1 baseado na utilização de hidrogéis de alginato modificado com RGD, que permitem um ambiente bem definido e regulável. As descobertas alcançadas com esta Tese de Mestrado poderão vir a ser úteis para o estabelecimento de sistemas de alto rendimento para a investigação em progressão de cancro e formação de metástases.

# ACKNOWLEDGMENTS

A realização desta Tese de Mestrado só foi possível devido ao empenho de inúmeras pessoas, que incansavelmente me apoiaram, ajudaram e que de alguma forma contribuíram para o meu crescimento como "bioengenheira", mas mais do que isso, como pessoa. A todos aqueles que não pude mencionar nesta Tese, mas que também me amparam ao longo dos últimos meses, e em alguns casos, ao longo dos últimos cinco anos, o meu mais sincero agradecimento.

À minha orientadora, Dra. Cristina Barrias, por quem desenvolvi um enorme apreço e admiração ao longo dos últimos meses, por me ter dado a oportunidade de participar neste projeto e por toda a simpatia, carinho e preocupação que foram constantes desde o primeiro dia em que reunimos no INEB. Muito obrigada por toda esta experiência!

À Patrícia Oliveira e à Sílvia Bidarra, as minhas co-orientadoras, que foram incansáveis e se mostraram sempre disponíveis para me ajudar. Obrigada por terem apurado o meu espírito crítico e pelas várias discussões científicas que permitiram o desenvolvimento deste trabalho.

À Dra. Carla Oliveira, por também ter permitido que eu entrasse neste projeto e pelo papel fundamental que teve no curso desta Tese. Apesar de não ser minha orientadora ou co-orientadora oficial, agradeço toda a simpatia, apoio e esforços dedicados ao meu trabalho e a forma tão aberta com que fui recebida no grupo *Expression Regulation in Cancer*.

A todos os elementos dos dois grupos de investigação dos quais fiz parte no INEB e no IPATIMUP (ERiC e BIOCARRIER) que, sem exceção, me acolheram e me fizeram sentir "*em casa*". Agradeço toda a vossa ajuda, não só no que diz respeito ao dia-a-dia no laboratório, mas também científica, e a constante preocupação comigo e com o meu trabalho.

Às minhas colegas e amigas Ipatimupianas, Cristina, Filipa, Inês e Joana por terem suportado o meu stress, alguns maus humores e horas de lamúrias, mas também pelos almoços mais divertidos e pelos regulares cafés de pausa, que facilitaram (e muito) o tempo passado no IPATIMUP. Ainda não me esqueci do passeio pelo Porto e do jantar que ficou prometido!

Às minhas colegas de curso, mas mais do que isso, às minhas amigas Joana e Maria, companheiras das muitas horas de desespero, problemas e noites mal dormidas que enfrentamos ao longo dos últimos anos. Nunca irei esquecer o vosso apoio em tempos mais difíceis, nem tão pouco as celebrações dos nossos esforços e da nossa amizade. Mais do que agradecer, desejo que consigamos continuar a alcançar sucessos, juntas!

Ao ex-bioteco/futuro médico Francisco pela amizade e apoio desde o primeiro ano de curso. Obrigada por todas as piadas "à Chico", por todos os conselhos, paciência e pela companhia diária nas viagens de comboio de regresso a casa.

À Patrícia, a minha amiga dos PCR's! Nunca pensei que daquele estágio no terceiro ano pudesse surgir uma amizade como a nossa. O teu apoio e confiança em mim foram e continuam a ser uma fonte de entusiasmo para continuar este percurso.

À Sara e à Ana, amigas de longa data, que me mostraram que uma verdadeira amizade supera distâncias físicas e temporais. Depois de tantos anos, é impossível fazer referência a tudo aquilo que já fizeram por mim, e tudo aquilo que já vivemos juntas. Meninas, muito obrigada por estarem sempre disponíveis a apoiar-me!

Aos meus pais, Helena e António, para os quais não tenho (nem nunca conseguirem ter) palavras suficientes para descrever o quão grata e privilegiada me sinto por ser vossa filha. Obrigada por todo o (enorme!) esforço que fizeram para que eu pudesse ter uma boa educação e formação. Obrigada pela dedicação com que me criaram e sempre acompanharam ao longo da vida, e por todas as experiências que me proporcionaram. Sem vocês nada disto seria possível, e tudo o que sou e todos os meus sucessos são, e continuarão a ser também vossos. Espero um dia conseguir retribuir tudo que fizeram por mim! Adoro-vos, são os melhores pais do mundo!

Às minhas maninhas, Sílvia e Sofia, que são sem dúvida as melhores irmãs que eu poderia pedir. Obrigada por partilharem tudo comigo e por me terem apoiado incondicionalmente em todos os capítulos da minha curta história. Agradeço-vos por todo o esforço que fizeram por mim. Sei que já vivemos situações complicadas, mas permanecemos sempre unidas, como aliás iremos continuar! Mais do que irmãs, vocês são as minhas melhores amigas.

Aos meus avós, sempre prontos a mimar-me um pouco mais, pelo constante interesse que demonstraram ao longo do meu percurso académico. Obrigada avó, pelo carinho com que me criaste. Obrigado avô, pelo entusiasmo com que vês a minha contribuição para a ciência.

Finalmente, não poderia deixar de agradecer aos dois meninos dos meus olhos!
Ao João Filipe, que apesar de não perceber nada do que a madrinha faz, é a minha fonte de força para superar as adversidades do dia-a-dia. Tu és a razão de eu acreditar na ciência e naquilo que esta pode fazer por nós. Fizeste-me ver que tudo é possível, basta acreditar!
Ao Pedro, a minha fonte de inspiração! Obrigada por todos os momentos de apoio e motivação. Obrigada por acreditares em mim, e por me teres apoiado quando mais precisei. Contigo aprendi um novo lema de vida, "*querer sempre mais, e fazer sempre melhor*", e graças a isso percebi que nenhum sonho é impossível se acreditarmos e trabalharmos para ele. Obrigada por teres vivido todas estas experiências comigo, tanto as boas como as mais difíceis. Um agradecimento nunca irá verdadeiramente refletir tudo aquilo que fizeste e fazes por mim.

# TABLE OF CONTENTS

# LIST OF TABLES

# LIST OF FIGURES

# LIST OF ABBREVIATIONS

| | |
|---|---|
| *2D* | Two-dimensional |
| *3D* | Three-dimensional |
| *α-SMA* | Alpha-smooth muscle actin |
| *bHLH* | Basic helix-loop-helix |
| *BSA* | Bovine Serum Albumin |
| *CLSM* | Confocal laser scanning microscopy |
| *CSC* | Cancer stem cell |
| *ECM* | Extracellular matrix |
| *EMT* | Epithelial to mesenchymal transition |
| *FBS* | Fetal Bovine Serum |
| *GDL* | Glucose delta-lactone |
| *GSK* | Glycogen synthase kinase |
| *HIF-1α* | Hypoxia-inducible factor 1-alpha |
| *HT* | High-throughput |
| *ILK* | Integrin linked kinase |
| *MAPK* | Mitogen-acivated protein kinase |
| *MET* | Mesenchymal to epithelial transition |
| *miR* | microRNA |
| *MMP* | Matrix metalloproteinases |
| *NFκB* | Nuclear-factor kappa B |
| *PA* | Polyacrylamide |
| *PBS* | Phosphate-buffered saline |
| *PEG* | Polyethylene glycol |
| *PGA* | Poly(glycolic acid) |
| *pHEMA* | Poly(2-hydroxyethyl methacrylate) |
| *PI(3)K* | Phosphoinositide 3-kinase |
| *PLA* | Poly(lactic acid) |
| *PLG* | Poly/lactide-co-glycolide) |
| *RFU* | Relative fluorescence units |
| *RGD* | Arginine-glycine-aspartic acid peptide |
| *ROS* | Reactive oxygen species |
| *R-Smad* | Receptor Smad |
| *TBS* | Tris-buffered saline |
| *TGF-β1* | Tumour growth factor-beta 1 |
| *TGFβRI* | Tumour growth factor-beta receptor type I |
| *TGFβRII* | Tumour growth factor-beta receptor type II |
| *TKR* | Tyrosine kinase receptor |
| *YIGSR* | Tyrosine-isoleucine-glycine-serine-arginine peptide |

# CHAPTER I

# Thesis Overview

## 1. Thesis Context

Epithelial to mesenchymal transition (EMT) has been described as a phenomenon through which epithelial cells undergo multiple biochemical modifications that enable them to transdifferentiate into cells that evidence a mesenchymal phenotype[1]. During this biological process, epithelial cells lose their characteristic intercellular adhesion and polarization, and gain mesenchymal features, namely enhanced production and deposition of extracellular matrix (ECM) components, along with enhanced migratory capacity and invasiveness[2–4]. EMT is a crucial embryonic developmental process that can be recapitulated in adulthood during wound healing and that may be harnessed by cancer cells[5]. Indeed, epithelial neoplastic cells may undergo EMT and develop the ability to invade through the basement membrane and metastasize, therefore allowing for cancer progression and systemic dissemination of the primary tumour, originating metastasis[6]. In fact, metastasis are responsible for more than 90% of cancer-related deaths and is currently handled as a dynamic and complex process that holds profound implications for cancer diagnosis, prognosis and treatment[7,8]. The success of the metastatic process is accomplished when the disseminated cancer cells give rise to a secondary tumour, which entails the reacquisition of an epithelial-like phenotype that can be the outcome of the reverse process of EMT, named mesenchymal to epithelial phenotype (MET)[9].

## 2. Problem Statement

The metastatic process and particularly the contribution of the EMT/MET molecular programs to its success are difficult to study both *in vitro* and *in vivo*, due to the lack of proper models. As a matter of fact, the role of EMT in cancer remains dubious since it is difficult to prove and identify a full EMT phenotype in clinical carcinomas and metastases[10]. Some clinical observations may support the concept of a transient EMT that is only induced in a small number of cancer cells[5]. During the past 10 years a notable effort was made in order to develop biological models that could contribute to a better understanding of the EMT molecular regulation and signature. Nowadays, EMT studies are driven by the eagerness to discover new molecular targets and therapies, however there is a concerning gap between the results obtained using the *in vitro* systems and their clinical outcome. Therefore, improved biological systems that better mimic

the three-dimensional (3D) microenvironment of the tumour need to be developed in order to closely reproduce the EMT transcriptional program that occurs *in vivo*. The development of artificial 3D ECM-like matrices may constitute a valuable tool to unravel the molecular mechanisms underlying the metastatic process.

## 3. Aims and Objectives of the Thesis

The primary aim of this Master Thesis was to establish an advanced 3D culture model of EMT/MET induction that would be useful to complement previous studies performed using traditional two-dimensional (2D) and *in vivo* models. The model gathers near-normal mouse mammary epithelial cell line EpH4 and alginate hydrogels as synthetic ECM, to create a Tumour Growth Factor (TGF)-β1-induced EMT/MET model with tuneable biochemical and mechanical properties. This model is expected to facilitate the analysis of the cellular behaviour in a well-defined and biologically relevant microenvironment; will allow the identification of several ECM features, to setup an EMT/MET induction within a 3D EpH4 culture; and will provide insight into cell-matrix interactions in this context.

The first objective was to further develop the 2D *in vitro* model of TGF-β1-driven EMT/MET induction previously established in the group, by characterizing the stemness properties of the cells at different stages of the process, as well as their ability to produce Matrix metalloproteinases (MMPs). The second objective consisted on the establishment of the 3D model that comprised three main tasks, which are identification of the most suitable culture conditions (e.g. stiffness and cell density), determination of TGF-β1 concentration and the time of culture that is necessary in order to achieve each cellular stage of the EMT/MET process, and monitoring of cell behaviour in the 3D artificial environment, in order to evaluate the interaction between epithelial/mesenchymal cells with the surrounding environment, as an integrated system. The final objective was comparison between the 2D and the 3D *in vitro* models to understand the impact of the third dimension, in the study of EMT/MET processes *in vitro*.

## 4. Thesis Outline

Chapter I, Thesis Overview, entails a short context of the Thesis and the problem statement that together represent the motto of this project; the main aims and tasks of the project are also exploited in Chapter I. Chapter II, Introduction, gives a detailed background on the subject that underlies this Thesis, by gathering a review on the extensive knowledge on EMT, particularly related to cancer, and the state-of-the-art of *in vivo* and *in vitro* biological models that have been

developed, in order to study this process. Chapter III, Material and Methods, describes the methods that were implemented during this experimental work, as well as main materials that were used. Chapter IV, Results, reports the observations and findings that resulted from the 2D model study, and from the establishment and validation of the EMT/MET-induction model in the 3D system. Chapter V, Discussion, analyses the obtained results, compares the 2D and 3D EMT/MET systems and correlates them with other models described in literature, offering a critical perspective of the work developed. Chapter VI, Conclusions, reviews the main achievements of this work, their implications, limitations and potential applications. Future research opportunities and perspectives are addressed in the final chapter, Chapter VI.

# CHAPTER II

# Introduction

## 1. General introduction

Epithelial cells are defined as cells highly polarized along a basal-apical axis, which normally interact with basement membranes via basal adhesive junctions. These cells are connected by basal and cell-cell adhesive contacts, such as tight and gap junctions, and they are arranged in mono or multilayers giving rise to the epithelium[11]. The epithelium is a robust tissue that supports the structure of embryos and organs, and acts as an effective barrier against pathogens. It is also recognized by its remarkable dynamic cohesion and adhesion capacity that mainly relies in the establishment of the abovementioned adhesive contacts[1,11]. Under normal settings, these cells present limited motility due to the fact that they can only migrate laterally along the basal surface[12]. In certain circumstances, such as embryogenesis, wound healing and cancer, epithelial cells may undergo the EMT transcriptional program that enable them to transdifferentiate into a mesenchymal phenotype[1]. Mesenchymal cells can be amoeboid or polarized in the anterior-posterior orientation and interact weakly with the ECM components and neighbouring cells leading to an enhanced migratory capacity and invasiveness, two key features of cells that undergo EMT[3,4]. The EMT process is not an irreversible conversion to a mesenchymal state; cells may suffer a reverse process – MET – by which they are able to partially recover an epithelial phenotype and associated features[1,9,13]. The microenvironment in which these events occur is a major regulator of the EMT/MET program, thus biomimetic model systems are necessary to study such influence. Over the past years several EMT studies have been performed contributing to the extensive knowledge about this program and related events. The *in vitro* studies are an essential complement to the *in vivo* experiments and they have been upgraded accordingly to current technology, evolving from monocultures in monolayer to co-cultures systems, complex 3D environments, microfluidics systems and high-throughput (HT) models. The creation of systems with increasing complexity intends to achieve a more reliable representation of the *in vivo* microenvironment thereby enabling a consistent and improved study the EMT/MET biological dynamics.

# 2. Epithelial to Mesenchymal Transition

## 2.1 The biological context of EMT

EMT may occur under diversified, although highly specific settings leading to different functional and physiological responses. Accordingly, three main categories of EMT – type 1, 2 and 3 – have been proposed depending on the biological context in which the phenotypic transition is settled[1]. These three EMT types represent distinctive processes that rely on different biochemical and genetic modification programs that are not yet completely understood.

EMT type 1 comprises a well-known multi-step process that plays a central role during embryonic morphogenesis and development. Particularly, EMT type 1 is crucial for embryo implantation and organ development, since epithelial cells are not endowed with the flexibility required for the development of complex body structures as mesenchymal cells are[1,11,14,15]. Indeed, the differentiation of specialized cells and the complex 3D structure assembly that occurs, for instance, during the internal organs formation, requires sequential rounds of EMT and MET programs, giving rise to the nominations of primary (e.g. gastrulation), secondary (e.g. nephogenesis) and tertiary (e.g. heart formation) EMT[13,14].

EMT type 2 occurs as part of the inflammatory response during wound healing, tissue regeneration and organ fibrosis, in order to generate fibroblasts and related cells that enable the reconstruction and remodelling of the damaged tissue[1]. For instance, during skin wound healing, keratinocytes recapitulate the EMT process through the acquisition of an intermediate phenotype, called “metastable” phenotype, through which cells display simultaneous epithelial and mesenchymal features that allow the movement of these cells without the complete loss of contact[16]. The wound healing of the ovarian surface epithelium at each menstrual cycle in another example of the importance of EMT type 2[17]. In contrast to EMT type 1, EMT type 2 can be associated to disease, since it enables the conversion of epithelial cells into myofibroblasts that secrete excessive amounts of collagen, which accumulate in the organ creating fibrotic collagen networks that compromise organ function[13]. This EMT-mediated conversion during fibrosis was already shown in several organs, such as kidneys, liver, lung and heart[18–21].

The third type of EMT is also associated to pathophysiological conditions as it has been proposed to occur in neoplastic cells and is thought to be a crucial step for cancer progression. Due to genetic and epigenetic alterations that occur in tumour cells, mechanisms thought to regulate EMT suffer modifications that lead to outcomes far different that those described for EMT type 1 and 2[1]. In the initial steps of carcinogenesis in epithelial tumors, transformed epithelial cells are associated to a gaudy proliferation and angiogenesis, and in the final stages these cells develop the ability to invade through the basement membrane and some of them to metastasize

leading to a systemic dissemination of the tumour. This malignant phenotypic change has been proposed as being consequence of the activation of an EMT program; furthermore, the eventual dissemination of these cells to originate secondary tumours at distant sites implies the reacquisition of an epithelial phenotype, which may occur via MET[6]. In some cases, epithelial cells may not be fully transformed into mesenchymal cells, thus accumulating features of both epithelial and mesenchymal phenotypes, suggesting the occurrence of a metastable phenotype[22] that could be the result of a partial EMT[1,23].

The physiological and pathophysiological conditions in which EMT may be activated, illustrate the biological relevance and highlight the need to study the fundamental mechanisms underlying this process. All three EMT types have been subject of extensive research, however there are many open questions that could break new grounds for improved therapies against cancer, chronic fibrosis and other EMT-associated diseases[24]. The specific signal or signals that trigger EMT and MET, the molecular stakeholders that orchestrate the response to those signals and the signalling pathways involved are some of the questions that are still not fully understood, particularly in EMT type 2 and 3.

## 2.2 Cellular and molecular basis of EMT

The molecular modifications inherent to the EMT program have been associated to key signalling pathways that may be responsible for the implementation of the cellular response to extracellular signals arising from the cell microenvironment (Figure 1), as it is the case of TGF-β ligand. Indeed, TGF-β signalling pathway is one of the best studied mechanism of EMT induction and its relevance for tumour progression has been intensively investigated and reviewed[25–29]. Under normal circumstances, TGF-β is a pleiotropic cytokine that is essential to development, differentiation and homeostasis of almost all kinds of mammalian cells and tissues, being a suppressor of uncontrolled proliferation and transformation[25,29]. However, dysregulation of TGF-β signalling may confer an oncogenic behaviour to this molecule that induces EMT and metastasis. Such functional switch is known as “TGF-β Paradox” and it has been studied in order to further understand the mechanisms underlying EMT induction and eventually to identify novel pharmacological agents that could prevent such mechanisms[26]. TGF-β superfamily is considered as primary inducer of EMT and it was found to be capable of inducing all three types of EMT[9]. Although different elements of the family are responsive to different extracellular signals, they share the same transcriptional network and cellular response. To initiate the TGF-β signalling pathway, TGF-β ligands bind with high affinity to TGF-β receptor type II (TGFβRII), a constitutively active cell surface receptor belonging to the serine/threonine kinase family. When the ligand binds to TGFβRII, a conformational change occurs in the receptor allowing the

recruitment of an appropriated TGF-β receptor type I (TGFβRI) and therefore, the formation of a tetrameric complex. TGFβRI can directly phosphorylate the receptor Smad (R-Smad) enabling the formation of a complex of two R-Smads and one Smad4 that accumulates in the nucleus and prompts the EMT transcriptional program[30]. The activation of Smad3 by TGF-β may induce the activation of the Notch pathway that regulates the expression of BMP family members, Notch ligands (e.g. Jagged 1) and targets (e.g. Hey1) and that is associated to E-cadherin repression, enhancement of MMP2/9 and alfa-smooth muscle actin (α-SMA) expression, some of the well-known EMT markers[31–33]. TGF-β signalling may also induce non-Smad pathways, including Mitogen-activated protein kinases (MAPKs), Phosphoinositide 3-kinase/Akt (PI(3)K/Akt) and Nuclear-factor kappa B (NFκB)[13,34,35]. All of these pathways converge in the initiation of a transcriptional program that leads to the inhibition of epithelial features and induction of a mesenchymal phenotype. Such outcome results from the activation of key transcription factors such as Snail, Slug, Twist, ZEB1/2, HMGA2, coupled with changes in microRNA (miR) expression, as it is the case of the downregulation of miR-200 family[27,36]. This specific transcriptional program accounts for characteristic changes in cell-surface, cytoskeletal and ECM protein expression that are understood as EMT markers. The decreased expression of E-cadherin, Cytokeratin and Laminin1, and enhanced expression of N-cadherin, Vimentin and Fibronectin are some of the most common reported changes during EMT at the protein level. TGFβRII may also be triggered in tight junctions where Occludin, Claudin and JAM proteins bind to ZO family proteins, connecting the cell to its neighbour and regulating its own polarity. Once activated, TGFβRII facilitates the interaction between Par6 and Occludin, via Par6 phosphorylation, leading to RhoA inhibition by Smurf1 and consequent polarity loss[9,37].

Besides the TGF-β-mediated EMT induction, other signalling pathways have demonstrated an important role in the induction of this event. Wnt signalling can be correlated to the inactivation of glycogen synthase kinase (GSK)-3β, that blocks the activation of the transcription factors Snail and LEF-1, thus inducing the EMT and cell migration via E-cadherin expression decrease and enhanced mesenchymal markers[9,38–40]. The Tyrosine kinase receptors (TKR) signalling may promote EMT through the induction of Ras-MAPK pathway that eventually activates the transcription factors Snail and Slug[13]. Met, FGF, IGF, EGF, HGF and PDGF families are some of the TKRs inherently associated with the 3 types of EMT[9,17,41]. The NFκB pathway can also be seen as an important regulator of type 2 and type 3 EMT, since it leads to the induction of Snail transcription in carcinoma cell lines and mesothelial fibrosis. Indeed, this pathway proved to be fundamental for EMT implementation, since the EMT is blocked when NFκB pathway was inhibited by IκB[13,34].

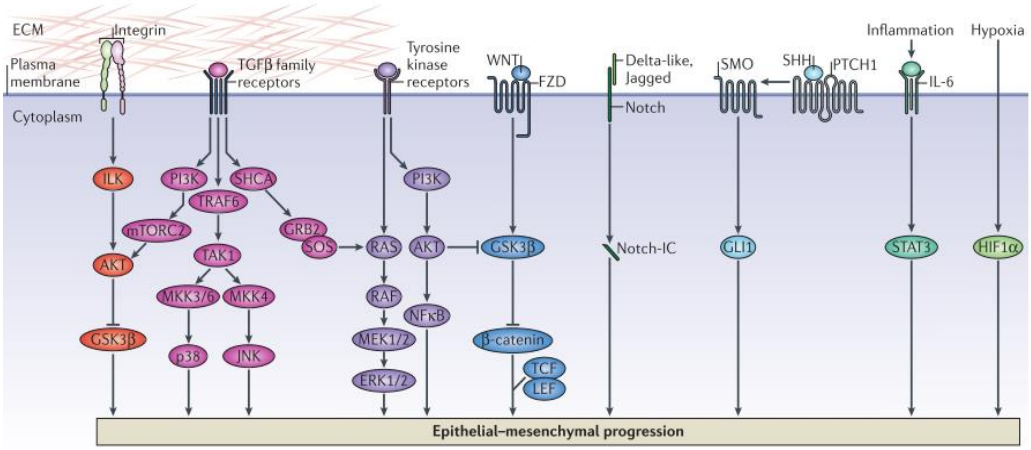


**Figure 1. Summary of major regulators and signalling pathways involved in EMT progression.** Retrieved from Lamouille, Xu and Derynck (2014)[42].

Despite of the several EMT induction mechanisms, the outcomes of the transcription program that is implemented always seem to include the loss of functional E-cadherin, which is why this feature is recognized as one of the most important hallmarks of EMT. Indeed, the loss of E-cadherin is widely correlated to all three types of EMT and it has been associated with carcinoma progression and poor prognosis both in human and mouse tumours[43]. E-cadherin function may be impaired through different mechanisms, which may be developed at the genetic, epigenetic, transcriptional and post-transcriptional levels[44]. Although rare, mutations in the E-cadherin gene (*CDH1*) may lead either to the protein absence or truncation, thus impairing E-cadherin mediated cell-cell adhesion. *CDH1* inactivating mutations were firstly found in diffuse-type gastric carcinomas[45]; now, they are known to occur in other types of cancers, such as lobular breast carcinomas[46] and synovial sarcomas[47]. Regarding the epigenetic mechanisms, hypermethylation of the 5' CpG islands of *CDH1* promoter seems to be an important mechanism of E-cadherin silencing and it has been reported in some types of cancers as it is the case of invasive breast ductal carcinoma[48], esophageal squamous cells carcinoma[49] and gastric cancer[50]. Indeed, in gastric cancers the hypermethylation of *CDH1* was found to be correlated with cancer aggressiveness and metastasis[51]. The transcriptional repression of *CDH1* can be accomplished through the EMT direct activation of zinc-finger transcription factors Snail, Slug and ZEB1/2 that are able to directly bind to E-box repressive elements in the promoter of *CDH1*[52,53]. Nevertheless, some EMT inducers, such as Twist1, FOXC2 and Goosecoid, have shown the ability to activate the EMT program in epithelial cells without binding directly to *CDH1* promoter[9]. The post-transcriptional modification of E-cadherin commonly occurs through phosphorylation or glycosylation. For instance, adherens junction formation can be negatively regulated by tyrosine kinases, such as Met and Src, which phosphorylate β-catenin and the short cytoplasmic tail of E-

cadherin[54]. On the other hand, the loss of E-cadherin function during EMT may be accomplished by a specific modification of the E-cadherin glycosylation via *Mgat3* glycogene expression and GnT-III-mediated glycosylation[55]. Despite the countless reports that show the loss of E-cadherin function in cells undergoing EMT, it is very important to highlight that when such loss occurs in normal epithelial cells, the result is often cell death rather than EMT, which suggests that E-cadherin loss is not, per se, an EMT inducer[9]. The loss of cadherin is associated to a cadherin switch in which N-cadherin is up-regulated[56] and has an important role in tumour progression. Furthermore, P-cadherin has also been associated with tumour progression and increased migration and invasion[57], however its contribution cannot be generalized due to divergent data obtained from independent studies in different types of cancer[45].

The mesenchymal differentiation, cell migration and invasion are also recognized hallmarks of EMT and they can be accomplished mainly through post-translational modifications that regulate the activity, subcellular localization and stability of SNAIL, basic helix-loop-helix (bHLH) and ZEB factors (Figure 2), as described by Lamouille, Xu and Derynck[42].

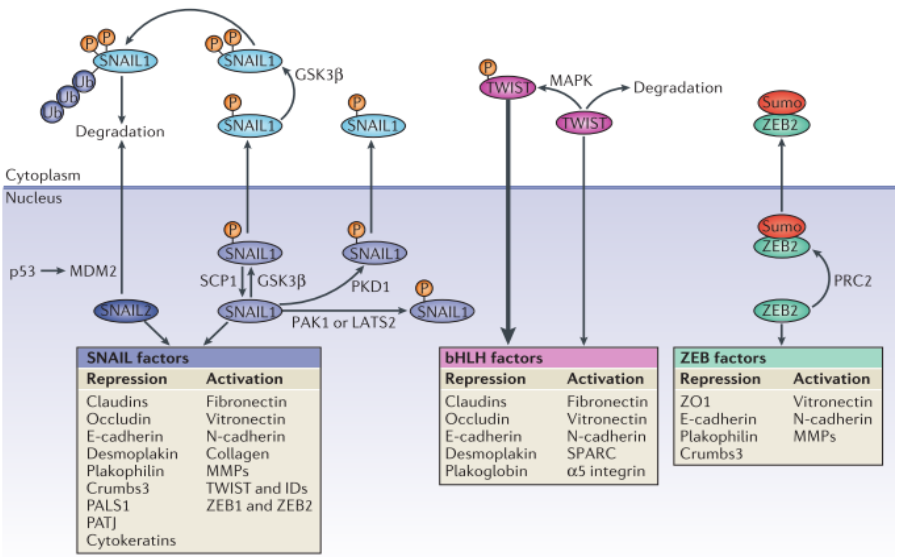


**Figure 2. Post-translational modifications in major EMT regulators SNAIL, bHLH and ZEB.** Adapted from Lamouille, Xu and Derynck (2014)[42].

The depicted signalling pathways are very complex and can regulate numerous elements such as transcription factors, effector proteins and microRNAs; additionally, other pathways can be involved in EMT induction. Hence, the precise role of each component and how it affects the EMT program requires further clarification.

## 2.3 Role of EMT in cancer

The concept of hallmarks of cancer proposed by Hanahan and Weinberg in 2000, and reviewed in 2011[58], gathered important insights that are seen as crucial pieces in the complex biological puzzle that is cancer. The great knowledge produced worldwide around the EMT mechanisms and its key drivers shows that there is a correlation between EMT implementation and several cancer hallmarks, such as activation of invasion and metastasis, immune system evasion and cell death resistance, which supports the existence of EMT type 3.

Several independent studies have shown that EMT type 3 may be induced mainly by TGF-β and Wnt signalling pathways via microenvironmental stimuli[59,60]. Hypoxia has also been revealed as a driving force of EMT events. At early stages, hypoxia supports the Snail up-regulation via Reactive oxygen species (ROS)-dependent GSK-3β inactivation and Notch signalling[61] and Twist expression may be induced via Hypoxia-inducible factor-1alpha (HIF-1α) activation[62]. In late stages of the EMT process, invasion, basement membrane degradation and ECM remodelling might be promoted by HIF-1α-mediated Wnt/β-catenin pathway[63]. Extracellular matrix molecules, such as Collagen type I, may as well contribute to EMT activation[64]. Collagen type I interacts with α2β1 integrin triggering the increase of Akt, GSK-3β and IκB phosphorylation via integrin linked kinase (ILK) that eventually enables the activation of EMT-related transcription factors, such as NF-κB, Snail and LEF-1, as well as E-cadherin down-regulation[38,65]. Beyond the multitude of extracellular signals that could be further described in EMT type 3, it is equally important to note the existence of some intracellular stimuli that have been identified as EMT promotes. One of those cases is the intracellular calcium signalling that has been studied in the growth of the primary tumour context and that recently showed some evidences that it may have an important role in cancer cell invasion and migration[66,67].

EMT type 3 relies on a transcriptional program that is different from the other two types of EMT, therefore the outcomes of this program will also differ from the ones observed in EMT type 1 and 2. In addition to the general hallmarks of EMT, other cell features were already shown such as cell death evasion, cell cycle and senescence regulation, angiogenesis, immunosuppression induction, resistance to therapy, and also acquisition of stem cell properties, in close resemblance to cancer progression[6,9,68]. Indeed, the tumour metastasis process is only possible due to a core of tumour cells that retain the self-renewing ability and stem cell features that enable them to initiate new tumours. These cells, named cancer stem cells (CSCs), can be recognized by a $CD44^{high}/CD24^{low}$ phenotype, which allowed the identification of their presence in breast, colon and brain carcinomas[69–71] or through a $CD44^{high}/CD29^{high}$ phenotype in squamous cell carcinomas[72]. Through the induction of EMT in immortalized human mammary epithelial

cells, Mani and colleagues showed that cells undergoing EMT also present features of CSC, suggesting that EMT can be involved in the formation of CSC[73]. The hypothesis of EMT/MET occurrence in these cells could explain how cells that gain motility and invasion capacity are also able to disseminate and initiate another tumour in distant tissues and organs[73,74]. Tsuji and colleagues suggested that EMT cells might cooperate with non-EMT cells in order to allow a spontaneous metastasis process. In their study, EMT cells induced extracellular matrix degradation enabling invasion and intravasation of both EMT and non-EMT cells[75]. Unfortunately, none of the studies performed until now demonstrates how these cells can initiate a tumour with similar features in a different microenvironmental niche[76]. Recent studies showed that the acquisition of an EMT-associated stem cell phenotype can be correlated with decreased expression levels of miR-200c – by p53 loss of function – and miR-203, suggesting that the restoration of the expression levels of this microRNA family may inhibit metastasis[77–79]. Despite of the lack of irrevocable evidences of EMT in human cancer tissues, the increasing number of studies reporting the potential role of EMT in promoting CSC features and chemoresistance[8,80], lead some authors to suggest the development of therapies based on the use of CSC or EMT markers to target CSCs and consequently reduce the tumour growth, metastasis and patient chemoresistance[81]. Others, propose the use of drugs to induce cancer cells to differentiate into benign stromal fibroblasts[82].

The strong evidences of the EMT importance for tumour development and dissemination, and the hypothetical role of MET in the establishment of metastases (Figure 3)[83] suggest that EMT/MET and associated signalling pathways could be useful to improve cancer treatment and find new cancer therapies. Moreover, the identification of clinically validated EMT/MET markers would lead to an improved and perhaps earlier diagnosis, which could be translated into better prognosis. Such expectation has been nourishing several studies that aim to magnify the knowledge about EMT and its potential role in cancer therapy.

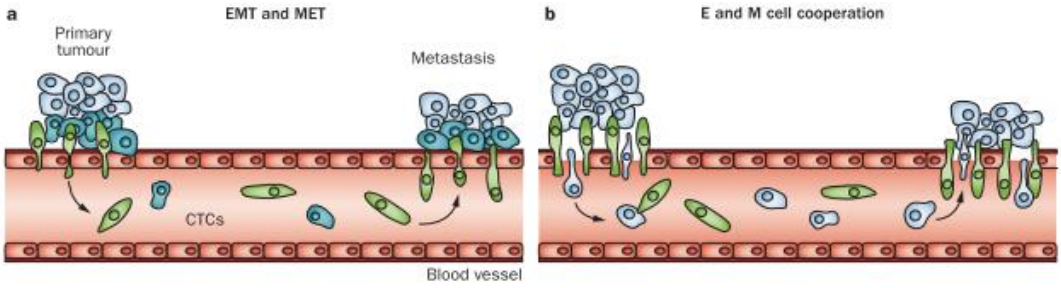


**Figure 3. Two proposed mechanisms of tumour cell dissemination in which EMT and MET are involved. A.** EMT as a complete or partial process. Primary epithelial tumour cells (blue cells) undergo EMT either partially (turquoise) or completely (green), and then undergo MET at a distant site to form the metastatic lesion. **B.** EMT and cell cooperation. Mesenchymal cells (green) invade the vasculature, enabling epithelial (blue) cells to pass through as passengers. Adapted from Krebs *et al.* (2014)[84].

# 3. *In vivo* and *In vitro* Models to Study EMT

## 3.1 *In vivo* models

There is no doubt about the outstanding contribution of the scientific studies performed *in vivo* for cancer research purposes and for biomedical research in general. *In vivo* studies are currently the ultimate barrier to the implementation of new therapies and treatments in all therapeutic classes, and for that reason these models are extensively used for screening purposes. These models are also largely employed to study the complex biological environment and dynamics, however it is important to highlight the high cost and ethical issues intrinsically associated with their implementation. Furthermore, these models are very time consuming and in some cases they fail to reflect the human condition, which may lead to a failure in the translation of the research outcomes[85–87]. In the particular case of cancer research, the most common models arise from the surgical implantation of tumour cells in animals, which are frequently immunodeficient, or the generation of genetically-engineered models that accomplish a spontaneous tumour formation[88]. A major lack in this field is the development of animal models that recreate deadly cancers[89]. Additionally, classical animal models and *in vivo* studies are associated to a higher degree of unpredictability of the model behaviour and ethical issues. These limitations suggest the need for better animal models that would enable to follow the spatial and temporal modifications in tumour cells. Until now, *in vitro* 2D systems have been used as an additional and complementary tool in order to overcome the considerable restrictions of *in vivo* models. Regarding the particular case of the EMT study, the *in vivo* study is even more complex due to the lack of proper biomarkers that would allow the identification of the EMT associated cells[90]. Indeed, despite the large number of biomarkers identified through 2D standard *in vitro* cultures, the success rate of their implementation in clinics is extremely low which translates the need for more reliable and representative models[91].

## 3.2 EMT *in vitro* models

### 3.2.1 2D EMT studies

The conventional 2D studies accomplished in flat culture plastic have given rise to major advances in the understanding of EMT. These systems are particularly interesting to study the effect of individual variables and factors, or to achieve constant and stringent conditions of analysis[92]. In fact, these models provide almost total control over the biochemical and topographical properties of cells and they can be easily manipulated and integrated with a wide range of techniques[93]. For all these reasons, 2D models have an important role in understanding the influence of the individual EMT intervening factors in the global biological process and to relate them with the observed outcomes.

Although 2D studies represent an easy, flexible and accurate way to analyse EMT related effects, they fail in reconstructing the 3D complex environment in which the EMT takes place. One of the major criticisms concerning studies in 2D is that when cells are removed from their biological environment they tend to show a non-natural behaviour that may induce modifications in the global process. Once cultured in monolayer, cells become polarized with only part of their surface anchored in the substrate while the remaining surface is exposed to the culture media, hence cells are limited to their planar and spread morphology which can lead to the loss of their tissue-specific functions[93,94]. When tissue derived cells or cell lines are cultured in 3D scaffolds they tend to develop complex networks of cell-cell and cell-matrix interactions that affect the penetration of nutrients, biological factors (hormones and growth factors) and drugs, thus influencing cell growth, differentiation and death[95]. Other restrictions of 2D models are the lack of stromal components and reduced cell-matrix interaction, which are essential stimuli found in the *in vivo* environment[95]. In order to overcome some of these limitations, several studies attempt to incorporate ECM-like components on the 2D model by coating the flat dishes with various proteins, such as Collagen, Fibronectin and Laminin, creating a natural basal adhesion. The most complex 2D models also include co-cultures that intend to recreate the natural intercellular communications. In any case, cells remain in a monolayered arrangement that impairs the generation of a multidimensional structure.

### 3.2.2 Advances of 3D *in vitro* models

The limitations of both 2D cell models and *in vivo* animal models provided the opportunity to the establishment of 3D models that aim to bridge the outcomes derived from the traditional models, and simultaneously to connect cell culture and human biology, both in physiological and pathological conditions. Such models attempt to recapitulate the tumour biology at all levels, which includes tumour gene signatures, cellular morphology, proliferation and differentiation, phenotypic heterogeneity of the population and the tumour microenvironment, through a fine balance between 2D *in vitro* simplicity and *in vivo* complexity (Figure 4).

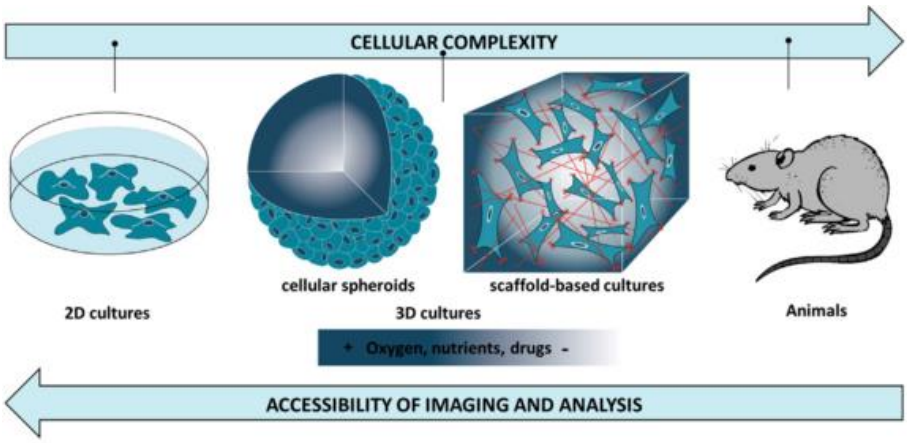


**Figure 4. Balance of main considerations of *in vivo* and *in vitro* models.** 3D cultures that recreate the complex cellular microenvironment more precisely than traditional 2D cultures, due to the incorporation of multiple physical, mechanical and chemical cues that arise from ECM–cell and cell–cell interactions. Animals do not capture important facets of human behavior and they are not feasible for HT screening applications. Adapted from Alemany and Semino (2014).

The differences between 2D and 3D systems were noticed for the first time in the beginning of the 20$^{th}$ century, when Ross Harrison cultured embryonic frog cells in different conditions and observed a different cell behaviour in 2D and 3D hanging drop cultures[96]. Another type of 3D cell culture had its beginning in 1957 when McLimans and its colleagues reported a "*disturbing feature*" of HeLa cells grown in shake culture that was the formation of "*large matrices of cells*"[97]. This was the first time that a multicellular spheroid derived from mammalian cells was described. Three years later, in 1960, Wichterle and Lim proposed the use of poly(2-hydroxyethyl methacrylate), also known as pHEMA, in contact lenses giving rise to the concept of hydrogels[98]. It took twenty years to expand this concept to cell culture that came in the first place through cell encapsulation[99]. The 3D culture concept was brought to the cancer field by Miller and its colleagues that showed that tumour cells exhibit greater drug resistance when grown as multicellular spheroids in a collagen gel than when cultured in monolayer[100]. Since then, many important achievement have been accomplished as it is the case of the pioneer work

of Mina Bissell that used 3D culture systems to model the molecular mechanisms underlying breast cancer cell invasion and revealed that when cells from tumour of epithelial origin are cultured in Matrigel, their shape is changed and resembles what is seen in *in vivo* tumour progression[101]. These findings sparked the interest of the scientific community, which led to the improvement of the 3D cell culture systems. Important advances were achieved in the field of biomaterials, giving rise to the concept of biologically active materials. The bioactivity of synthetic polymers could be accomplished by the incorporation of cell-recognition sites, such as adhesion factors and enzymatic cleavage moieties[102]. One example of those bioactive biomaterials are the polyethylene glycol (PEG) hydrogels designed by West and Hubbell (1999) that incorporated peptide domains susceptible to cellular proteases, which allowed the hydrogel degradation by cells[103]. A few years later, the work of Mooney's group in adapting scaffolds initially developed for tissue engineering purposes for cancer research, allowed for the first time the combination of these scaffolds with human carcinoma cells for *in vitro* and *in vivo* experiments[104]. Since then, many other groups have expanded the applications of the 3D *in vitro* models in cancer, for instance, Hutmacher and Clements lab developed 3D *in vitro* models for breast and prostate cancer bone metastasis[90] and currently there are several groups trying to develop HT systems to produce and analyse 3D cultures, which can be very important to improve the screening of anticancer drugs and to develop personalized therapies.

According to the tumour microenvironment and its characteristics, or a particular process/feature that is aimed to mimic, different 3D models can be used, differing not only in their composition but also in terms of cell culture methodology and analysis (Table 1). Regarding the composition of these systems, they can be constituted by purely natural to purely synthetic materials[105]. Models derived from natural materials encompass as main advantages their cytocompatibility, ease usage, the ability to create a porous matrix or fibrous structure, and the possibility of modulating the stiffness simply through modulation of polymer composition and gelling conditions. Additionally, ECM-derived materials are provided with bioactivity due to the presence of cell adhesion sites in their composition. Despite of the broadly usage of these materials, they present relevant limitations, such as batch-to-batch variability and their complex or sometimes unknown molecular composition that challenges the reproducibility of the experiments. While studying EMT, it is important to understand that the unknown and variable composition on growth factors, namely TGF-β, may strongly compromise the replicability of the outcomes. Some examples of naturally derived materials are Matrigel® (derived from the basement membrane of murine sarcoma), ECM components from animal tissues such as Collagen type I, Laminin and Fibrin, and components derived from other biological sources as it is the case of Alginate[106] and Chitosan[107]. Both Matrigel and Collagen have been largely used in

cancer research, and EMT studies are not an exception, however they present weak mechanical strength and the modification of the matrix mechanics often alters the matrix biochemistry. Alginate is a natural polymer derived from polysaccharides that has been used in tissue engineering, for instance to transplant cells[108]. Nevertheless, 3D alginate scaffolds, such as AlgiMatrix™, have already proved their value as tumour models, namely for anticancer drug screening[109]. The typical slow biodegradation of the alginate hydrogels[93,110] can be adjusted through their partial oxidation, combination of polymer chains with different molecular weight[111] or even the incorporation of MMP-sensitive peptides[112].

Synthetic materials can also be used to engineer 3D models for cancer research, being their main advantage the great control over the experimental conditions. Additionally, they provide batch-to-batch uniformity and allow a selective tuning of physical and biochemical composition. The major lack of these models is the absence of intrinsic bioactivity since their ultimate goal is the recreation of a physiological microenvironment that mimics as closely as possible the *in vivo* scenario. Therefore, hydrogels and scaffolds based in synthetic materials can be modified giving rise to hybrid artificial matrices. The incorporation of cell adhesive peptides (e.g. Arginine-Glycine-Aspartic acid (RGD) and Tyrosine-Isoleucine-Glycine-Serine-Arginine (YIGSR)) and proteins (growth factors); the sensibility to cellular matrix-proteases (e.g. MMPs); and the modulation of the scaffold stiffness and surface topography are some of examples of matrices modifications[93,113,114]. Among the most commonly used synthetic materials are PEG[115], poly(lactide-co-glycolide) (PLG)[116] or polyacrylamide (PA)[117]. PEG hydrogels are biocompatible and resistant to protein adsorption, since they have high hydrophilicity, neutrality and mobility. PEG bioactivity can be easily tuneable and controlled, and it has been used as an hydrogel to culture different types of cells[118,119]. PLG is a synthetic and biocompatible polymer that allows for an easy reproduction and is convenient to use, which enables its utilization in a large-scale, for instance for cancer progression research and antitumor drug screening[104]. PA models are ideal to study mechanoregulatory mechanisms in the tumour; indeed, these models enabled researchers to understand that matrix stiffness improves tumorigenesis and that increased cellular traction stresses, as a response to increased stiffness, may be considered as an index of enhanced malignant potential[120]. Other synthetic materials can be used depending the microenvironment that is aimed to mimic, thus enabling the study of different metastatic sites. For instance, poly(lactic acid) (PLA), poly(glycolic acid) (PGA) or the combination of these two polymers provide a very high stiffness that can be used to biomimic the bone ECM[121].

**Table 1. Most common 3D cell culture methodologies.**

| Cell culture Methods | Fundamentals |
|---|---|
| **Multicellular Spheroids** | *Cells undergo self-assembly when in the absence of an attachment surface or scaffold, leading to the formation of cellular aggregates*[122] |
| Spinner culture | Constant stirring cell collision, thus avoiding single cells in suspension to settle and promoting the spheroid formation.[122,123] This technique allows the formation of heterotypic spheroids and the control over spheroid characteristics via medium changes, stirring time and agitation speed. Mass diffusion along the spheroid can be promoted by fluid movement, avoiding the gradient of soluble components. This process can be easily scaled up, however it cannot be used for culturing low cohesive, shear sensitive or adherent cells. Additionally, cell visualization during aggregation is not possible due to the constant mixing.[122,124] |
| Liquid overlay | Cells are seeded in flat tissue culture dishes made of low-adhesive surface (e.g. coated with agar, agarose and pHEMA) and spheroid formation is achieved by rocking the plates, together with a small amount of shaking. This technique is easy to perform, yet spheroids present a heterogeneous size and shape.[122,124] |
| Rotating wall vessel | Cell suspension is slowly rotated about an x-axis, creating a microgravity environment.[95] As cells start to aggregate, the rotation speed is increased to avoid its settlement. Through this method high yield of spheroid formation can be achieved, using low levels of shearing forces. Moreover, the culture medium can be easily changed by perfusion allowing long-term studies or changing conditions during the process.[125] Nevertheless, the size of the spheroids is highly variable and it is difficult to track spheroid assembly. |
| Hanging drop | A small volume of a cell suspension is pipetted in the inside part of the lid of a tissue culture plate, and when the lid is inverted, the drop will stay attached due to surface tension and spheroid formation occurs through gravity-enforced cell self-assembly.[126,127] This method allows for a high-throughput spheroid formation, with a fine spheroid size and cellular composition regulation.[128] In this system, it is difficult to track spheroid assembly and to change or add cell culture medium/drugs. |
| Concave plate | Cells are isolated in microwells of non-adhesive substrates allowing them to cluster and grow into compact cell spheroids through cell-cell adhesion. This method enables the creation of a high-throughput system of spheroid production, as well as easy track of spheroid formation and medium change. |
| External force | External forces, such as ultrasound, electric and magnetic fields induce an increase in cell concentration into a high density that facilitates spheroid formation. Physiological cell changes induced through this method are still not well characterized.[122] |

(Table 1 continues in next page)

(Table 1 continuation)

| **Scaffolds** | *Cell-cell and cell-matrix interactions induce cell spheroid mimicking the ECM behaviour*[95,105] |
|---|---|
| Microporous scaffolds | Cells interact with the substrate being lodge within the porous. Due to the large size of those porous (≈100 µm), cells tend to adhere and form few cell-cell interaction which leads to a 2D-like culture rather than a 3D culture.[105] |
| Nanofibrous scaffolds | Cells interact with a fibrous substrate that provides a 3D architecture for cell culture. Yet, these substrates tend to be structurally weak to handle the stress needed for mechanotransduction.[105] |
| Hydrogels | Cells interact with crosslinked networks that are characterized by high porosity and water content that enable free diffusion of nutrients, oxygen, growth factors, cell metabolites and other soluble components.[93,105] These matrices closely mimic the nature of most soft tissues and allow the study of cell behaviour in different conditions, since the medium can be easily changed. Retrieving the cells from the 3D culture seems to be the main difficulty associated to this method.[124] |

Regardless the cell culture methodology or composition of the 3D model, epithelial cells tend to form cellular spheroids that provide a more physiological arrangement that the 2D cultures (Figure 5), that can be generally described by additional mechanical inputs, dissimilarity in morphology, distinct cell adhesion and contraction, as well as modified intracellular signalling, which may ultimately change the functional behaviour of these cells[129,130].

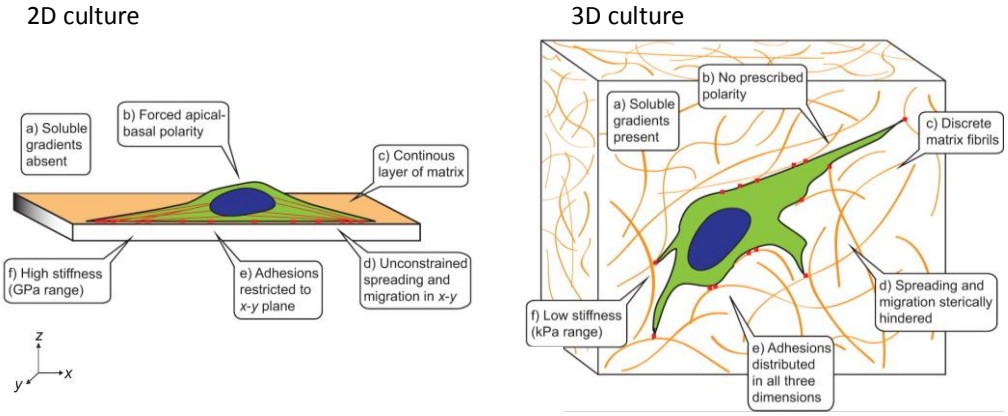


**Figure 5. Adhesive, topographical, mechanical, and soluble cues in 2D and 3D.** The cues encountered by a cell are strikingly different between an ECM-coated glass or plastic surface (2D) and a typical 3D ECM. Adapted from Baker and Chen (2012)[130].

### 3.2.3 EMT studies using 3D *in vitro* models

In an attempt to create research approaches that better resemble the *in vivo* conditions in which EMT takes place, many groups have been exploiting different 3D models based on a wide range of materials and technologies. This divergence of models also differs in respect of the EMT inducer; indeed, TGF-β remains one of the most common EMT inducers[131–135], however other stimuli have also been studied such as Snail[136], BMP7[137], HGF[138], collagen type I[38,65,139,140], matrix stiffness[141–143] and endothelial cells co-culture[144].

The initial 3D studies on EMT were designed to address the cellular behaviour and cell-matrix interactions. The work of Maschler and colleagues is a great example of such studies. Using EpH4 cells transformed by oncogenic Ha-Ras, this group showed that TGF-β1 induced EMT results in secretion and deposition of the extracellular matrix protein tenascin-C when cells are cultured in 3D collagen scaffolds but not when traditionally cultured in 2D[145]. Indeed, tenascin-C was found to be overexpressed in breast carcinomas and it is associated with a migratory and invasive tumour cell phenotype[146]. Additional studies on this model also showed the important role of functional α5β1 integrin in cell invasiveness associated with EMT[147] and that Annexin A1, an important cellular mediator that is highly reduced during tumour progression and metastasis in breast cancer and that correlates with reduced patient's survival, is an efficient EMT/metastasis suppressor[148,149]. In an independent study, Loessner and colleagues compared the cell-ECM interactions between two human cancer cell lines – epithelial ovarian cancer and serous adenocarcinoma cell lines – that despite the similarity in 2D culture, showed different proliferation rates in RGD-modified PEG hydrogels[113]. The authors showed that proliferation in the hydrogel was dependent on cell-integrin engagement but also on the cellular ability to remodel the surrounding matrix. In fact, the surrounding matrix plays a crucial role in defining the EMT success, both in a biochemical and in a mechanical manner. For that reason, some studies propose models with independently tuneable chemical and mechanical properties to better understand the EMT process. In 2012, Gill and colleagues proposed a PEG modified scaffold for miR-200-dependent EMT/metastasis on 344SQ metastatic cell line and showed that matrix stiffness and concentration of cell-adhesive ligands influences the epithelial morphogenesis at different levels, namely at the expression of epithelial markers, apoptosis, proliferation and lumenization of epithelial spheres in MMPs-degradable hydrogels[118]. They also showed a successful EMT induction by TGF-β1 regardless the matrix composition. Markowski and colleagues exploited this question by culturing alveolar epithelial cells (RLE-6TN cell line) on top of PA gels with different concentrations of bisacrylamide and different recombinant variants of the RGD sequence in Fibronectin[150]. Their work suggested that TGF-β1 induced EMT is only

supported on stiff substrates that present adhesive ligands that preferentially bind αv integrins. Recently, it was shown that the increase of ECM stiffness alone may induce malignant phenotypes, however that effect can be abrogated with the concomitant increase of basement membrane ligands[151]. This phenomena was observed in the human mammary epithelial cells (MCF10A) cultured in a matrix composed by a combination of Matrigel and alginate and it is dependent on integrin β4, Rac1 and PI3K signalling pathway, as suggested by the authors. Nevertheless, stiffness is not the only physical property that should be considered and the topography of the culture surface has becoming more and more relevant. Last year, Foroni and colleagues demonstrated that aligned-PLA scaffolds are prone to produce more aggressive phenotypes than PLA fibers randomly orientated[152].

With all the knowledge conquered with these studies even more complex systems have been created. Decellularized tissue matrices, co-cultures in 3D structures, microfluidic devices and high throughput methods have been produced and tested in order to develop new methods for drug screening, diagnosis or personalized treatments related to cancer and EMT in particular (Table 2). All of these engineered–based systems have been developed to increase complexity of standard methods and simultaneously reduce the complexity of the disease. Nevertheless, these systems need to be further improved to truly fill the gap between *in vitro* and *in vivo* outcomes.

**Table 2. Innovative 3D *in vitro* models for EMT and cancer research**

| Relevance | System | Cell Model | Reference |
|---|---|---|---|
| Usefulness of the radial flow type bioreactor for 3D culture systems | Hydroxyl apatite matrix in a radial flow type bioreactor | A431 squamous carcinoma cell line | Shibata *et al.* (2009) [153] |
| Hydrogel-based microfluidic system for tumour spheroid formation and drug screening | In situ gelation of alginate within microchannels | LCC6/Her-2 breast tumour cells | Chen *et al.* (2010) [154] |
| High-throughput system for tumour spheroid formation and drug screening | 384-well platform for hanging drop spheroid culture | COS7 kidney fibroblast cells; ES-D3 embryonic stem cells; A431.H9 epithelial carcinoma cells | Tung *et al.* (2011) [128] |
| High-throughput system for 3D EMT and metastatic breast cancer drug screening | Single spheroids cultured in 1536-well plates coated with Matrigel™ | MDA-MB-231 breast carcinoma cells | Li *et al.* (2011) [155] |
| Microfluidic chip for deterministic patterning of multicellular spheroids | Chip coated with Pluronic copolymers that induce spheroid formation via cell aggregation | SKOV3 ovarian cancer cells | Kuo *et al.* (2012) [156] |
| Microfluidic system for 3D EMT monitoring and drug screening | 3D spheroid culture in collagen type I hydrogels integrated with co-culture of endothelial cell monolayer | A549 lung carcinoma cells in co-culture with HUVECs | Aref *et al.* (2013) [157] |
| 3D culture of tumour cells and tumour biopsies for EMT study and personalized cancer therapy | EMT inducing 3D nanofibrous scaffold of PLGA, PLA and methoxy PEG | MCF-10A and MCF7 breast cancer cells; PC3 protate cancer cells; B16 melanoma cells; BG1 ovarian cells; LLC1 Lewis lung cancer cells | Girard *et al.* (2013) [158] |
| Customized microfluidic platform to study flow induced EMT and metastasis | 3D nodules culture on growth-factor reduced Matrigel | NIH:OVCAR5 ovarian cancer cells | Rizvi *et al.* (2013) [159] |
| Complex 3D cell culture for lung cancer model | Intestinal decellularized tissue matrix | HCC827 and A549 lung carcinoma cells | Stratmann *et al.* (2014) [160] |
| Microchip filter platform for isolation of heterogeneous population of cells with CTCs and EMT markers | 3D cell culture in ultralow adherent dishes for spheroid formation; 3D flow for cell separation in slit arrays via CAV1-EpCAM conjugated microbeads | MDA-MB-231, MDA-MB-436, MCF-10A and SK-BR3 breast cancer cells; NCI-H1650 and HCC 827 lung cancer cells; PC3 and LNCap prostate cancer cells | Kim *et al.* (2014) [161] |

# CHAPTER III

# Material and Methods

The literature review provided on Chapter II identified several factors that must be taken in consideration when establishing an EMT/MET model based on 3D cell culture. Additionally, different methods have been described regarding the characterization of EMT/MET processes at the behavioural, cellular and molecular levels[162]. Therefore, this chapter describes the approach and methods used for the development of the 3D *in vitro* EMT/MET.

## 1. 2D culture of EpH4 cells

EpH4 cell line[163] was maintained in normal culture medium constituted by Dulbecco's Modified Eagle Medium with Glutamax (DMEM/F12 GlutaMAX™, Gibco) supplemented with 5% v/v Fetal Bovine Serum (FBS, Biowest), 1% v/v Penicilin/Streptomycin (Pen/Strep, Gibco) and 5µg/mL Insulin solution human (10mg/mL; Sigma). Mesenchymal cells cultures were grown in normal culture medium supplemented with 8ng/mL of TGF-β1 recombinant human protein (Gibco) for 7 days. For EMT reversion, mesenchymal cells were cultured for 4 days in normal culture medium. Cultures were maintained at 37°C in a 5% v/v $CO_2$ humidified atmosphere in order to maintain physiological conditions.

## 2. Alginate hydrogels preparation and formation

Alginate hydrogels were prepared under cytocompatible and controlled conditions using RGD-modified alginate at 1.7 and 2.7 wt-% in 0.9 wt-% sodium chloride (NaCl, Sigma). PRONOVA ultra-pure alginate (FMC Biopolymers) with a molecular weight of 150kDa and a high glucuronic acid content (68%) was modified as previously described by Fonseca and colleagues[164], by covalent grafting of the oligopeptidic sequence of (Glycine)4-Arginine-Glycine-Aspartic acid-Serine-Proline ($G_4$-RGDSP, Peptide International) performed by aqueous carbodiimide chemistry[165]. Alginate gelling process was accomplished by ionic crosslinking of alginate solution promoted by calcium[166]. For that purpose, alginate precursor solutions were homogeneously mixed with a suspension of calcium carbonate ($CaCO_3$, Fluka) in 0.9 wt-% NaCl at a $CaCO_3$/COOH molar ratio of 1.6, and the gelling process was triggered through the addition of a filtered (0.2µm) fresh glucose solution of delta-lactone (GDL, Sigma) in 0.9 wt-% NaCl at a $CaCO_3$/GDL molar ratio of 0.125. A final RGD-modified alginate concentration of 1 and 2 wt-% with 200µM of RGD is obtained by adding the previous solution to the cell suspension. *In situ* crosslinking (30min, at

37°C) was allowed after quickly applying small drops (14 and 20µL) of the mixture between Teflon plates separated by spacers with appropriate height (500 and 750µm, respectively); larger matrices – with 60µL of volume – were crosslinked within a QGel™ 3D disc caster device (QGel) that allows for the production of consistent and reproducible discs with high volume. After *in situ* crosslinking, the matrices were transferred to a 24-well culture plate (Falcon) coated with pHEMA (Sigma) and incubated with fresh culture medium at 37°C. The coating with pHEMA permanently reduces the adhesiveness of plastic tissue culture dishes[167] which prevents cell migration from the hydrogels to the bottom of the wells. After 30-60min, the culture medium was changed accordingly to E, M and TS cell culture requirements.

## 3. 3D culture of EpH4 cells within alginate-RGD hydrogels

In order to immobilize the EpH4 cells within the RGD-modified alginate hydrogel, cells in 2D culture were harvested before reaching confluence through the incubation with 0.05% w/v trypsin/50mM ethylenediamine tetraacetic acid (EDTA) solution (Gibco) at 37°C, a solution that disrupts both cell-cell and cell-subtract adhesions. Trypsin/EDTA was inactivated with normal culture medium, and after centrifugation (1200rpm, 5min) and supernatant removal, EpH4 cells were ressuspended in 0.9 wt-% NaCl and homogeneously mixed, at the desired densities, with the alginate gel precursor and the crosslinking agents. After the crosslinking process, described in section 2, cells were kept at 37°C in a 5% v/v $CO_2$ humidified atmosphere. Epithelial cultures were maintained in normal culture medium and mesenchymal cultures in normal culture medium supplemented with TGF- β1 recombinant human protein.

## 4. Cell viability

Cell viability under different 3D culture conditions was assessed by staining with Cytrak Orange™ (1:200 dilution; Biostatus) and DRAQ7™ (1:1000; Biostatus) fluorescent dyes. Cytrak Orange™ is a membrane-permeant dye that stains both nucleus and cytoplasm of live cells, whereas DRAQ7™ is a DNA counterstain that only stains the nuclei in dead or permeabilized cells. This live/dead staining was performed by incubating the cells cultured within the alginate-RGD hydrogels (height: 500µm; volume: 14µL) with the abovementioned fluorescent dyes for 10min at 37°C. Then, cells – within the hydrogel – were analyzed by confocal laser scanning microscopy (CLSM; Leica TCS-SP5 AOBS). Spheroid formation and morphology in the hydrogel were also analyzed through this 3D imaging.

## 5. Metabolic activity

Cell metabolic activity was determined through a resazurin-based assay. To this end, hydrogels containing cells (height: 750µm; volume: 20µL; n=3) were incubated with 20% v/v of stock resazurin solution (0.1mg/mL, Sigma-Aldrich) in normal cell culture medium for 2h at 37°C and in the dark. After this incubation, 200µL of supernatant were transferred to a 96-well black plate (Greiner) and fluorescence measurements were performed using a microplate reader (Biotek Synergy MX) with excitation/emission at 530/590nm. Thereafter, samples were washed with Tris-buffered saline (TBS)/Calcium Chloride ($CaCl_2$, 7.5mM, Merck) and EpH4 cells were retrieved from the alginate-RGD hydrogels for total protein quantification. The protein quantification was used to normalize data collected from the resazurin assay. Cell retrieval was accomplished by dissociating the matrix using 0.05% w/v trypsin/50mM EDTA solution, followed by centrifugation at 1200rpm for 5min. At that point, cells were washed with 1x Phosphate-Buffered Saline (PBS) and again centrifuged (1200rpm, 5min) with removal of supernatant. In order to promote cell lysis, cells were incubated with 1% v/v Triton X-100 (Sigma-Aldrich) for 1h at 250rpm and 4°C. After a 1:10 dilution in 1xPBS, PierceTM BCA Protein Assay Kit (Thermo Scientific) was used for quantification of total protein. Accordingly to manufacturer's instructions, samples were transferred to a 96-well plate, mixed with the BCA working reagent and incubated for 30min at 37°C, in the dark, to allow the colorimetric detection. Absorbance was measured at 540nm using a microplate reader. Absorbance was converted to µg/mL using a standard curve in the range of 0-2000µg/mL.

## 6. Transcriptional analyses by real-time PCR

Gene expression quantification was performed by quantitative real-time polimerase chain reaction (real-time PCR). At each time point alginate-RGD hydrogels (height: 500µm; volume: 20µL; n=3) were collected, washed with TBS/$CaCl_2$ and cells were retrieved by dissolving the matrices using 0.05% w/v trypsin/50mM EDTA solution, followed by centrifugation (1200rpm, 5min) and supernatant removal. Before cell pellet storage at -80°C until further analyses, cells were washed 3 times with 1xPBS. Total RNA was extracted using the *mir*Vana™ miRNA Isolation Kit (Ambion, Life Technologies), following the manufacturer instructions, and quantified by using NanoDrop™ 1000 spectrophotometer (Thermo Scientific). For single stranded cDNA synthesis, 1µg of total RNA was incubated during 10min at 70°C with random hexamer primers (0.1µg/µL) in DNase/RNase-free distilled water (Gibco), to prime reverse transcription reaction. After 2min on ice, a reaction mix containing 0.1M DTT (Invitrogen), 10mM dNTPs (Invitrogen), 8U RNase inhibitor (rRNasin® 40U/µL, Promega) and 150U reverse transcriptase (SuperScript®II 200U/µL,

Invitrogen) in 5x first-strand buffer (Invitrogen) was added to the samples for a final volume of 20µL. Reverse transcription reaction was allowed via incubation at 37°C during 1h. Real-time PCR reaction mix was prepared on ice, by mixing the single stranded cDNA samples (50ng) with probes for target genes (0.5µL; Table 3) and master mix (5µL, TaqMan) in DNase/RNase-free distilled water for a final volume of 10µL. Samples were run in triplicates in the ABI Prism 7000 Sequence Detection System and data was analysed by the comparative 2(-ΔΔCT) method[168] and normalized to *GAPDH*.

**Table 3. Fluorescent probes for expression analysis of target genes by real-time PCR**

| Marker | Symbol | Reference | Supplier |
|---|---|---|---|
| E-cadherin | *CDH1* | Mm00486909 | Applied Biosystems |
| Occludin | *Ocln* | Mm.PT.47.16166845 | Integrated DNA Technologies |
| Mgat3 | *Mgat3* | Mm00447798_s1 | Applied Biosystems |
| N-cadherin | *CDH2* | Mm00483212_m1 | Applied Biosystems |
| Vimentin | *Vim* | Mm01333430_m1 | Applied Biosystems |
| ZEB2 | *Zeb2* | Mm.PT.47.13169136 | Integrated DNA Technologies |
| Twist | *Twist* | Mm.PT.97.12853943 | Integrated DNA Technologies |
| Dies1 | *Dies1* | Mm00472312_m1 | Applied Biosystems |
| ID2 | *Id2* | Mm00711781_m1 | Applied Biosystems |
| ID3 | *Id3* | Mm00492575_m1 | Applied Biosystems |
| GAPDH | *GAPDH* | 4352932-0912031 | Applied Biosystems |

## 7. Immunocytochemistry analysis

Immunocytochemistry was conducted to analyze the expression and cellular localization and organization of the epithelial marker E-cadherin (24E10 Rabbit mAb, #3195, Cell Signaling Technology), and mesenchymal markers Fibronectin (2755-8 Mouse mAb, #sc-69681, Santa Cruz Biotechnology) and α-SMA (Mouse mAb, #M0851, Dako), during EMT/MET induction. Immunocytochemistry was performed in alginate-RGD hydrogels (height: 500µm; volume: 14µL) that were collected at each time point, washed 3 times with TBS/$CaCl_2$, fixed with 4% v/v Paraformaldehyde (PFA, Merck) with 7.5mM $CaCl_2$ for 20min at RT and washed again. TBS was used instead of PBS since the presence of phosphate in PBS could sequester the calcium ions that maintain the ionic crosslinking of the hydrogels, which would induce a mechanical instability in the hydrogel[169] that may lead to its degradation. Before the immunostaining, the alginate-RGD hydrogels containing cells are incubated with 50mM Ammonium chloride ($NH_4Cl$,

Calbiochem) in TBS/$CaCl_2$ for 10min, and permeabilized with 0.2% Triton X-100 in TBS/$CaCl_2$ for 5min; both incubations were performed at RT and hydrogels were washed 3 times after each incubation. To block unspecific signal and enhance specific fluorescence, samples were incubated with 5% Bovine Serum Albumin (BSA, Fisher Scientific) in TBS/$CaCl_2$ during 1h, and then incubated overnight at 4°C with primary antibodies in 5% BSA TBS/$CaCl_2$. After the immunoreaction, samples were washed 3 times with TBS/$CaCl_2$ and then incubated with secondary antibody Alexa Fluor® 594 Goat Anti-Rabbit (Life Technologies) and/or Alexa Fluor® 488 Goat Anti-Mouse (Life Technologies) in TBS/$CaCl_2$ for 2h in the dark. After washing 4 times with TBS/$CaCl_2$, Vectashield® Mounting Media with DAPI (Vector Labs) was added to the samples. 3D imaging of the samples was accomplished by CLSM (Leica TCS-SP5 AOBS) and data analysis was performed using ImageJ software (http://rsb.info.nih.gov/ij/).

## 8. 3D culture characterization

For the characterization of spheroids geometry and number, alginate-RGD hydrogels were collected as described in section 7 and cell nuclei stained using Vectashield® Mounting Media with DAPI (Vector Labs). For image acquisition, hydrogels were transferred to a µ-Plate 96 well (ibidi) and the plate was read by an IN Cell Analyzer 2000 microscope (GE Healthcare). Bright field and fluorescence (excitation/emission for DAPI: 350/455nm) images were taken using a x10 objective lens and an advanced 2D deconvolution method with a 0.030 seconds exposition. Several fields were acquired in order to obtain images of the entire hydrogel. The obtained images were analyzed in the IN Cell Developer Toolbox software (GE Healthcare) that enables an individual characterization of each spheroid and their automatic counting. In order to improve spheroid recognition by the software, a protocol based on spheroid area, form factor, DAPI intensity and standard deviation of the signal was established.

## 9. Population molecular characterization by Flow Cytometry

Flow cytometry was carried out to assess the presence of E-cadherin, CD44 and CD29 antigens in the surface of EpH4 cells at different stages of EMT/MET. E-cadherin surface levels are critically reduced when cells are treated with peptidases commonly used for cell dissociation, such as trypsin, since E-cadherin mediated-intercellular adhesion is strongly dependent on calcium. Therefore, it is advisory the use of other cell dissociating agents such as Versene, a calcium-chelating agent. For this instance, alginate-RGD hydrogels (volume: 60µL; n=4) were collected at each time point and cells were retrieved using Versene (Gibco). After cell dissociation, cells were washed twice with 3%BSA in 1xPBS followed by centrifugation (1500rpm, 5min, 4°C) and supernatant discard. Unspecific signal blocking was accomplished by incubation

with 3% BSA in 1xPBS for 30min on ice. Upon centrifugation (1500rpm, 5min, 4°C) and supernatant discard, samples were incubated with the conjugated antibodies diluted in 3% BSA in 1xPBS for 1h on ice in the dark. The conjugated antibodies used were: PE anti-mouse/human CD324 (BioLegend); PE anti-mouse CD44 (Miltenyi Biotec); APC anti-mouse CD29 (Miltenyi Biotec). For removal of unbinding antibody, samples were washed twice with 3% BSA in 1xPBS and fixed with 4% v/v PFA during 20min at RT. Samples were washed and resssuspended in 1xPBS before running in the flow cytometer. Data was acquired using Accuri™ C6 Flow Cytometer (BD Biosciences) and data was analyzed using FlowJo software.

## 10. Matrix metalloproteinases secretion by gelatin zymography

To analyse the presence of secreted MMPs (MMP2 and MMP9), cell culture supernatants corresponding to the previous 24h of culture of each time point were collected (n=3), centrifuged at 1200rpm for 10min in order to remove cell debris and stored at -20°C for further analysis. Protein quantification was performed using the Pierce™ BCA Protein Assay Kit (Thermo Scientific), as described in section 5, with a previous sample dilution of 1:4 in distilled water. For zymography, the preparation of 10% polyacrylamide gels containing 0.1% of gelatin as substrate (Table 4) and the electrophoresis were performed in a Mini-PROTEAN® Tetra Cell system (Bio-Rad). Samples were prepared in order to load a final volume of 15µL, containing 5µL of Tris-Sucrose SDS sample buffer and 10µL of sample diluted to yield 16µg or 32µg of total protein. Normal culture medium was used as a control. Electrophoresis was set at a constant voltage of 80V in 1xTris-Glycine SDS running buffer (Bio-Rad), for one gel, and it was stopped when the 25kDa marker of the Precison Plus Marker (Bio-Rad) runs out of the gel. Once the electrophoresis was complete, the gel was washed twice with 2% Triton X-100 for 15min on an orbital shaker to remove the SDS remnants, and incubated with MMP substrate buffer (50mM Tris-HCl, pH 7.5, 10mM $CaCl_2$) for 16h at 37°C to allow the gelatin degradation by the MMPs. For zymogram development, the gel was washed with distilled water and incubated with 0.1% w/v Coomassie Brilliant Blue solution for staining. Thereafter, the gel was washed with distilled water, scanned using the GS-800 Calibrated Densiometer (Bio-Rad) and analysed through the QuantityOne software (Bio-Rad).

**Table 4. Separating gel and Stacking gel preparation for MMPs analysis via *in gel* zymography**

| Solution | Separating gel* | Stacking gel* |
|---|---|---|
| Distilled water | 1800µL | 1020µL |
| 30% acrylamide-bisacrylamide (Bio-Rad) | 1480µL | 249µL |
| 10% SDS (Merck) | 60µL | 15µL |
| 1% gelatin (Sigma Aldrich) | 600µL | - |
| 0.5M Tris-HCl pH 6.8 | - | 189µL |
| 1.5M Tris-HCl pH 8.8 | 1500µL | - |
| 10% APS (Sigma-Aldrich) | 60µL | 15µL |
| TEMED (Sigma-Aldrich) | 2.4µL | 1.5µL |

*For preparation of 1gel

## 11. Statistical Analysis

Data are expressed as mean values of the independent experiments ± s.d., when more than one biological replica was analysed. Student's t-tests were performed to determine statistically significant differences (* $p < 0.05$).

# CHAPTER IV

# Results

The central aim of this study was the generation of a 3D *in vitro* model of EMT/MET. As a cellular model we chose the near-normal mouse mammary EpH4 cell line, previously described as a nontumorigenic cell line[163]. This cell line was isolated from spontaneously immortalized mouse mammary gland epithelial cells, which means that they have not a fully normal phenotype, however the occurrence of unknown cellular features, such as mutations, rearrangements and even loss of chromosomes that could be seen as drivers of the outcomes of this model, should be reduced. Furthermore, EpH4 was already used in other EMT studies both for stable and transient inductions[145,147,149,170–174]. In our study, a transient EMT induction was accomplished using a classical inducer, TGF-β1, and MET was established by removing this stimulus from the cell culture environment. As mentioned in Chapter II, TGF-β1 is one of the most common EMT inducers used, mainly due to the high frequency of activation of TGF-β signalling pathway in cancer[28].

This chapter details the process of establishment of a 3D *in vitro* EMT/MET model, using ECM-like hydrogels based on RGD-modified alginate, as described in chapter II. In addition, we also describe the additional studies performed on the previously established 2D *in vitro* EMT/MET model in order to complement the definition of its outcome.

## 1. Complementary studies to characterize the 2D *in vitro* model of TGF-β1-induced EMT/MET in EpH4 cell line

The 2D TGF-β1-driven EMT/MET model in EpH4 cell line (Figure 6) was previously established and validated within our research group[55]. According to this model, for EMT induction, epithelial cells were cultured for 7 days in normal culture medium supplemented with TGF-β1, which allowed cells to acquire a mesenchymal-like phenotype (2D-M7 cells). The mesenchymal nature of these cells was further confirmed by the *de novo* expression of several mesenchymal markers. As a biological control, epithelial cells were grown without TGF-β1 supplementation for 7 days (2D-E7 cells). The reverse process, MET, was achieved by culturing the 2D-M7 cells in normal culture medium, without TGF-β1 supplementation, for another 4 days (2D-TS11 cells). Cells resulting from this reversion revealed a heterogeneous phenotype that although displaying an overall reacquisition of an epithelial-like phenotype, retained differential expression of some

mesenchymal markers. This population was named TS cells as they resemble a "transient state" phenotype between epithelial and mesenchymal cells (unpublished data).

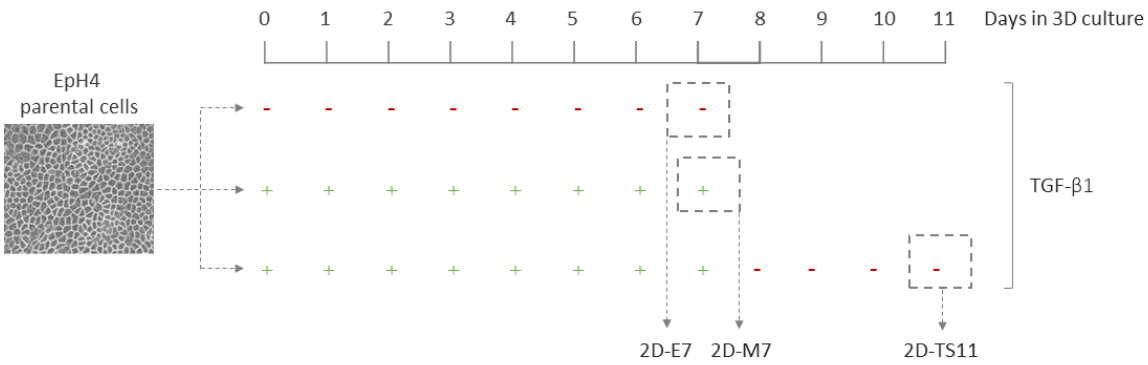


**Figure 6. Representation of the 2D *in vitro* TGF-β1-driven EMT/MET induction.** For EMT induction cells were cultured for 7 days in normal culture medium supplemented with 8 ng/mL of TGF-β1 – 2D-M7 cells. For MET induction, cells were cultured 7 days with TGF-β1 (8ng/mL) followed by 4 days without TGF-β1 supplementation – 2D-TS11 cells. Epithelial cells (2D-E7 cells), the biological control, were seeded at the same density and cultured during the same period of time as 2D-M7 cells, without TGF-β1 supplementation.

Several studies concerning expression at the RNA level of epithelial/mesenchymal markers, as well as functional assays, were previously performed by our research group, in order to characterize the 2D-E7, M7 and TS11 cells (data not shown). To further complement the characterization of the 2D *in vitro* model of EMT/MET induction, we measured the proportion of 2D-E7, 2D-M7 and 2D-TS11 cells that were positive for CD29 and CD44 markers by flow cytometry. Together these markers are able to identify cell sub-populations with stem properties, a feature known to be associated with EMT induction[72]. We observed that 2D-M7 cells were enriched in $CD29^+/CD44^+$ subpopulation in comparison to the 2D-E7 epithelial control (41.8% and 35.4% respectively, p=0.4194). Moreover, the $CD29^+/CD44^+$ subpopulation was significantly reduced in 2D-TS11 (17.4%, p=0.0246) (Figure 7A), supporting the occurrence of EMT reversion. The enrichment in $CD29^+/CD44^+$ cells in 2D-M7 appeared to be associated with the gain of a subpopulation that highly expressed CD44 (p=0.0716), which was lost in the 2D-TS11 cells (Figure 7B). Indeed, 2D-TS11 cells accumulated not only a significant decrease of $CD44^+$ cells (p=0.1152) but also a reduction of $CD29^+$ cells (p=0.429).

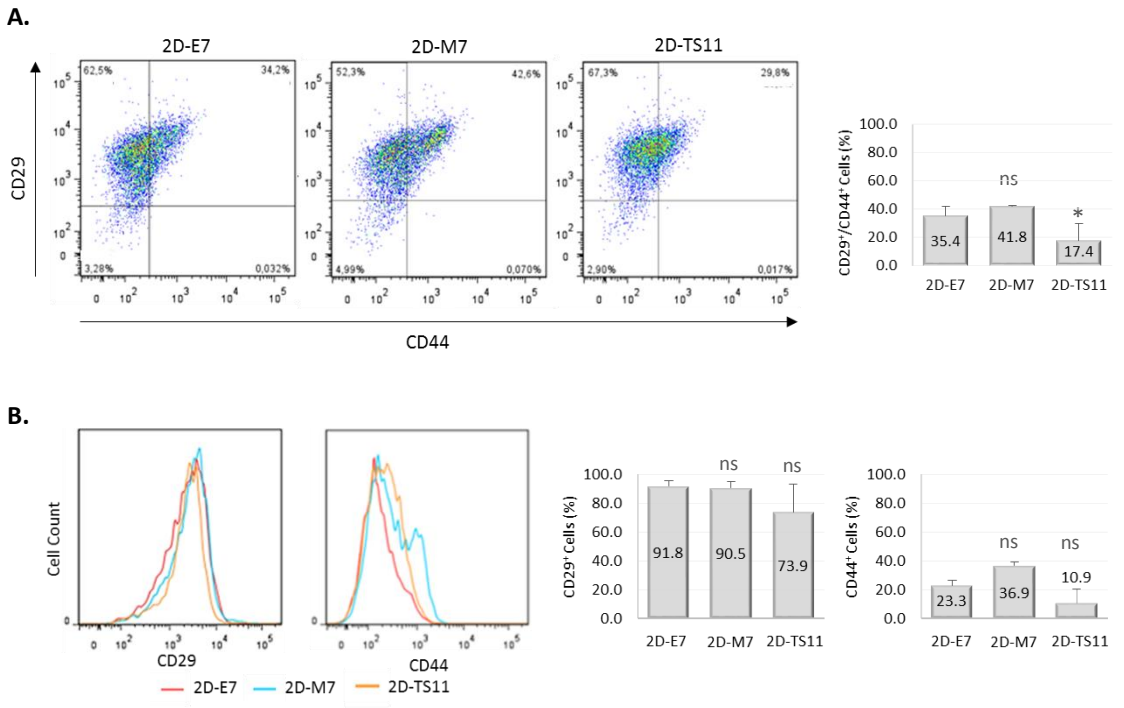


**Figure 7. CD29 and CD44 expression during EMT/MET induction in the 2D *in vitro* model.** Flow cytometry was used to determine the expression of CD29 (integrin-β1) and CD44 in EMT-derived cells (2D-M7) and MET-derived cells (2D-TS11), compared to the epithelial control (2D-E7). **A.** CD29/CD44 double-staining. **B.** CD29 and CD44 single-staining for 2D-E7 (red), 2D-M7 (blue) and 2D-TS11 (orange) populations. Results were described as mean ± standard error of two biological replicas. Single asterisk corresponded to p≤0.05 and ns corresponded to non-significant changes.

Next, we evaluated the ability of cells at different stages of the EMT/MET process to secrete MMP2 and MMP9, also known as gelatinase A and B, respectively. The results showed an increase of MMP9 expression in 2D-M7 (1.75-fold) compared to the epithelial control (2D-E7) (Figure 8). Furthermore, in 2D-TS11 cells, the basal levels of MMP9 were almost fully recovered (1.13-fold), in agreement with reversion to an epithelial-like phenotype. Regarding MMP2 expression, no significant variations were recorded, however it was possible to identify a slight increase both in 2D-M7 and 2D-TS11 cells. Together these results indicated that expression of MMP9 but not MMP2, was induced during EMT in this 2D model.

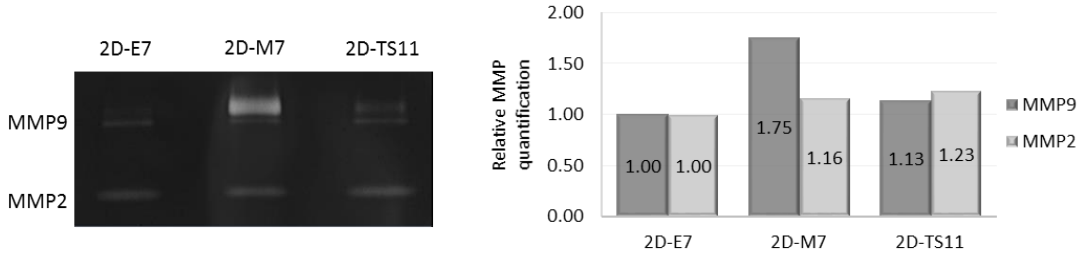


**Figure 8. Effect of EMT/MET induction on MMP2 and MMP9 secretion.** Relative quantification was performed to basal level expressed by epithelial cells (2D-E7). 32ug of total protein were loaded for each sample. (n=1 biological replica)

# 2. Establishment of a 3D in vitro model of TGF-β1-induced EMT/MET in EpH4 cell line using ECM-like hydrogels

The 3D model reported on this document derived from the 2D *in vitro* model previously established, as it makes use of the same cell type – EpH4 cell line – and the same method for transient EMT/MET induction, TGF-β1 supplementation to the culture medium. In order to build a well-defined 3D system, RGD-modified alginate hydrogels were used as an artificial ECM-like matrix for 3D *in vitro* culture[108].

## 2.1 Definition of the 3D *in vitro* culture conditions

In order to determine the best culture conditions to study the EMT/MET process, EpH4 cells were cultured for 14 days in normal culture media (3D-E14) within RGD-modified alginate hydrogels with different concentrations (1 and 2 wt-%) and at different cell densities ($5x10^6$ and $10x10^6$ cells/mL).

We assessed the viability of EpH4 cells in the 3D environment through a live/dead staining and we observed that the majority of cells was viable in all conditions tested (Figure 9). The best scenario, i.e diminished presence of dead cells, was found when cells were cultured in the 1 wt-% RGD-alginate hydrogels (Figure 9A and 9B). Additionally, it was observed that when cells were seeded at a density of $5x10^6$ cells/mL in 1 wt-% RGD-alginate hydrogels, larger sized spheroids were detected in comparison with the corresponding higher density condition (Figure 9A and 9B). Moreover, in the 1 wt-% RGD-alginate hydrogels, cells cultured in a density of $10x10^6$ cells/mL (Figure 9B) formed what seems to be a monolayer in the surface of the hydrogel in addition to the matrix-embedded spheroids. In accordance with these results, 1 wt-% RGD-alginate hydrogels and cell density of $5x10^6$ cells/mL was the best option for culturing EpH4 cells in a 3D *in vitro* environment, enabling the formation of large spheroids with very high cell viability. Therefore, we chose these conditions to perform the subsequent tests.

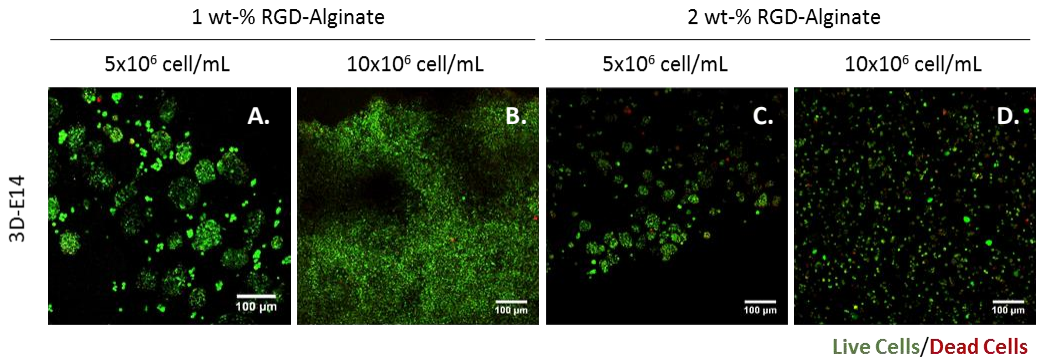


**Figure 9. Effect of the 3D *in vitro* environment on cell viability using the Cytrak Orange™/DRAQ7™ live/dead staining.** Immunofluorescence of 3D-E14 cells cultured in 1 wt-% RGD alginate hydrogels **(A, B)** and in 2 wt-% RGD alginate hydrogels **(C, D)** with a cell density of $5x10^6$ cells/mL **(A, C)** or $10x10^6$ cells/mL **(B, D)**. Live cells were shown in green and dead cells in red. The scale bar corresponded to 100µm.

## 2.2 Characterization of the EpH4 cell line behaviour in the RGD-alginate hydrogel model

To better understand the EMT induced phenotype it was important to assess whether EpH4 cells maintained an epithelial behaviour in the selected 3D culture system. For that purpose, EpH4 cells at a cell density of $5x10^6$ cells/mL, were cultured in the 1 wt-% RGD-alginate hydrogels with normal culture medium and monitored for 21 days both at RNA and protein level. Additional studies regarding the metabolic activity and spheroid morphology were also performed.

The measurement of the metabolic activity (resazurin-based method) showed that the overall metabolic activity of cells in each hydrogel disk increased with time reaching a 2.62-fold increase at day 21 (3D-E21 cells in comparison with 3D-E3 cells, Figure 10A). Regarding spheroid morphology, although there was a decrease in spheroid number (Figure 10B), an increase in spheroid area was observed (Figure 10C).

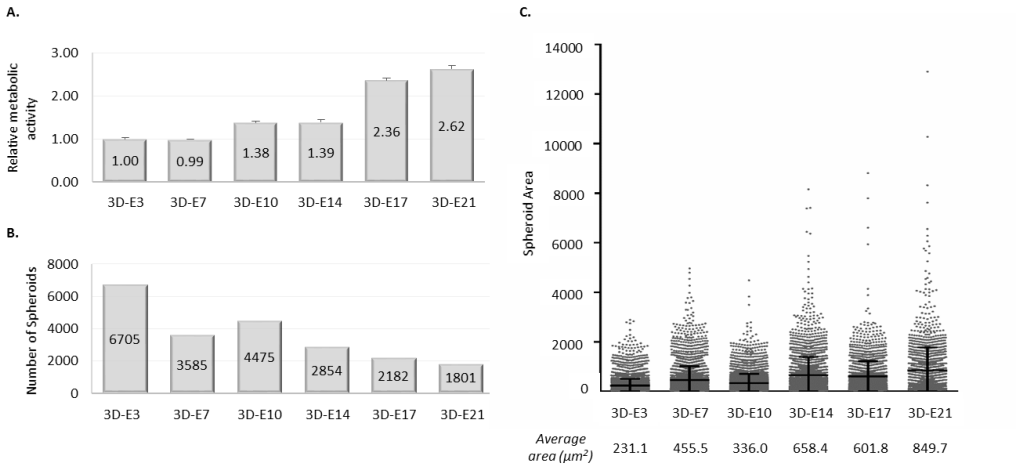


**Figure 10. Morphological and metabolic characterization of EpH4 spheroids in the 1wt-% RGD-alginate hydrogels. A.** Metabolic activity of cells embedded within the hydrogels (n=3 independent hydrogel disks in each time-point). **B.** Number of spheroids and **C.** Spheroid area measured in the best confocal plan and plans immediately above and below, using the same acquisition and segmentation strategy in all disks (n=1 hydrogel disk in each time-point). Data was normalized for 3D-E3 in each assay.

Epithelial and mesenchymal markers, respectively E-cadherin and α-SMA, were assessed during the 3D culture in order to characterize phenotypic changes at protein level. We observed E-cadherin staining at the cell membrane in 3D-E7 cells, while little or no expression was detected in 3D-E3 cells (Figure 11A and 11D). E-cadherin staining at the cell membrane was also detected in all other time-points analysed, from 3D-E10 to 3D-E21 (Figure 11G, 11J, 11M and 11P). Regarding the α-SMA staining, no expression was detected both in 3D-E3 and 3D-E7 cells (Figure 11B and 11E). Nevertheless, in 3D-E10, 3D-E14, 3D-E17 and 3D-E21 cells, expression of this marker was detected (Figure 11H, 11K, 11N and 11Q). Interestingly, we noticed that when E-cadherin and α-SMA co-localized in the same spheroid, the area in which α-SMA is expressed displayed a weaker, and in some cases cytoplasmic E-cadherin staining, suggesting functional impairment (Figure 11L, 11O and 11R).

To complement these studies, we addressed the secretion of MMPs by EpH4 cells across time. However, no changes both in MMP9 and MMP2 expression were observed (Figure 12).

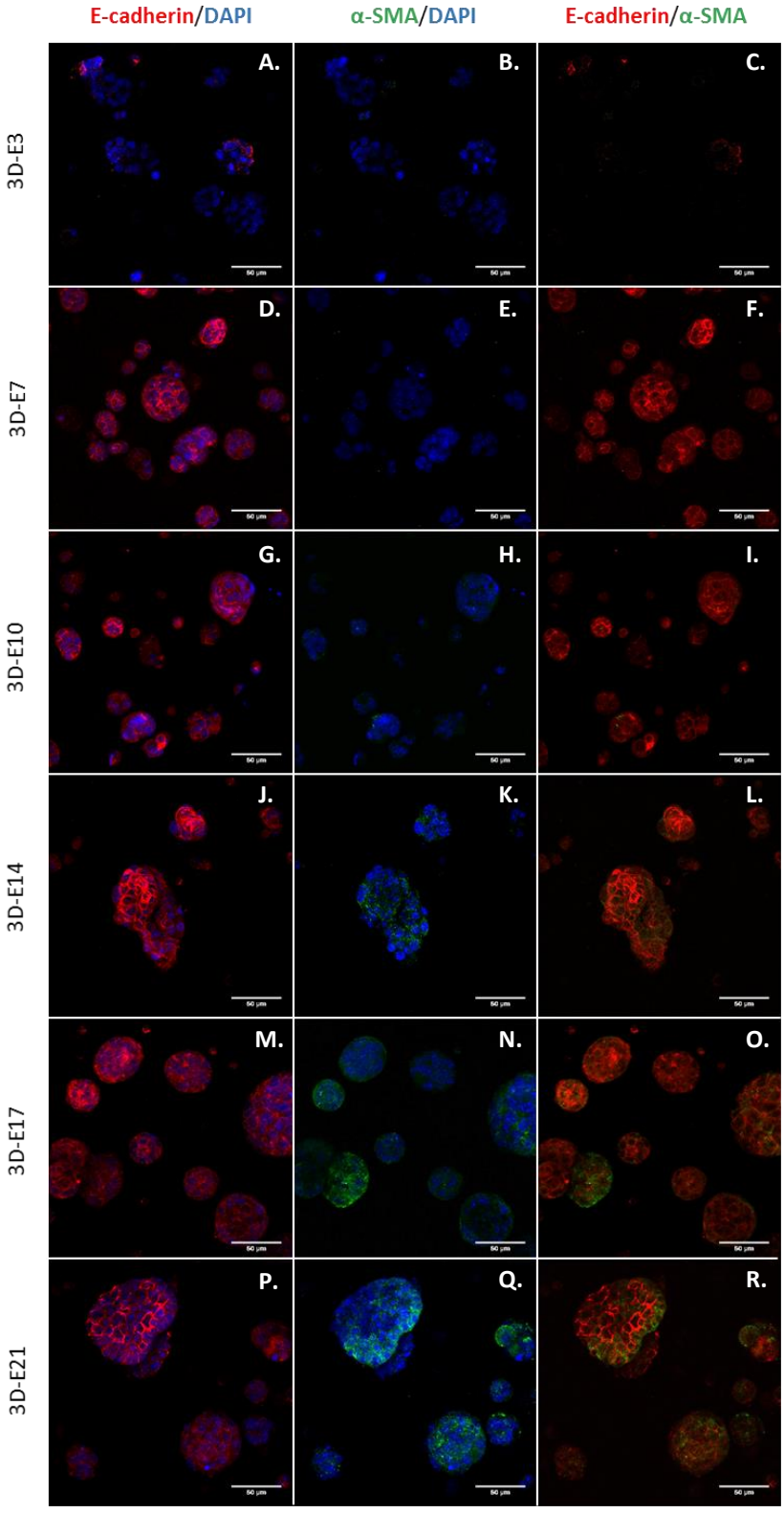


**Figure 11. Assessment of the expression of epithelial and mesenchymal markers in 3D epithelial cultures.** Co-immunofluorescence for E-cadherin (red) and α-SMA (green) in 3D-E3 cells **(A-C)**, 3D-E7 cells **(D-F)**, 3D-E10 cells **(G-I)**, 3D-E14 cells **(J-L)**, 3D-E17 cells **(M-O)** and 3D-E3 cells **(P-R)**. Merged images illustrated the presence of E-cadherin at the membrane since day 7 in culture **(F, I, L, O, R)** and the gain of α-SMA expression after 14 days in culture **(L, O, R)**. The scale bar corresponds to 50µm.

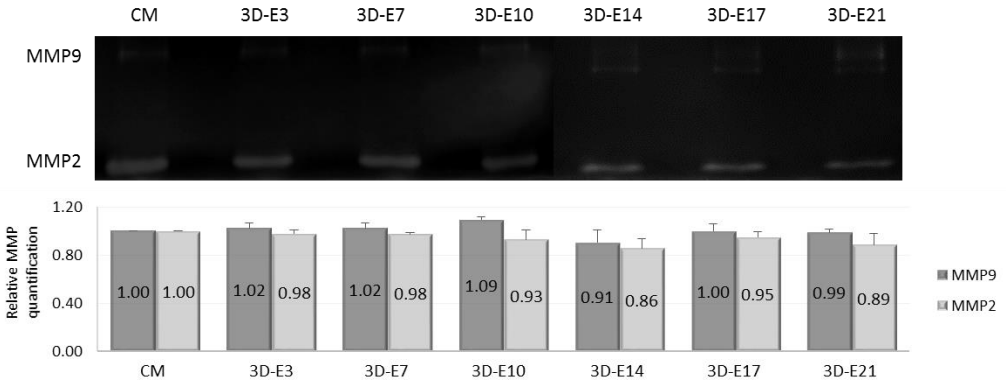


**Figure 12. MMP secretion profile of EpH4 cells cultured in the 3D *in vitro* system.** MMP2 and MMP9 secretion. Relative quantification was performed to normal culture medium (CM). 16ug of total protein were loaded for each sample (n=2 biological replicas).

Next, we analysed the RNA extracted from the cell populations obtained across time (Figure 13), in order to assess transcriptional modifications that occurred in EpH4 3D-E cells. Given that very few cells were obtained at day 3 (3D-E3), no markers were assessed for this time-point. For all subsequent comparisons, expression levels of 3D-E7 cells were used for normalization purposes. We observed that E-cadherin coding gene, *CDH1*, was slightly upregulated in 3D-E10 cells, with a 1.3-fold increase in comparison with 3D-E7 cells, the first time-point assessed in which we also had observed E-cadherin staining at the cell membrane. However, in 3D-E17 and 3D-E21 cells, *CDH1* was found to be strongly downregulated, with a 0.4 and 0.1-fold decrease in comparison with 3D-E7 cells, respectively (Figure 11). For the epithelial marker *Ocln* (Occludin), we observed a marked increased expression in 3D-E10 cells, both in comparison with 3D-E7 and 3D-E14. Due to technical problems, *Ocln* expression could not be assessed in 3D-E17 and 3D-E21 cells. For the mesenchymal marker, *CDH2* (N-cadherin), a wave-like expression pattern was detected: we observed an increased expression (1.6-fold) in 3D-E10 cells, which was later abrogated in 3D-E14 cells (0.9-fold). Afterwards, *CDH2* expression was again increased in 3D-E17 cells (2.3-fold) and later abolished in 3D-E21 (0.7-fold). In turn, the mesenchymal marker *Vim* (Vimentin), presented a slightly different pattern since no variations were found until day 14 (3D-E14 cells); still, in 3D-E17 cells a peak in the expression of this marker was detected (4.1-fold) but such expression was reduced in 3D-E21 cells (1.9-fold). We further complemented this analysis by assessing the expression of genes that encode for two transcriptional factors involved in the EMT induction, *ZEB2* and *Twist1*[175]. We observed that *ZEB2* was downregulated in 3D-E14 cells (0.5-fold) and upregulated in 3D-E17 (2.3-fold), being this increased expression abolished in 3D-E21 cells (0.5-fold) in a perfect correlation with the results obtained for both mesenchymal markers assessed. We did not find any significant variations concerning *Twist1* expression.

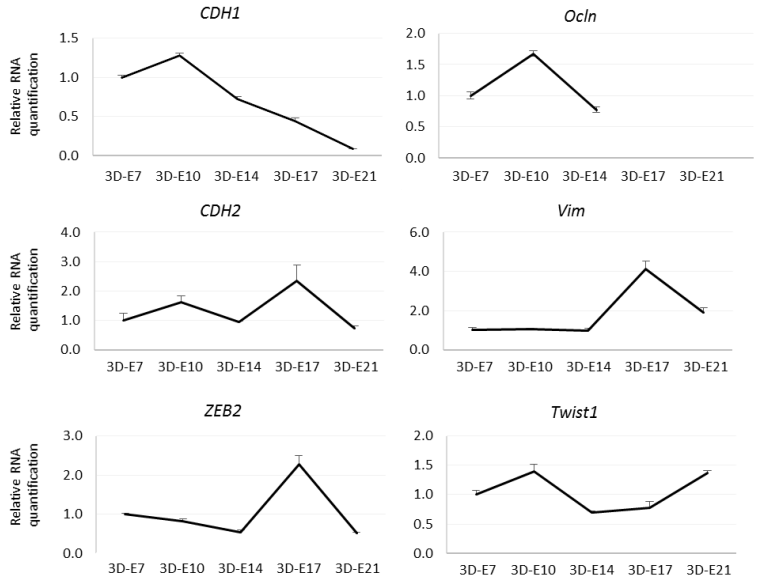


**Figure 13. RNA signature of EpH4 cells cultured in the 3D *in vitro* system.** n=1, and 3 technical replicates used for each measurement. Data was normalized to 3D-E7. Due to technical problems, *Ocln* expression could not be assessed in 3D-E17 and 3D-E21 cells.

Overall, these results showed that EpH4 cells displayed a stable epithelial phenotype until day 14 (3D-E14). In addition, we observed that longer periods of 3D culture of these cells could induce changes in the expression of epithelial and mesenchymal markers, both at RNA and protein levels.

## 2.3 Characterization of EMT induction in EpH4 cells cultured in the RGD-alginate hydrogel model

For EMT induction, we cultured EpH4 cells at $5x10^6$ cells/mL in a 1wt-% RGD-alginate hydrogels in the presence of TGF-β1 (16 ng/mL) during 3, 7, 10 and 14 days, thus generating 3D-M3, 3D-M7, 3D-M10 and 3D-M14 cell populations and assessed several cellular features (Figure 14).

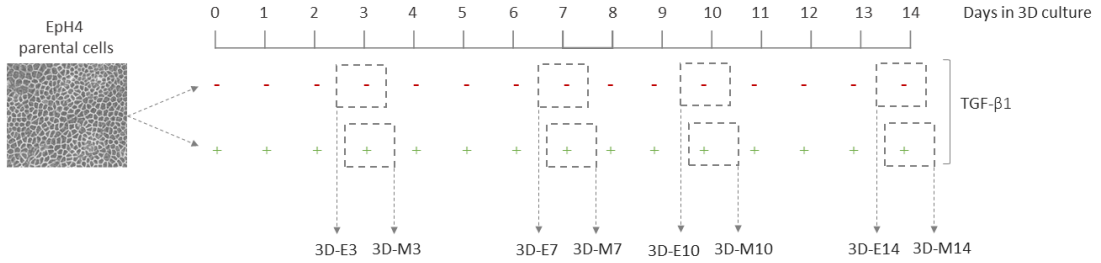


**Figure 14. Representation of the 3D *in vitro* TGF-β1-driven EMT.** For EMT induction, EpH4 parental cells (2D) were cultured for up to 14 days with TGF-β1 supplementation. Cells were harvested at day 3 (3D-M3 cells), day 7 (3D-M7 cells), day 10 (3D-M10 cells) and day 14 (3D-M14 cells) to assess EMT associated features. Epithelial cells (3D-E3, 3D-E7, 3D-E10 and 3D-E14) were cultured in the same conditions, without TGF-β1 supplementation.

Firstly, we measured the metabolic activity of each cell population and observed that it was consistently decreased during the period of culture analysed (Figure 15A and 15B). In fact, the metabolic activity decreased approximately 30% in 3D-M10 and 3D-M14 cells, in comparison to 3D-M3 cells (Figure 15B). As we compared the metabolic rates of 3D-M cells with the corresponding 3D-E cells, we observed that in the initial phase of culture the metabolic rate was very similar for both cell types, as seen for day 3 and day 7 (3D-M3 vs. 3D-E3; 3D-M7 vs. 3D-E7). However, for longer periods of TGF-β1 treatment, the difference in metabolic activity between 3D-M and 3D-E cells started to be noticeable. In fact, both 3D-M10 and 3D-M14 cells displayed a massive decrease in metabolic rate when compared with the respective biological controls, 3D-E10 and 3D-E14 cells (0.4-fold decrease, Figure 15C).

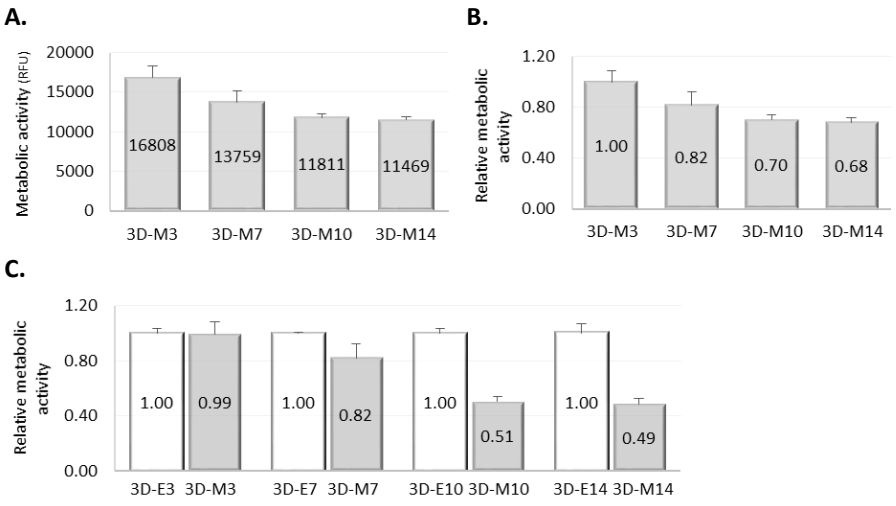


**Figure 15. Metabolic activity during EMT induction. A-B.** EpH4 cells cultured in the 3D *in vitro* system in normal culture medium supplemented with TGF-β1 (16 ng/mL). **(A)** Raw values of metabolic activity in relative fluorescence units (RFU) **(B)** Data normalized to 3D-M3 cells. **C.** Comparison between epithelial and mesenchymal cultures. Data normalized to correspondent epithelial control cells. n=1, technical triplicates for independent hydrogel disks in each time-point.

To evaluate the EMT phenotype during the time of induction – at protein level – we assessed the expression of E-cadherin and α-SMA by co-immunostaining, and MMPs secretion. Concerning E-cadherin, we observed an overall decreased membrane staining, however never was complete loss of expression protein observed in any of the analysed days. In fact, 3D-M3 and 3D-M7 cells (Figure 16A and 16D) revealed a weaker expression of this epithelial marker, which was detected in the cytoplasm of cells rather than in the cell membrane, suggesting functional impairment. This cytoplasmic delocalization of E-cadherin was also observed in 3D-M10 (Figure 16G) and 3D-M14 (Figure 16J), although with increased expression levels when compared to 3D-M3 and 3D-M7 cells. In addition, 3D-M14 displayed increased presence of E-cadherin at cell membrane. Regarding the mesenchymal marker α-SMA, its expression was

detected in all samples analysed: while in 3D-M3 cells the expression detected was weak (Figure 16B), it became stronger in 3D-M7, 3D-M10 and 3D-M14 cells (Figure 16E, 16H and 16K). Concerning MMPs, both MMP9 and MMP2 secretion was not altered during this experiment and the only variations found indicated a slight increase of MMP2 secretion (Figure 17A). When comparing these results with the MMP secretion by the corresponding 3D-E cells, no relevant differences were observed and the only trend found was a small increase in MMP2 secretion across all 3D-M cells (Figure 17B).

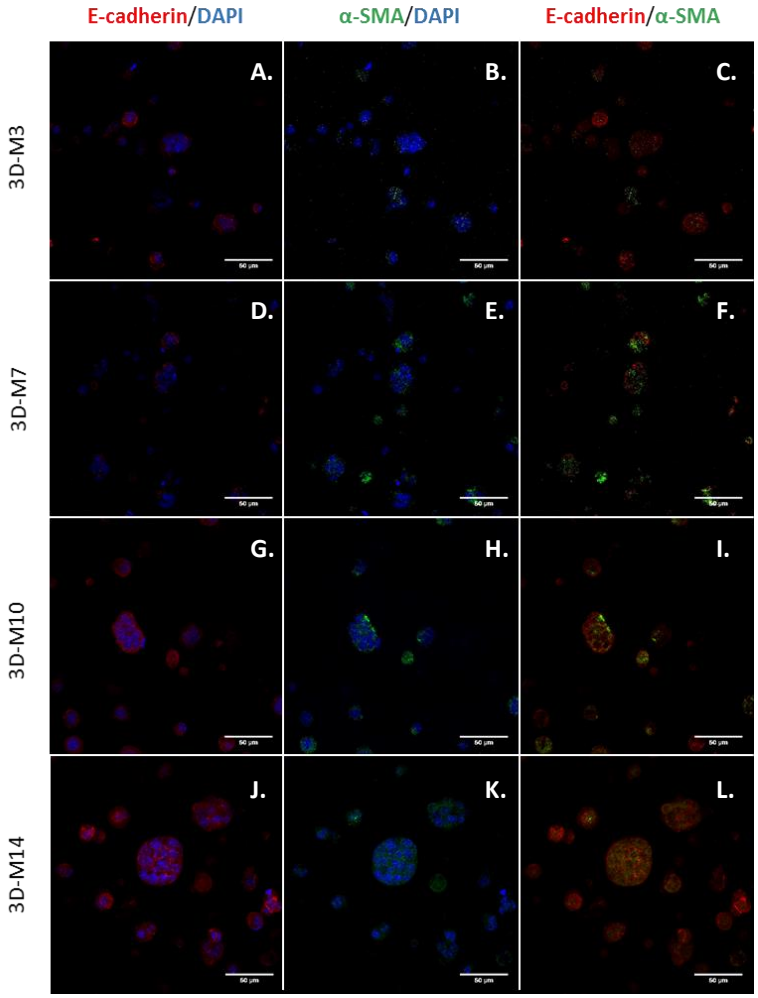


**Figure 16. Assessment of the expression of epithelial and mesenchymal markers in 3D mesenchymal cultures.** Co-immunofluorescence for E-cadherin (red) and α-SMA (green) in 3D-M3 cells **(A-C)**, 3D-M7 cells **(D-F)**, 3D-M10 cells **(G-I)** and 3D-M14 cells **(J-L)**. Merged images illustrate the presence and localization of E-cadherin and α-SMA during the 14 days of culture. The scale bar corresponds to 50µm.

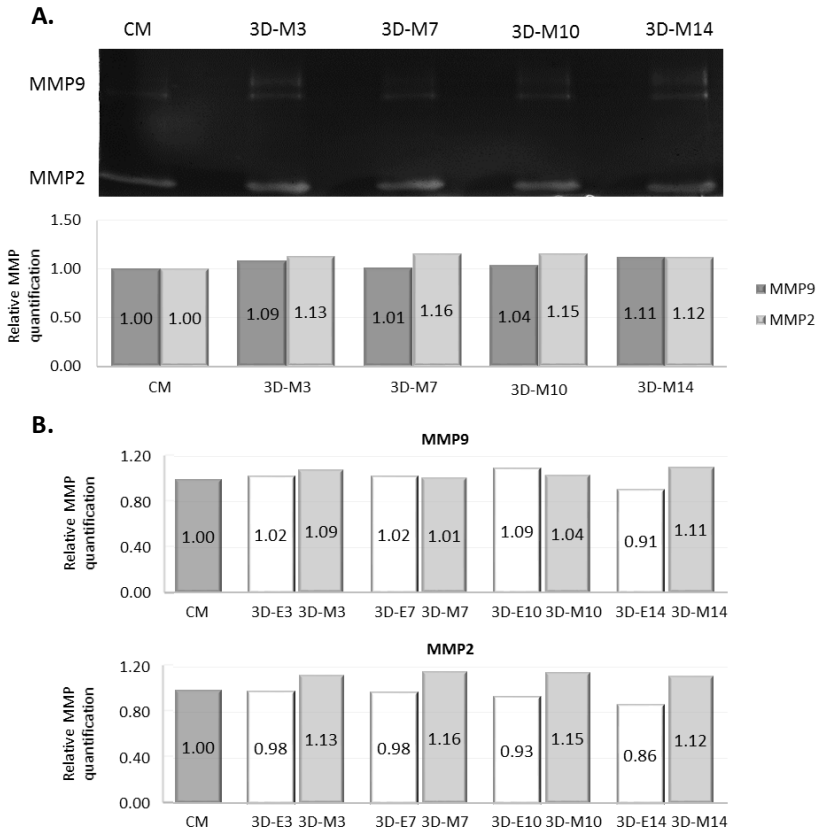


**Figure 17. MMP secretion profile of EpH4 cells cultured in the 3D *in vitro* system in normal culture medium supplemented with TGF-β1. A.** MMP2 and MMP9 secretion. Relative quantification was performed to normal culture medium (CM). 32ug of total protein were loaded for each sample. **B.** Comparison of MMP secretion in epithelial and mesenchymal cultures. Data was normalized to the normal culture medium run in each experiment. n=1 biological replica

The abovementioned changes were further explored by quantification of the RNA expression of the same epithelial and mesenchymal markers, as well as *ZEB2* and *Twist1* (Figure 18). No information could be collected concerning 3D-M3 cells due to lack of biological material. Concerning *CDH1* expression, we observed that all 3D-M cell populations displayed increased levels of this epithelial marker than the equivalent 3D-E cells. When focusing only in the 3D-M populations (normalized to the corresponding 3D-E cells), we observed that 3D-M10 cells displayed the highest levels of *CDH1* (8.09-fold in comparison with 3D-E10 cells). Concerning *Ocln*, the lowest levels of expression were detected in 3D-M10 cells (0.48-fold in comparison to 3D-E10 cells). However this downregulation may be an artefact due to the previously detected increase in *Ocln* expression in 3D-E10 cells. Regarding *CDH2*, *Vim* and *Zeb2*, all 3D-M cells revealed a consistent increased expression in comparison with the corresponding 3D-E cells, in agreement with acquisition of mesenchymal properties (ranging from 1.86 to 9.52-fold). Concerning *Twist1*, only 3D-M7 cells displayed increased expression of *Twist1* comparing with the respective 3D-E7 cells (1.51-fold). For both 3D-M10 and 3D-M14, *Twist1* expression was below or at the same levels as observed in 3D-E10 and 3D-E14, respectively (0.46 and 1.06-fold).

Similarly to *Ocln*, 3D-E10 cells displayed an increased expression of *Twist1* in comparison with 3D-E7 cells (1.40-fold), hampering the observations made for *Twist1* expression in 3D-M10.

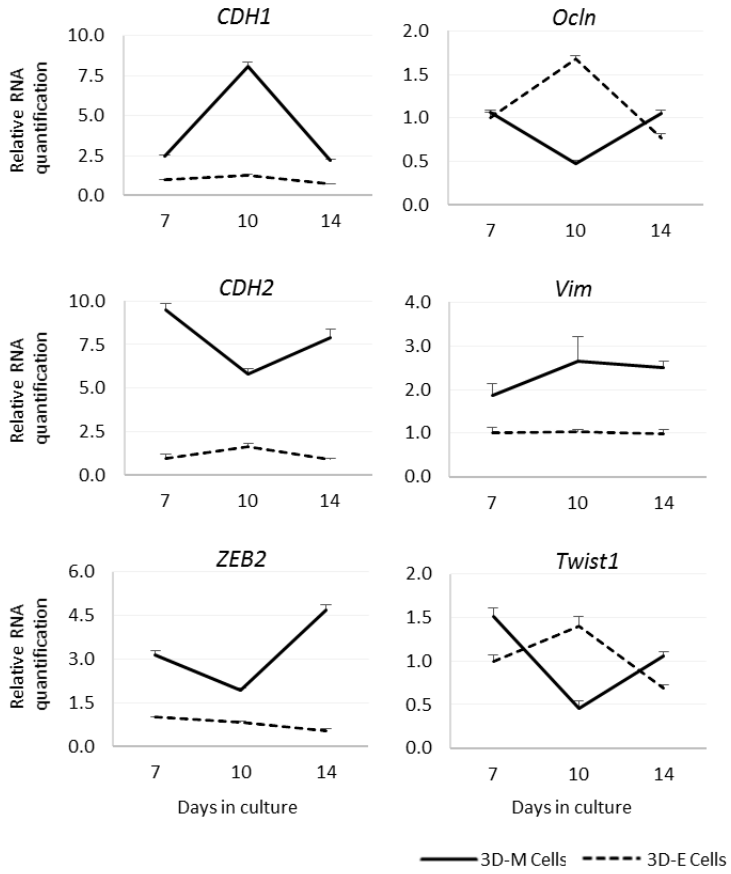


**Figure 18. RNA signature of 3D-M cells and comparison to epithelial RNA profile.** N=3 replicates were used for each measurement. Data for 3D-M cells was normalized to the corresponding 3D-E cells (3D-M7 vs. 3D-E7, 3D-M10 vs. 3D-E10, 3D-M14 vs. 3D-E14). Data for 3D-E cells was normalized to 3D-E7 cells.

Altogether, these findings suggested that both 3D-M7 and 3D-M14 cells already display a mesenchymal-like phenotype. However, while 3D-M7 cells displayed E-cadherin functional impairment, as suggested by its cytoplasmic localization, in 3D-M14 cells, E-cadherin was present at cell membrane. Moreover, *CDH2*, *Vim* and *ZEB2* expression was enhanced in 3D-M7 and 3D-M14 as was α-SMA expression, all of which hallmarks of mesenchymal/EMT cells. Despite these similarities, we selected 3D-M7 cells as the end-point of our 3D EMT induction, due to the observed differential E-cadherin cellular localization.

## 2.4 Characterization of MET induction in EpH4 cells cultured in the RGD-alginate hydrogel model

As previously mentioned, when MET was induced in the 2D *in vitro* model developed by our research group, a "transient-state" population was obtained, with simultaneous expression of epithelial and mesenchymal markers and an overall epithelial-like. In order to assess the behaviour of the same cell line in the 3D *in vitro* model upon MET induction, EpH4 3D-M7 cells (7 days with TGF-β1) were further cultured without TGF-β1 supplementation. Metabolic activity, MMPs secretion, E-cadherin/α-SMA co-immunostaining and RNA expression of epithelial and mesenchymal markers was assessed in two time-points: 3 and 7 days post-TGF-β1 removal from the culture system (3D-TS10 and 3D-TS14, respectively, Figure 19).

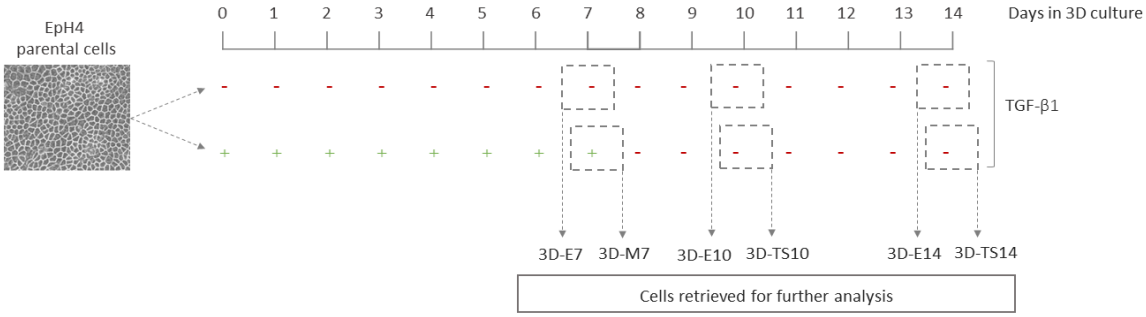


**Figure 19. Representation of the 3D *in vitro* TGF-β1-driven EMT/MET induction.** For MET induction, 3D-M7 cells were cultured for up to 7 days without TGF-β1 supplementation. Cells were harvested at day 10 (3 days post-TGF-β1 removal, 3D-TS10 cells) and day 14 (7 days post-TGF-β1 removal, 3D-TS14 cells) to assess MET associated features. Epithelial cells (3D-E7, 3D-E10 and 3D-E14) were cultured in the same conditions, without TGF-β1 supplementation.

Firstly, we measured the number and size of spheroids and we found that 3D-M7 (EMT-induced cells) disks presented higher number of spheroids (Figure 20A), although with smaller size (Figure 20B), compared to the epithelial control 3D-E7 (1678 spheroids with average size of 349.2μm$^2$ vs. 1285 spheroids with average size of 645.6μm$^2$, respectively). A similar scenario also occurred when comparing 3D-TS10 with 3D-E10 (1656 spheroids with average size of 473.4μm$^2$ vs. 1422 spheroids with average size of 856.5μm$^2$). Interestingly, 3D-M7 spheroids (size and number) were similar to those observed in 3D-TS10 cells. We also observed that despite a similar average size, 3D-TS14 cells displayed a diminished spheroid number than both 3D-M7 and 3D-TS10 cells (1058 spheroids vs. 1678 and 1656 spheroids, respectively). These results suggest that MET might be inducing a change on spheroid growth, potentially by increasing proliferation. To address this question we measured the metabolic rate of these cells and observed that all 3D-E cells (3D-E7, 3D-E10 and 3D-E14) exhibited higher levels of metabolic activity than the corresponding 3D-M/TS cells (Figure 20C). While 3D-M7 cells displayed a 50%

decrease in metabolic rate in comparison with 3D-E7 cells, both 3D-TS10 and 3D-TS14 seemed to recover their metabolic activity to levels closer to those registered for their counterparts (0.59-fold for 3D-TS10 and 0.73-fold for 3D-TS14, Figure 20C). These observations also support that MET might be inducing cell proliferation or at least a metabolic change in 3D-TS10 and 3D-TS14 cells.

Given that the number of cells in each hydrogel disk might significantly impact the metabolic activity measured, we decided to normalize the abovementioned values to the total protein content (Figure 20D). This rationale assumed that protein content was directly proportional to the total cell number. In fact, the measured protein content increased steadily from 3D-M7 up to 3D-TS14, as did the respective epithelial controls (Figure 20D). Upon normalization, we observed that, unlike all the previous results, there was a decrease in normalized metabolic activity in both 3D-E10 and 3D-E14 cells in comparison to 3D-E7 cells (Figure 20E). Moreover, 3D-TS10 cells were more active in terms of normalized metabolic rate, than the corresponding 3D-E10 cells (2.70-fold increase in 3D-TS10 cells, Figure 20E). Finally, 3D-TS14 cells displayed a similar normalized metabolic activity comparing with 3D-E14 cells (0.86-fold decrease in 3D-TS14, Figure 20E).

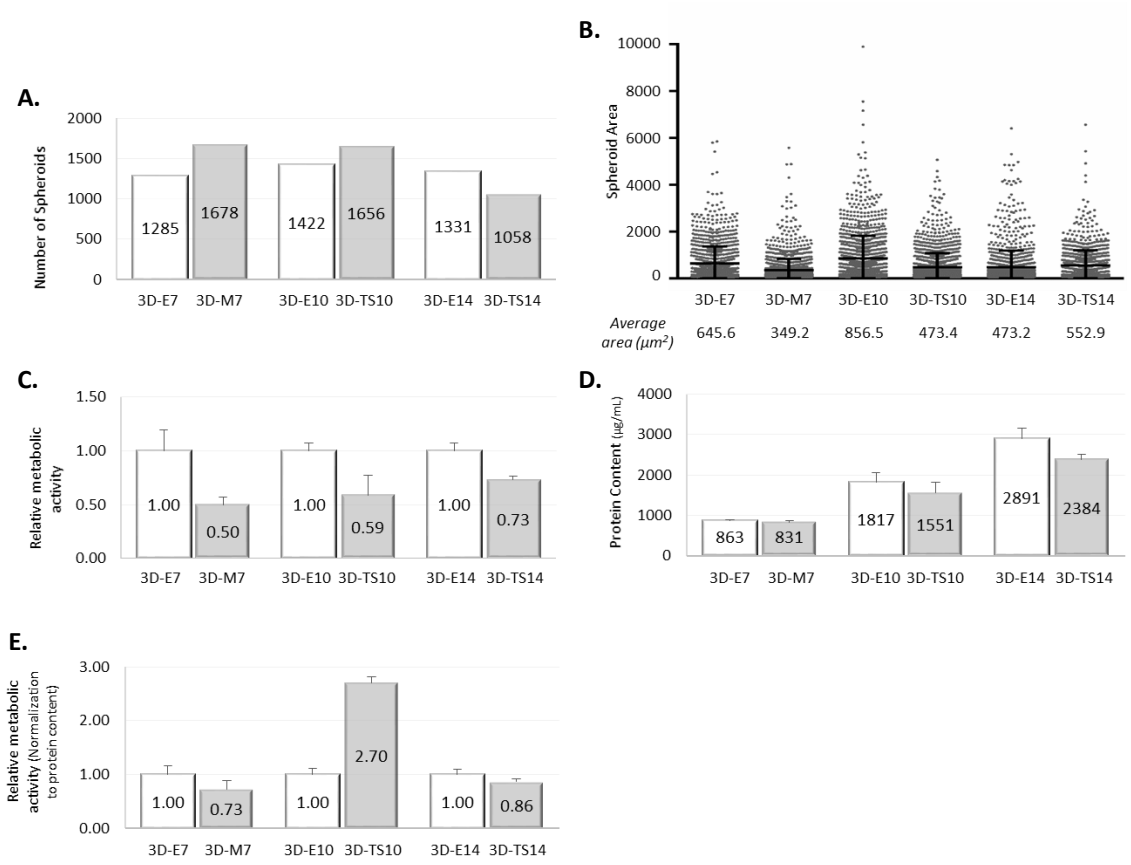


**Figure 20. Morphological and metabolic characterization of EMT/MET populations obtained in the 3D *in vitro* system. A.** Number of spheroids and **B.** Spheroid area measured in the best confocal plan and plans immediately above and below, using the same acquisition and segmentation strategy in all disks (n=1 hydrogel disk in each time-point). **C.** Metabolic activity of cells embedded within the hydrogels. Data normalized to correspondent epithelial control cells. **D.** Cellular protein content of different cell types (μg/mL). **E.** Metabolic activity of cells embedded within the hydrogels normalized with protein content. Data normalized to correspondent epithelial control cells. n=1, technical triplicates for independent hydrogel disks in each time-point.

The evaluation of MMP secretion revealed that 3D-TS10 and 3D-TS14 cells tend to secrete higher amounts of MMP9 in comparison to 3D-M7 (Figure 21A). Furthermore, 3D-TS14 cells also secreted more MMP2 than both 3D-TS10 and 3D-M7 cells. When comparing to the corresponding 3D-E cells, we observed that 3D-TS14 cells secreted higher levels of MMP9 and MMP2, while 3D-TS10 cells only showed this increased secretion for MMP9 (Figure 21B).

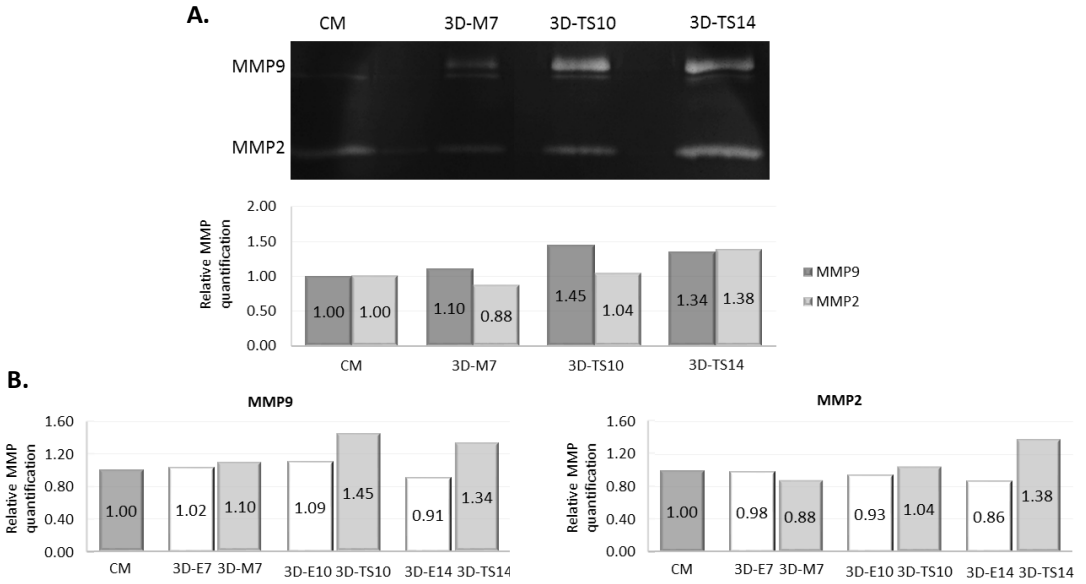


**Figure 21. MMP secretion profile during EMT/MET in EpH4 cells cultured in the 3D *in vitro* system. A.** MMP2 and MMP9 secretion. Relative quantification was performed to normal culture medium (CM). 32ug of total protein were loaded for each sample (n=1 biological replica). **B.** Comparison of MMP secretion during EMT/MET induction and in epithelial cultures. Data was normalized to the normal culture medium run in each experiment.

By immunostaining, we assessed the presence of E-cadherin and observed that this marker was strongly expressed at the cell membrane in 3D-E7, 3D-E10 and 3D-E14 (Figure 22A, 22G, 22M), as described in previous experiments. Again, 3D-M7 cells expressed low levels of E-cadherin which was mainly localized at the cytoplasm of the cells (Figure 22D). In 3D-TS10 and 3D-TS14 it was possible to observe an increase in E-cadherin expression, particularly in 3D-TS14 cells. Indeed, in 3D-TS10 cells E-cadherin seems to be mostly localized in the cytoplasm (Figure 22J), while in 3D-TS14 cells we observed a heterogeneous pattern, since in some spheroids E-cadherin was localized in membrane and in others in the cytoplasm (Figure 22P). Regarding the α-SMA marker, almost no expression was detected in 3D-E7 cells (Figure 22B), however in 3D-E10 and 3D-E14 samples some spheroids were found to exhibit expression of this marker (Figure 22H and 22N). We also observed expression of α-SMA in 3D-M7, 3D-TS10 and 3D-TS14 spheroids (Figure 22E, 22K and 22Q), although this expression seemed to be decreased in 3D-TS10 cells.

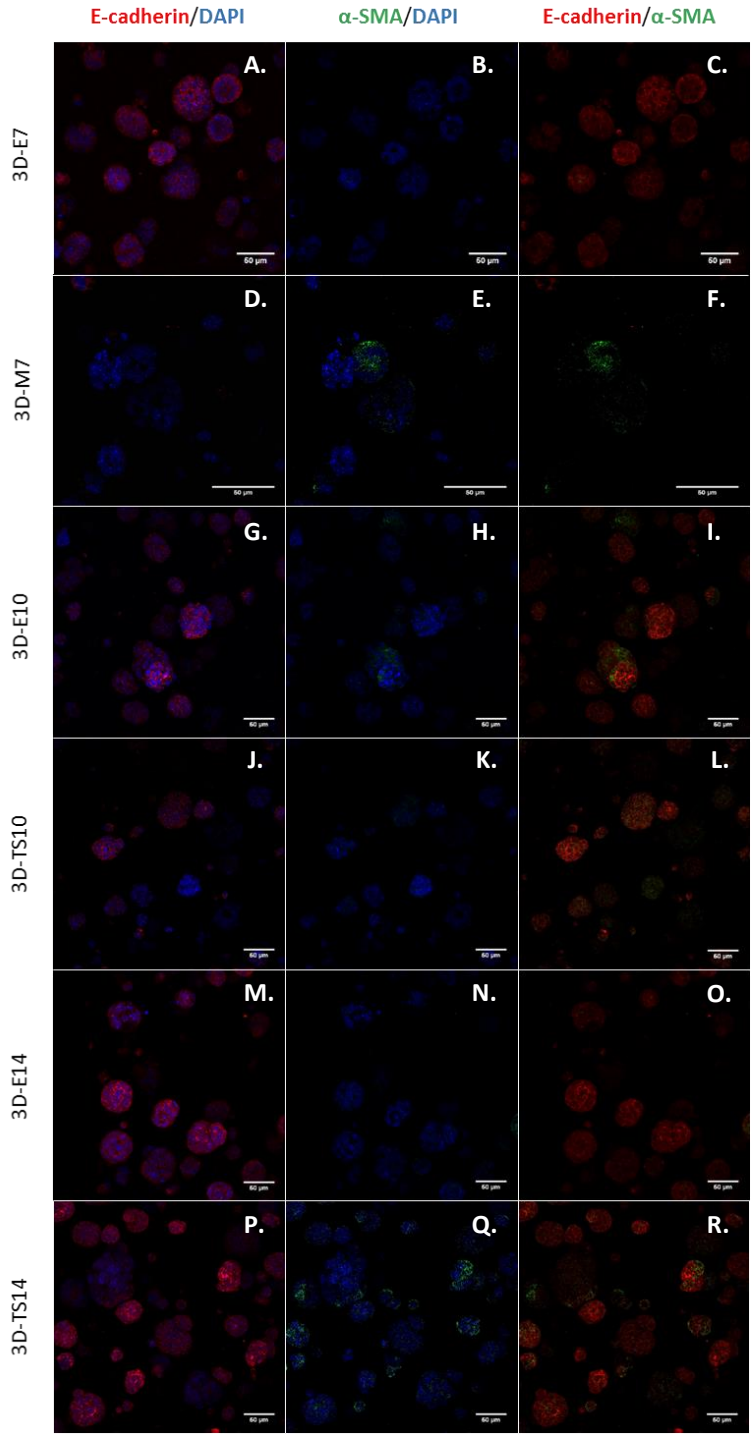


**Figure 22. Assessment of the expression of epithelial and mesenchymal markers during EMT/MET induction in EpH4 cells cultured in the 3D *in vitro* system.** Co-immunofluorescence for E-cadherin (red) and α-SMA (green) in 3D-E7 cells **(A-C)**, 3D-M7 cells **(D-F)**, 3D-E10 cells **(G-I)**, 3D-TS10 cells **(J-L)**, 3D-E14 cells **(M-O)** and 3D-TS14 cells **(P-R)**. The scale bar corresponds to 50µm.

Additionally, we measured the presence of CD29 and CD44 in the membrane of these cells by flow cytometry. We observed a decrease in the $CD29^{+}/CD44^{+}$ subpopulation in 3D-TS10 and 3D-TS14 cells both comparing with 3D-M7 cells and the epithelial counterparts (Figure 23A). In addition, 3D-TS14 cells displayed a smaller $CD29^{+}/CD44^{+}$ subpopulation than 3D-TS10 cells

(17.8% vs. 30.4%), similarly to their epithelial counterparts (23.9% for 3D-E14 and 44.6% for 3D-E10). Interestingly, the difference between 3D-TS14 and 3D-E14 (6.1% decrease in 3D-TS14 cells) was less than half of the difference between 3D-TS10 and 3D-E10 (14.2% decrease in 3D-TS10 cells). These results pinpointed the pair 3D-TS14/3D-E14 cells as more similar than 3D-TS10/3D-E10 cells. Considering the 3D-E10/3D-TS10 counterparts, the decrease of the $CD29^+/CD44^+$ population was due to the decrease of $CD44^+$ cells whereas in 3D-E14/3D-TS14 cells, the reduction of the double positive population was due to a concomitant decrease of both $CD29^+$ and $CD44^+$ cells (Figure 23B). No relevant changes were reported for 3D-M7 comparing to 3D-E7. Moreover, we analysed the percentage of E-cadherin positive cells in these populations and verified that the presence of E-cadherin at the cell membrane was reduced in 3D-M7, 3D-TS10 and 3D-TS14 cells comparing to 3D-E7, 3D-E10 and 3D-E14, respectively (Figure 23B). Notwithstanding, the percentage of positive E-cadherin cells was low in all samples analysed, even in 3D-E7, 3D-E10 and 3D-E14 epithelial cells (ranging from 17.8% to 43.2% of E-cadherin membrane-positive cells).

We further investigated RNA expression of the markers used in the aforementioned experiments. In addition, we analysed the expression of *Mgat3*, *ID2* and *ID3* given they have been associated with MET induction in the 2D *in vitro* EpH4 model. *Mgat3* has been shown to be downregulated with EMT and upregulated with MET (similarly to an epithelial marker[55]) while both *ID2* and *ID3* were upregulated in EpH4 2D-MET (unpublished work by our research group). We started by comparing the RNA expression levels of all epithelial and mesenchymal markers in 3D-TS10 and 3D-TS14 cells against 3D-M7 cells, to understand the TGF-β1 removal effect (MET induction, Figure 24). We observed that *CDH1* expression was slightly diminished in 3D-TS10 cells and exhibited a trend for upregulation in 3D-TS14 cells (0.85 and 1.31-fold respectively). Concerning *Ocln*, its expression levels were increased only in 3D-TS14 cells (1.06 and 1.26-fold increase respectively). *CDH2* and *Vim* were found to be downregulated in 3D-TS14 (0.62 and 0.37-fold); in fact, *Vim* was already decreased in 3D-TS10 cells (0.56-fold). *ZEB2* was downregulated both in 3D-TS10 and 3D-T14 comparing to 3D-M7 cells, displaying a higher decrease in the 3D-TS10 cells (0.38 and 0.74-fold). In contrast, *Twist1* expression did not change in 3D-TS10 and increased in 3D-TS14 cells (1.02 and 1.72-fold). *Mgat3* exhibited a pattern similar to *ZEB2*, being downregulated in 3D-TS10 cells but recovering, in 3D-TS14 cells to the same expression level detected in 3D-M7 cells (0.26 and 0.97-fold). Finally, *ID2* and *ID3* showed a parallel upregulation in 3D-TS14 cells (1.48 and 1.19-fold), however in 3D-TS10 the behaviour of these markers was different, with *ID2* being upregulated and *ID3* downregulated (1.97 and 0.84-fold).

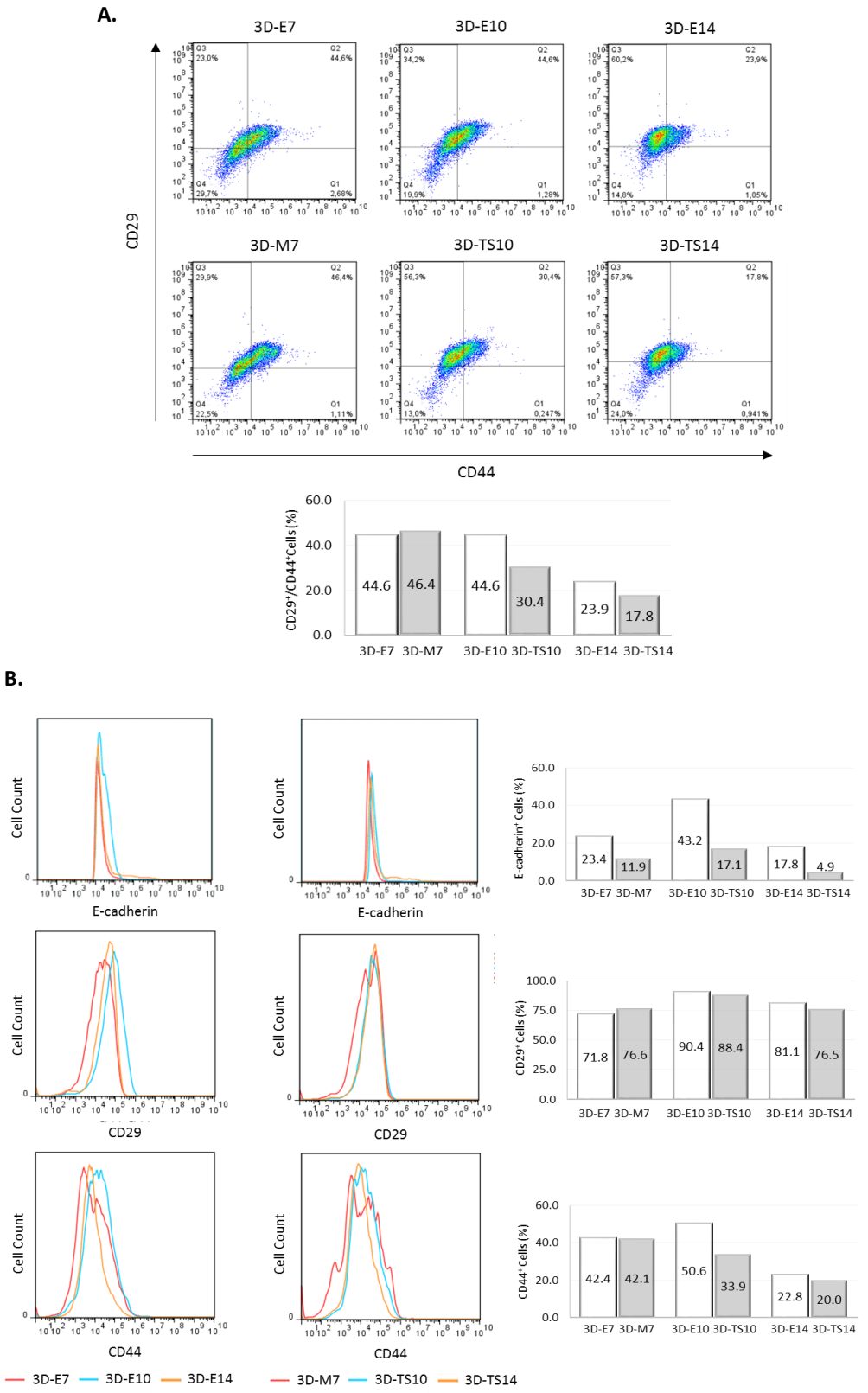


**Figure 23. E-cadherin, CD29 and CD44 expression during EMT/MET induction in the 3D *in vitro* system.** Flow cytometry was used to determine the expression of E-cadherin, CD29 (integrin-β1) and CD44 in EMT-derived cells (3D-M7) and MET-derived cells (3D-TS10 and 3D-TS14), compared to the epithelial controls (3D-E7, 3D-E10 and 3D-E14). **A.** CD29/CD44 double-staining. **B.** E-cadherin, CD29 and CD44 single-staining for 3D-E7 (red), 3D-M7 (blue) and 2D-TS11 (orange) populations. n=1, four independent technical replicates for each time-point.

Summarizing, 3D-TS10 cells were characterized by a strong downregulation of *Vim*, *ZEB2* and *Mgat3* and an increase of *ID2*. On the other hand, 3D-TS14 cells were characterized by a decreased expression of *CDH2* and *Vim*, concomitantly with an increase of *Twist1*. For this characterization we considered that a gene upregulated for RNA expression increase over 1.5-fold, and downregulated for a decrease below 0.66-fold.

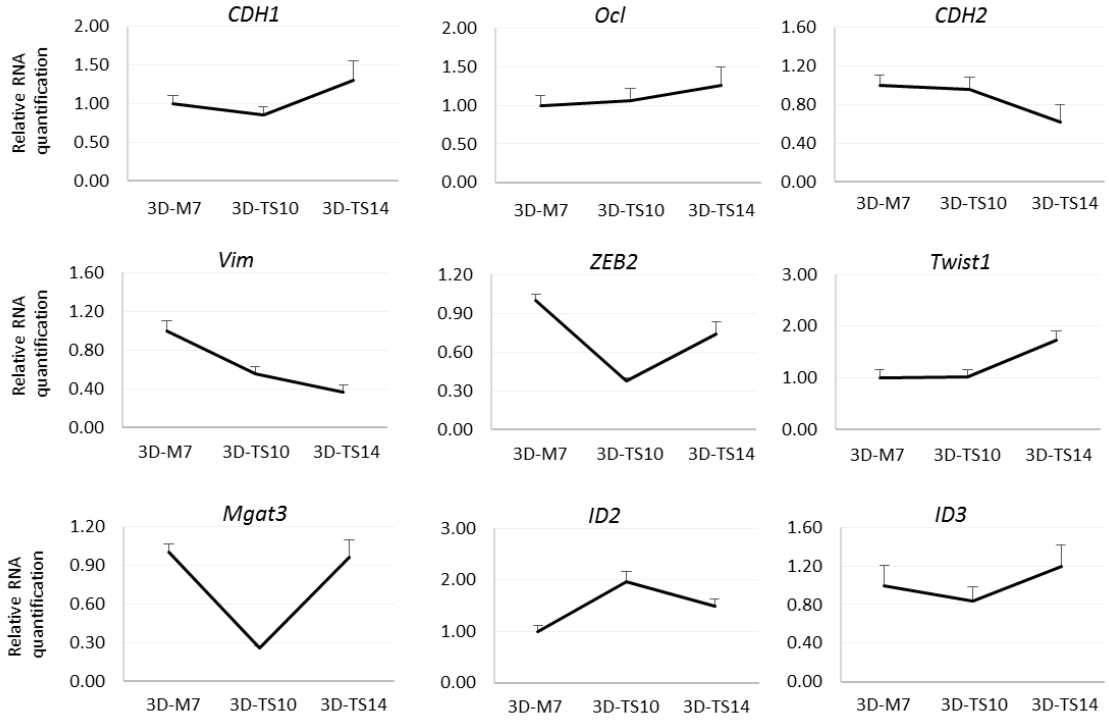


**Figure 24. RNA signature of cells undergoing EMT/MET in the 3D *in vitro* system.** N=3 replicates were used for each measurement. Data was normalized to 3D-M7 cells.

Finally, to understand how similar 3D-TS10 and 3D-TS14 cells were to epithelial cells, thus unveiling the reversibility of our 3D-EMT/MET model, we compared the RNA expression levels of all epithelial and mesenchymal markers in 3D-TS10 and 3D-TS14 cells against 3D-E7 cells, (Figure 25). Concerning *CDH1* and *Ocln*, 3D-M7, 3D-TS10 and 3D-TS14 cells displayed increased expression in comparison with 3D-E7 cells, however only 3D-TS14 cells showed a relevant upregulation of *CDH1* (1.57-fold). For 3D-M7 cells we observed an upregulation of all mesenchymal markers assessed (*CDH2*, *Vim*, *ZEB2* and *Twist1*, ranging from 1.23 to 7.38-fold), later on abrogated (*Vim* and *ZEB2*, 4.11 and 1.45-fold) or stabilized (*CDH2* and *Twist1*, 2.57 and 1.25-fold) in 3D-TS10 cells. Concerning *Mgat3*, *ID2* and *ID3*, 3D-M7 cells showed an overall downregulation (0.38, 0.43 and 0.67-fold). In 3D-TS10 cells, both *Mgat3* and *ID3* continued to decrease (0.10 and 0.56-fold) while *ID2* expression recovered to levels closer to 3D-E7 cells (0.85-fold). In 3D-TS14 cells, *Mgat3* and *ID3* expression increased to levels equal or above those

registered in 3D-M7 cells (0.37 and 0.80-fold), however *ID2* expression decreased (0.64-fold) although still at levels above 3D-M7 cells.

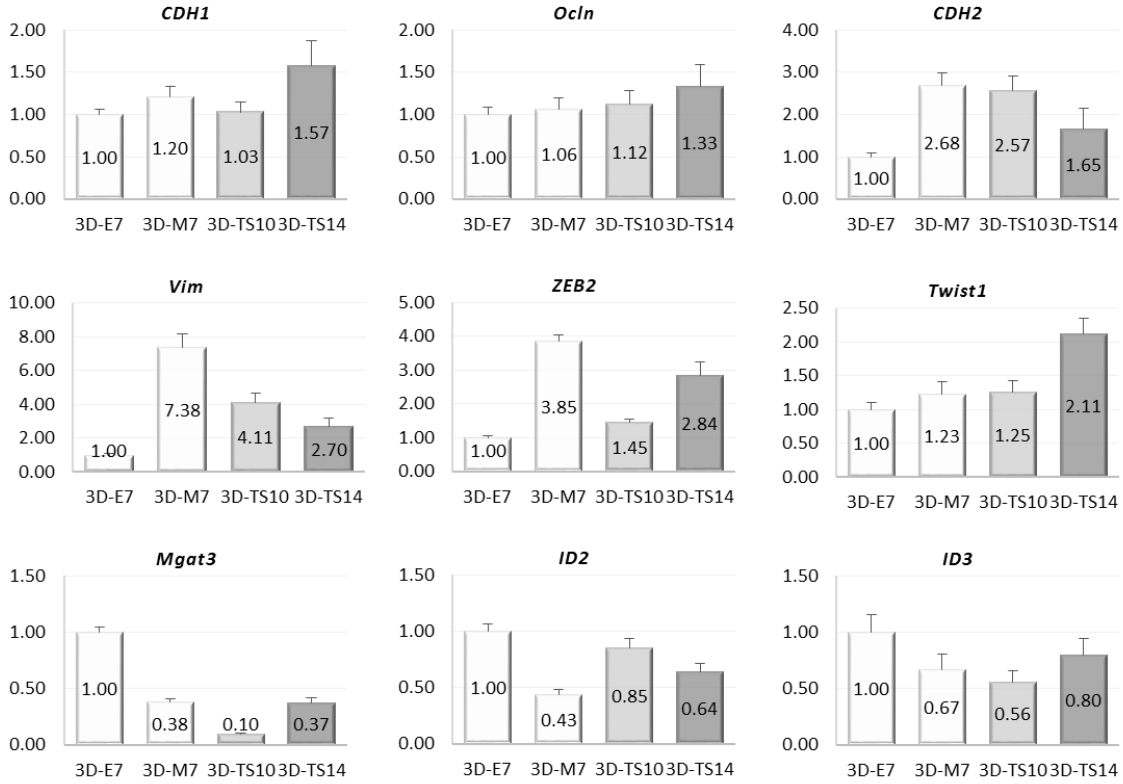


**Figure 25. RNA signature of cells undergoing EMT/MET in the 3D *in vitro* system.** N=3 replicates were used for each measurement. Data was normalized to 3D-E7 cells.

Overall, these results suggested that a partial MET was obtained in 3D-TS10/3D-TS14 cells. In both cell types, upregulation of MET-associated genes *ID2* and *ID3*, residual to low expression of α-SMA and decreased presence of $CD29^{+}/CD44^{+}$ cell subpopulation were observed, in comparison to 3D-M7 cells. However, 3D-TS10 cells despite showing an upregulation of *CDH1*, E-cadherin cytoplasmic staining suggested E-cadherin function impairment. Concerning 3D-TS14 cells, *Vim* was downregulated and a heterogeneous E-cadherin staining was observed, with expression detected both at cell membrane and in the cytoplasm, suggesting a partial recovery of E-cadherin function. Therefore, our findings suggest that EMT reversion was stronger in 3D-TS14 cells than in 3D-TS10 cells.

# CHAPTER V

# Discussion

The occurrence of the EMT/MET phenomenon in cancer progression and metastasis development remains rather controversial among the scientific and medical communities, despite of the snowball of evidences that have been reported linking the EMT/MET events to the depicted situations, both *in vitro* and *in vivo*. All the studies that have been performed to address this issue have revealed important information about fundamental mechanisms underlying the EMT/MET programs. However, a gap between their outcomes and the pathological *in vivo* situation unveiled the need for novel models that would better resemble clinical scenarios, in a fine balance of environmental simplicity and complexity.

In this Master Thesis, we focused on the establishment of a 3D model of EMT/MET *in vitro*. Such model could be further developed in order to generate data concerning novel EMT/MET-related targets with relevance in clinics. To establish our 3D *in vitro* EMT/MET model, we made use of a near-normal mouse mammary epithelial cell line (EpH4) that was previously used to establish a 2D *in vitro* EMT/MET model induced by TGF-β1 in our research group. Here, we also used TGF-β1 as trigger for the EMT induction in our 3D model since it has been extensively reported as a major inducer of EMT in *in vitro* and *in vivo* studies, but also due to its relevance in the clinical situation, as described in chapter II of this Thesis. TGF-β1 mediates diverse cellular responses, from amongst which cell proliferation suppression[176], disruption of cell-cell junctions[177] and cytoskeleton rearrangements[178]. To yield a 3D environment for this model, we have resorted to an alginate-based hydrogel covalently modified with the adhesion peptide RGD. Alginate polysaccharides are obtained from brown seaweed, therefore gathering important features of naturally derived-materials, such as biocompatibility and low toxicity. In addition, alginate lacks some of the most problematic characteristics of such materials – high variability and unknown composition – since commercially available alginates are nowadays well-defined and of ultra-pure grade. In fact, ultra-pure alginate are submitted to strict purification processes in order to remove heavy metals, endotoxins, proteins and polyphenolic compounds that are often present in the raw materials[179]. Alginate provides an ideal blank slate polymer to study specific cellular interactions with peptide ligands, such as the one studied in this project, once its hydrophilic nature impairs protein adsorption therefore hindering unspecific interactions with mammalian cells[165]. To simultaneously counteract this non-adhesive property of the material and regulate cell-substrate interaction, alginate was modified with RGD, a peptide derived from fibronectin

that is recognized by many integrins, such as $\alpha_5\beta_1$, $\alpha_8\beta_1$, $\alpha IIb\beta_3$, $\alpha V\beta_3$, $\alpha V\beta_5$, $\alpha V\beta_6$ and $\alpha V\beta_8$[180]. The concentration of this peptide is an important factor to be considered and it highly depends on the cell type used. Since no reports were found addressing the use of RGD in 3D systems for EpH4 cells, we adopted a final 200μM concentration of RGD that was used in studies previously performed in the group, although for other types of cells[108]. Preliminary studies of EpH4 cell culture in 200μM RGD-alginate hydrogels showed high cell survival and metabolic activity (data not shown), therefore we assumed this concentration for the following experiments. RGD-modified alginate was ionic crosslinked via calcium ions allowing the formation of hydrogels under mild and cytocompatible conditions. This process is reversible, allowing easy cell recovery in the presence of a calcium chelator. These features are especially relevant allowing the development of 3D embedded cultures and enabling cell retrieval after the experiment. Multiple studies have proved that cells cultured within 3D matrices form different integrin complexes when compared to 2D cultures[154], rapidly remodelling their microenvironment and depositing their own ECM molecules[93]. These modifications may trigger important consequences regarding cell adhesion and decision-making that can be translated, for instance, into a higher resistance to drugs and radiation better mimicking, for example, solid tumours and tumour nodules[154,179]. Matrix mechanics is one of the most relevant features of 3D systems as it modulates cell responses in different ways[181], albeit it is dynamically changed accordingly to cell density and time of culture-dependent matrix deposition[182]. In the particular case of hydrogels, stiffness modifications may also affect oxygen and nutrient permeability, as well as binding sites availability and water content[183]. Therefore, we investigated the possibility of using 1 and 2 wt-% alginate matrices (G'≈500 and 3500Pa, respectively) and cell densities of $5x10^6$ and $10x10^6$ cells/mL for our 3D EMT/MET model and evaluated EpH4 cellular responses to these culture conditions after 14 days in culture. The obtained results (Figure 9) demonstrated the impact of matrix stiffness in spheroid formation and cell viability through the different extents of spheroid size and live/dead cells that were observed. In accordance with such results, the softer matrix with lower cell density – 1 wt-% alginate matrix with $5x10^6$ cells/mL – allowed the formation of much larger spheroids in which almost all cells were viable. These results correlate with other studies that showed that in softer matrices of MMP-degradable PEG, significantly larger spheres could be obtained through a persistent cellular growth during the first 8 days of culture[118]. It is worth noting that, in our study, seeding a higher cell density in soft matrices resulted in cell escape to the periphery of the hydrogel and production of spheroids with smaller size. These evidences may reveal that a higher cell density can induce spatial limitation or that cell proliferation led to disk outgrowth. An important complement to this study would be the measurement of the stiffness of these matrices upon cell culture in each condition. Thus we

would be able to understand the effect of EpH4 cells in the matrix and not only the reverse influence. Additionally, this study could be of use to compare the ability of epithelial cells, EMT-derived cells, and MET-derived cells to modulate the surrounding microenvironment. The stiffness of the cells themselves, is also an important factor and indeed it was already correlated with the occurrence of EMT, when Wu and colleagues demonstrated that cells that underwent TGF-β1-induced EMT have higher compressive and tensile stiffness as well as increased adhesion force[184]. Therefore similar studies should also be performed in our different cell types.

Making use of the 1 wt-% alginate matrix with $5x10^6$ cells/mL we addressed another important issue, which is the definition of the TGF-β1 concentration needed for EMT implementation. Throughout the different studies in which EMT was induced, different concentrations of TGF-β1 have been used accordingly to the cell type, culture system (2D vs 3D) and period of induction. The only model reported in the literature in which EMT was induced in EpH4 cells was the previously 2D model established in our group, for which 8 ng/mL of TGF-β1 were used to induce EMT during 7 days of culture[55]. Other groups were able to establish a stable and irreversible EMT model by transforming EpH4 cell line with oncogenic H-Ras (EpRas), and supplementing their culture with 8 ng/mL of TGF-β1 during 24 hours[145] or 5 ng/mL during 72hours[172]; in another study, TGF-β1 supplementation (2.5 ng/mL) was complemented with 4-hydroxytamoxifen for Raf activation and EMT was analysed upon 6 days of treatment[173]. We attempted to induce EMT in the 3D system using 8 ng/mL of TGF-β1 as previously done in the 2D system, however even upon 14 days in culture – with the supplemented culture medium being renewed every 2-3 days – we could not observe a consistent EMT phenotype (Figure 26D-26F). Most likely, the 3D environment and proportion of cells for the available amount of TGF-β1 conditioned its activity, which explains why we were only able to observe minimal expression of Fibronectin and no delocalization of E-cadherin (Figure 26D-26F). By doubling the concentration of TGF-β1, we overcame that limitation which was demonstrated through the production of higher amounts of Fibronectin and lower expression of E-cadherin (Figure 26G-26I).

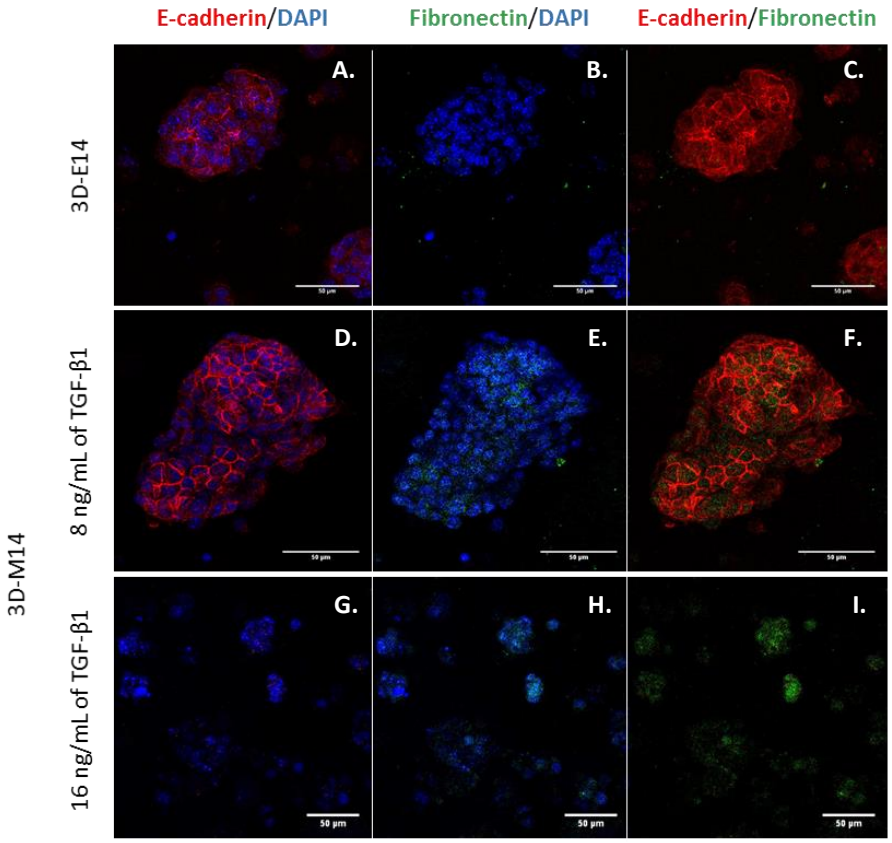


**Figure 26. Evaluation of the TGF-β1 potential to induce EMT in the 3D *in vitro* system.** Co-immunofluorescence for E-cadherin (red) and Fibronectin (green) in 3D-E14 cells **(A-C)** and 3D-M14 obtained with 8ng/mL **(D-F)** or 16ng/mL **(G-I)** of TGF-β1. Merged images **(C, F, I)** illustrate the loss of E-cadherin at cell membrane and the expression of *de novo*-Fibronectin in 3D-M14 cells derived from the exposure to 16 ng/mL of TGF-β1. The scale bar corresponds to 50µm.

Interestingly, we found that both in the presence and absence of TGF-β1, EpH4 cells tend to form spheroids with different 3D architecture and in some cases they form lumenized structures (Figure 27)[91]. In fact, EpH4 cells had already prove their ability to form acini-like[185] and branched organ-like structures[186] in Matrigel and 3D collagen gel, respectively. Further studies are needed in order to characterize the functionality and organization of the lumenized structures obtained in our model, thus enabling the comparison with the acini-like structures derived from other natural matrices[185,186]. The possibility of studying these structures in a more controllable and defined, yet biologically relevant system, such as ours, may be translated into important insights in normal breast development and ultimately breast cancer progression.

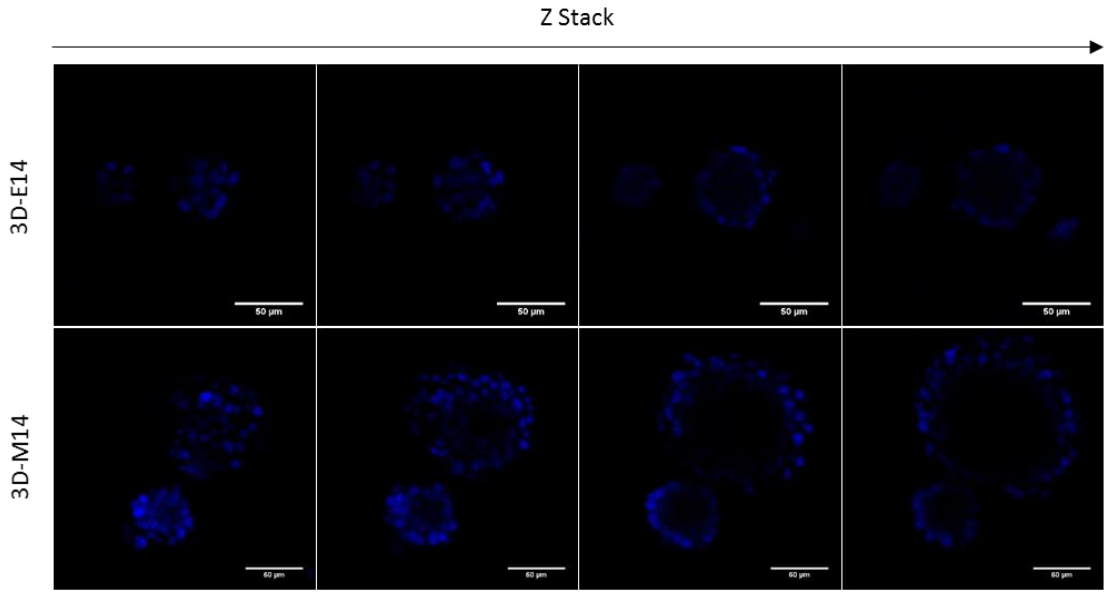


**Figure 27. Architecture of the lumenized spheroids found both in the 3D epithelial and EMT-derived cultures.** Representation of structures found at day 14, 3D-E14 and 3D-M14, at different Z Stacks. The size of the structures is not representative from each culture. Cell nuclei is stained with DAPI (blue). The scale bar corresponds to 50µm.

In order to optimize and further validate the TGF-β1-driven EMT model, we characterized the cellular behaviour of both epithelial and mesenchymal cultures in the 3D matrix. We observed a stable epithelial phenotype during the first 14 days of culture, and the establishment of EMT after 7 days of culture (3D-M7), characterized by E-cadherin delocalization to the cytoplasm (Figure 16 and Figure 23B), upregulation of *CDH2*, *Vim*, *ZEB2* and *Twist1* (Figure 18). Interestingly, 3D-M14 cells displayed similar features, although their metabolic activity was much lower (Figure 15). We measured the metabolic activity using the classic resazurin assay, in which this redox dye is reduced within the mitochondria by accepting the electrons resulting from the normal mitochondrial enzymatic activity[187]. Therefore, the observed decrease may be due to a metabolic shift that was also found in the 2D *in vitro* model (unpublished data). In fact, 2D-M7 cells displayed protein expression downregulation of several oxidative phosphorylation components with a concomitant increased level of lactate production. Given that resazurin was already proved to be a reliable method for identification of mitochondrial functional defects[188], we believe that the metabolic shift observed in the 2D EMT model may also be occurring in our 3D model. The observed decrease of metabolic activity may also be due to other features, such as reduced cell growth, which has already been associated with TGF-β1 treatment[25]. To elucidate the basis of this metabolic decrease, further studies should be performed, for instance, measurement of lactate production and glycose consumption together with the determination of growth rates in the 3D cultures.

Another function of TGF-β1 is the modulation of the balance of MMPs and their inhibitors, mainly the tissue inhibitors of MMPs (TIMPs) and the membrane-associated MMP inhibitor (RECK), thus modulating the cell motility and invasion[29,189]. Enhanced MMP activity has been correlated with cell migration and invasion of carcinoma cells, and it has been reported in a wide range of carcinomas such as colon, prostate, breast and ovarian carcinomas[190]. Therefore, an enhanced ability to produce MMP9/MMP2 would be expected in 3D-M cells compared to the epithelial control, as already observed in the 2D model (Figure 8). However, in our 3D *in vitro* conditions, no difference was found regarding the production of MMPs between epithelial cells and EMT-derived cells (Figure 17). This may be due to the short period of time (24h) in which the conditioned media used was exposed to cells. Therefore, by increasing this period of time (48h), our MMP evaluation methodology could be optimized, as we show for 3DE14 and 3DM14 cells (Figure 28). In addition, other techniques are available that may more accurately assess MMPs secretion and activity. For example, we could translate our 3D model into proteolytically degradable MMP-sensitive alginate hydrogels, and follow their degradation, by MMPs, using Safranin-O/light-green staining[112]. This method differs from the zymography given that we could observe, in real time, MMP activity, bypassing all the technical methodology associated with zymography.

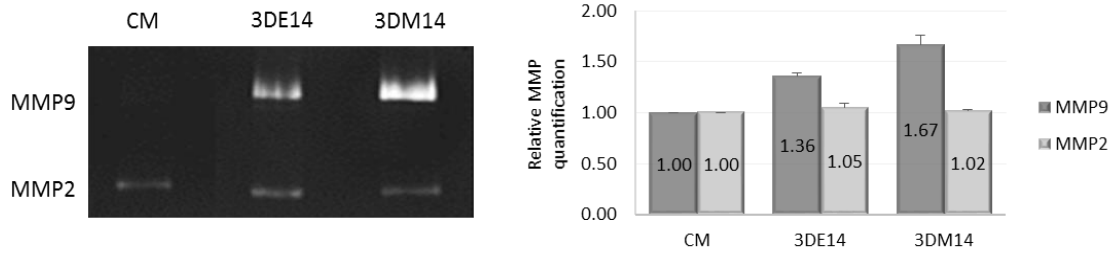


**Figure 28. MMP2 and MMP9 secretion for 3D-E14 and 3D-M14 cells.** Relative quantification was performed to normal culture medium (CM). 16ug of total protein were loaded for each sample (n=2 biological replicas). Conditioned media with 48h of culture was collected.

**Our characterization of the TGF-β1-induced EMT in the 3D *in vitro* system, showed that both 3D-M7 and 3D-M14 cells displayed a mesenchymal signature (Table 5).** However, 3D-M14 cells also displayed an unexpected increase in E-cadherin presence at the cell membrane. Moreover, a matrix-related effect was observed in the control epithelial culture starting after day 14, suggesting that the matrix itself alters these cells. This suggested that 3D-M14 cells may derive from a concomitant effect of TGF-β1 and the matrix itself. Therefore we selected 3D-M7 cells as our EMT end-point.

**Table 5. Summary of the characterization of TGF-β1-induced EMT in the 3D *in vitro* system**

| Criteria | | 3D-M7 | 3D-M10 | 3D-M14 |
|---|---|---|---|---|
| Gene Expression | *CDH1* | ++ | +++ | ++ |
| | *Ocln* | = | --- | = |
| | *CDH2* | +++ | +++ | +++ |
| | *Vim* | + | ++ | ++ |
| | *ZEB2* | +++ | ++ | +++ |
| | *Twist1* | + | --- | + |
| Protein Localization | E-Cadherin | Cytoplasm | Cytoplasm | Cytoplasm & Cell Membrane |
| | α-SMA | Cytoplasm | Cytoplasm | Cytoplasm |
| Protein Expression | E-Cadherin | Low/Absent | Medium | Medium |
| | α-SMA | Low | Medium | Medium |
| MMP production | MMP9 | = | = | = |
| | MMP2 | = | = | = |
| Metabolic activity | | = | -- | -- |

**Legend of symbols:** (---) <0.33-fold; (--) 0.33-0.50-fold; (-) 0.50-0.67-fold; (=) 0.67-1.50-fold; (+) 1.50-2.00-fold; (++) 2.00-3.00-fold; (+++) >3.00-fold. Data normalized to 3D-E7 cells.

By removing the TGF-β1 stimulus after EMT, i.e. after 7 days of culture, we observed a strong reversion from the mesenchymal to an epithelial-like phenotype in the 3D-TS14 cells. This phenotype was characterized, when comparing with 3D-M7 cells, by upregulation of *Twist1* and also of the genes *ID2* and *ID3,* which derived from the characterization of EMT reversion previously obtained in the EpH4 EMT/MET 2D model. Moreover, 3D-TS14 cells also exhibited downregulation of *Vim* (Figure 24) and heterogeneity regarding E-cadherin and α-SMA staining in the spheroids (Figure 22 and Figure 23B). Additionally, the metabolic activity of 3D-TS14 cells increased, which could be due to a higher cell density resulting from a higher proliferation rate (Figure 20). In order to address this question, we measured cell protein content, assuming that it would mirror cell density. Our results in fact suggested that protein cell content increased along with time of culture. However, after normalizing the metabolic activity to those values, we found a considerable difference between normalized and non-normalized metabolic rates (Figure 20). Despite these differences, in 3D-TS14 cells both non-normalized and normalized metabolic rates showed the same trend of recovery to 3D-E14 cells level. The main differences were observed in 3D-E7 to 3D-E10 and 3D-TS10 to 3D-TS14: both comparisons revealed that, after normalization to the protein content, 3D-E10 and 3D-TS14 displayed a halt in metabolic activity, which could be associated with high cell density. Additional studies to understand the basis of these metabolic changes are needed, such as live/dead assays as well counting the number of cells present at each time-point in each disk.

Regarding the MMP production, the increased secretion found in 3D-TS10 and 3D-TS14 (Figure 21) revealed a completely different behaviour from what was observed in the 2D *in vitro* system: 2D-M7 cells developed a higher ability to produce MMP9, while 2D-TS11 cells lost such feature (Figure 8). The inconsistencies found in the assessment of MMPs production in the 3D system were in fact similar to those previously discussed, reinforcing the need for either methodology optimization or implementation of novel technical strategies.

Due to the heterogeneity found within each population (2D/3D-E, M and TS cells), we attempted to find differences in the expression of surface markers that could help us analyse the stem-cell potential of these cells. We assessed the markers CD29 (integrin-β1) and CD44 due to their previous association with EMT and CSCs[72]. In fact, several works reported CD44 and CD29 as cell surface markers used to isolate CSC[191]. Additionally, breast cancer CSCs have been distinguished from cells lacking tumour initiating ability via $CD29^{hi}/CD44^{med}$ markers[69], and $CD29^{hi}/CD44^{hi}$ cells in squamous cell carcinoma have been associated with enriched CSC and EMT features[72]. In line with these studies, we observed a significant increase of the $CD29^{+}/CD44^{+}$ subpopulation in the 2D-M7 cells. However, in the 3D model, the same was not observed. Concerning the EMT reversion, the $CD29^{+}/CD44^{+}$ subpopulation was decreased in 2D-TS11 cells as well as in 3D-TS10 and 3D-TS14 cells (Figure 7A and Figure 23A). This common downregulation of the stem-cell like subpopulation in 2D/3D-TS cells narrows the gap between the two models. Nevertheless, more experiments should be performed using the 3D model, to confirm this hypothesis, such as testing other combinations of known EMT/CSC markers such as $CD44^{+}/CD24^{-}$ [69–71].

**Summing up, the characterization of the TGF-β1-induced EMT/MET in the 3D *in vitro* system showed that 3D-TS14 cells displayed a partial EMT reversion (Table 6).** This metastable phenotype is associated with a concomitant expression of α-SMA and membrane-located E-cadherin. Therefore, our model could be used to study transient phenotypes occurring during the metastatic process, enabling the monitoring of cellular interactions in a complex 3D environment. Indeed, the EpH4 EMT/MET 2D *in vitro* model previously established in our research group, also demonstrated the occurrence of a MET-derived metastable phenotype, in which different cell subpopulations were found (unpublished data). Further studies will be needed to understand if our 3D EMT/MET-derived cultures also display such distinct subpopulations. If those heterogeneous populations are indeed present in our 3D model, novel experiments addressing the cooperation between non-EMT and EMT cells, as well as the occurrence of diverse cycles of EMT/MET during cancer progression and metastasis, could be designed.

**Table 6. Summary of the characterization of TGF-β1-induced EMT/MET in the 3D *in vitro* system**

| Criteria | | 3D-M7 | 3D-TS10 | 3D-TS14 |
|---|---|---|---|---|
| Gene Expression | *CDH1* | = | = | + |
| | *Ocln* | = | = | = |
| | *CDH2* | ++ | ++ | ++ |
| | *Vim* | +++ | +++ | ++ |
| | *ZEB2* | +++ | = | ++ |
| | *Twist1* | = | = | ++ |
| | *Mgat3* | -- | --- | -- |
| | *ID2* | -- | = | -- |
| | *ID3* | = | - | = |
| Protein Localization | E-Cadherin | Cytoplasm | Cytoplasm | Cytoplasm & Cell Membrane |
| | α-SMA | Cytoplasm | Cytoplasm | Cytoplasm |
| Protein Expression | E-Cadherin | Residual | Low | Medium |
| | α-SMA | Low | Residual | Low |
| MMP production | MMP9 | = | = | = |
| | MMP2 | = | = | + |
| Metabolic activity | | = | +++ | = |
| Cellular Populations | $CD29^+$ | = | = | = |
| | $CD44^+$ | = | - | = |
| | $CD29^+/CD44^+$ | = | = | = |

**Legend of symbols:** (---) <0.33-fold; (--) 0.33-0.50-fold; (-) 0.50-0.67-fold; (=) 0.67-1.50-fold; (+) 1.50-2.00-fold; (++) 2.00-3.00-fold; (+++) >3.00-fold. Data normalized to 3D-E7 cells.

Alongside to the TGF-β1-induced EMT/MET model, we monitored the behaviour of the EpH4 epithelial cells in the 3D *in vitro* system for longer periods of culture. Interestingly, we observed that 3D-E17 cells displayed increased expression of the mesenchymal marker α-SMA (Figure 11), upregulation of *CDH2*, *Vim*, *ZEB2*, as well as decreased expression of *CDH1* (Figure 13). Together, these findings suggest that the 3D environment may be inducing the EpH4 cells to undergo a transient EMT. Possibly, the increased cellular density and eventual ECM deposition may induce an overall increase of stiffness that in turn triggers EMT, as previously discussed. Additionally, this mesenchymal signature was abrogated in 3D-E21 cells, indicating that a cyclic EMT induction modulated by the 3D environment may be occurring. Again, if true, this hypothesis would be of great interest to gain important insights regarding the cycles of EMT/MET during cancer progression and metastasis.

Our 3D *in vitro* EMT/MET model driven by TGF-β1 (Figure 29) emphasizes interesting features of both processes that are associated to important findings arising from *in vivo* studies. However, the work developed in this Master Thesis constitutes a preliminary data set that requires further

validation experiments, given that most of our results derived from a single biological replica. Nevertheless, the results obtained during this short approach encourage the application of this 3D system for the study of EMT/MET. Our results reveal the potential of this model to unravel novel mechanisms, biomarkers, and ultimately therapies associated with EMT/MET in the scope of cancer progression and metastasis establishment. Furthermore, our model may be useful to elucidate the origin of the high resistance to chemotherapy and radiotherapy in EMT-derived cells, which was not observed in MET-derived cells[83]. Such studies could help answer some questions that remain open: should subclinical tumours be induced to undergo MET to facilitate therapy? Can new biomarkers for EMT be useful to better understand cancer progression? Is MET stable in metastasis or secondary EMT may also occur? We believe that our 3D model and our ability to create EMT-cells and metastable-like cells could be a useful tool to answer such questions.

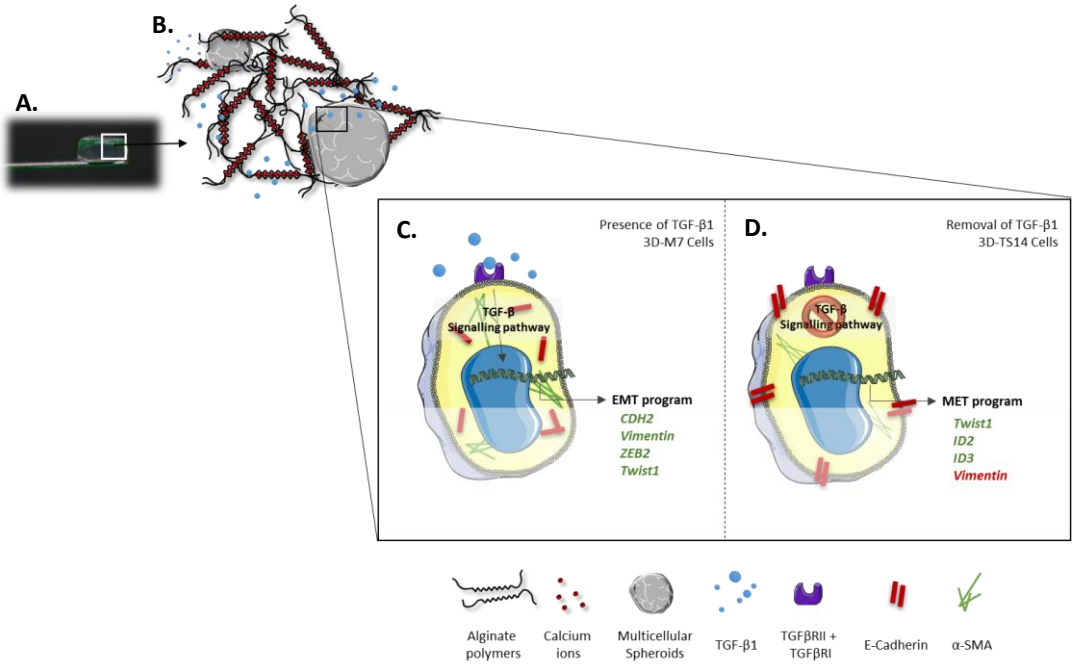


**Figure 29. Global representation of the 3D *in vitro* TGF-β1 induced EMT/MET model in RDG-modified hydrogels. A.** Appearance of a RGD-modified hydrogel, such as the ones used for the 3D cell culture. **B.** Alginate crosslinking via calcium ions. The resulting network allows the free diffusion of TGF-β1 molecules across the hydrogel. **C.** In the presence of TGF-β1 for 7 days, TGF-β1 signaling pathways lead to delocalization of E-cadherin to the cytoplasm and expression of α-SMA, as a result of the implementation of a transcriptional EMT program based in the upregulation of *CDH2*, *Vim*, *ZEB2* and *Twist1*. **D.** 7 days upon removal of the TGF-β1 stimulus and consequent signalling pathways, E-cadherin undergoes translocation to cell membrane and α-SMA is decreased due to the implementation of a MET program in which *Twist1*, *ID2* and *ID3* are upregulated while *Vim* is downregulated.

# CHAPTER VI

# Conclusions

The overall gap found between the outcomes of traditional 2D cancer models and its clinical success nourished the concretization of this Thesis, in which we aimed to establish a 3D *in vitro* model for EMT/MET induction.

First, we focused on complementing the 2D *in vitro* model of TGF-β1-mediated EMT/MET induction by addressing the expression of EMT and CSC-related molecules and the secretion of MMPs by EMT and MET-derived cells. This study revealed that EMT-derived cells present stemness features as well as increased ability to degrade the basement membrane and the ECM in comparison to EpH4 epithelial and MET-derived cells.

Secondly, we initiated the development of the 3D *in vitro* TGF-β1-driven EMT/MET system by culturing the EpH4 cell line within RGD-modified alginate hydrogels. We concluded that softer matrices with low cellular density allow the formation of large spheroid with different architectures that express classical epithelial markers, i.e. E-cadherin, in the absence of TGF-β1 supplementation. Additionally, we concluded that our 3D system can be used for epithelial culture of EpH4 cell line without significant phenotypic variations during the first 14 days of culture, which might be particularly interesting to study the epithelial morphogenesis and potentially the function of normal mammary gland. Moreover, the extension of the culture of these cells to 17 days showed the induction of an EMT-like program with upregulation of mesenchymal markers and downregulation of epithelial markers. This EMT program seems to be transient and probably resulting from cell-matrix interactions.

Using this 3D system, we observed that EMT can be achieved via TGF-β1 treatment, with E-cadherin delocalization to the cell cytoplasm, presence of α-SMA and upregulation of several EMT-related genes.

Thereafter, to complete the establishment of the EMT/MET model, we monitored the cellular behaviour of EMT-derived cells for 7 days in 3D culture without TGF-β1 supplementation. Our results showed a concomitant upregulation of *Twist1*, *ID2* and *ID3*, downregulation of *Vim*, increased E-cadherin expression with maintenance of α-SMA expression, and decreased stem-cell like subpopulation, suggesting the occurrence of a partial MET program.

In conclusion, we were able to translate a previously established 2D model of EMT/MET to a novel 3D *in vitro* system using TGF-β1 treatment. The main strength of this work was the identification of viable readouts of this 3D system, which enable its manipulation in the future,

by altering, for example, the matrix components. Following the insights described in this Thesis, a robust high-throughput and novel system can be established for further studies on cancer progression and metastasis formation.

# CHAPTER VII

# Future Perspectives

One of the major drawbacks of the work developed in this Master Thesis is that most results derive from a single biological replicate. Therefore, the first task that should be performed to better strengthen this project, is to reproduce all the experiments previously described.

In particular, as suggested in Chapter V, a clearer definition of metabolic states and growth/proliferation rates of the different cell populations should be addressed. In addition, activity of MMPs and stiffness measurements would also be of great importance to confirm some of the uncertainties identified during this Thesis.

The activity of MMPs could also be complemented with the design of migration/invasion studies that would ultimately show the efficiency of these cells in degrading the ECM and the basement membrane. Thereafter, matrix variations at chemical (composition) and physical (mechanics mesh size) levels could be introduced in order to investigate how cell in the different stages of the EMT/MET process would react and adapt to these environmental changes. For this purpose, the readouts defined in this Thesis will be crucial to rapidly and efficiently spot the phenotypic responses to those changes.

Due to the high levels of stress that cells may undergo when transferred from a 2D culture to a 3D environment, another interesting study would be the induction of EMT only after spheroid formation with cells already presenting a stable epithelial phenotype.

Analogous studies should be performed to evaluate the potential matrix-driven EMT induction that was observed in prolonged cultures of EpH4 cells, taking into account the biological relevance that this phenomenon may have in the process of understanding the crosstalk between EMT/non-EMT cells and the surrounding environment.

Our 3D EMT/MET *in vitro* TGF-β1 model would also benefit from a parallel study using other cell lines, such as a human derived cell lines. Having in mind a potential clinical usage of our model, for instance drug screening, it would be of outmost interest to test the potential of primary cultures in this system. If successful, this approach might indicate the possibility of culture

biopsies from patient's tumours, allowing a personalized therapy and perhaps help in the prognostic decision-making.

Finally, the characterization of the organized and lumenized structures formed by EpH4 could become an additional focus of this project, since it can be translated into a novel 3D complex system to study the normal mammary gland, and perchance the tumorigenic process in this cells.

In summary, our 3D *in vitro* EMT/MET model exhibits a myriad of potential applications in cancer research that are worth to pursue in future research projects.

# REFERENCES


1. Kalluri, R. & Weinberg, R. A. The basics of epithelial-mesenchymal transition. *J Clin Invest* 119, 1420–8 (2009).
2. Baldwin, A. *et al.* Epithelial-mesenchymal status influences how cells deposit fibrillin microfibrils. *J Cell Sci*, (2013).
3. Hay, E. The mesenchymal cell, its role in the embryo, and the remarkable signaling mechanisms that create it. *Dev Dyn* 233, 706–20 (2005).
4. Sahai, E. & Marshall, C. Differing modes of tumour cell invasion have distinct requirements for Rho/ROCK signalling and extracellular proteolysis. *Nat Cell Biol* 5, 711–9 (2003).
5. De Craene, B. & Berx, G. Regulatory networks defining EMT during cancer initiation and progression. *Nat Rev Cancer* 13, 97–110 (2013).
6. Thiery, J. Epithelial-mesenchymal transitions in tumour progression. *Nat Rev Cancer* 2, 442–54 (2002).
7. Yilmaz, M., Christofori, G. & Lehembre, F. Distinct mechanisms of tumor invasion and metastasis. *Trends Mol Med* 13, 535–41 (2007).
8. Wan, L., Pantel, K. & Kang, Y. Tumor metastasis: moving new biological insights into the clinic. *Nat Med* 19, 1450–64 (2013).
9. Yang, J. & Weinberg, R. A. Epithelial-mesenchymal transition: at the crossroads of development and tumor metastasis. *Dev Cell* 14, 818–29 (2008).
10. Brabletz, T. To differentiate or not - routes towards metastasis. *Nat Rev Cancer* 12, 425–36 (2012).
11. Baum, B., Settleman, J. & Quinlan, M. Transitions between epithelial and mesenchymal states in development and disease. *Semin Cell Dev Biol* 19, 294–308 (2008).
12. Guillot, C. & Lecuit, T. Mechanics of epithelial tissue homeostasis and morphogenesis. *Science (80-. ).* 340, 1185–9 (2013).
13. Thiery, J. P. *et al.* Epithelial-mesenchymal transitions in development and disease. *Cell* 139, 871–90 (2009).
14. Shook, D. & Keller, R. Mechanisms, mechanics and function of epithelial–mesenchymal transitions in early development. *Mech Dev* 120, 1351–83 (2003).
15. Micalizzi, D. S., Farabaugh, S. M. & Ford, H. L. Epithelial-mesenchymal transition in cancer: parallels between normal development and tumor progression. *J Mammary Gland Biol Neoplasia* 15, 117–34 (2010).
16. Arnoux, V. *et al.* Erk5 controls slug expression and keratinocyte activation during wound healing. *Mol Biol Cell* 19, 4738–49 (2008).

17. Ahmed, N. *et al.* Molecular pathways regulating EGF-induced epithelio-mesenchymal transition in human ovarian surface epithelium. *Am J Physiol Cell Physiol* 290, C1532–42 (2006).

18. Iwano, M. *et al.* Evidence that fibroblasts derive from epithelium during tissue fibrosis. *J Clin Invest* 110, 341–50 (2002).

19. Zeisberg, E. *et al.* Endothelial-to-mesenchymal transition contributes to cardiac fibrosis. *Nat Med* 13, 952–61 (2007).

20. Zeisberg, M. *et al.* Fibroblasts derive from hepatocytes in liver fibrosis via epithelial to mesenchymal transition. *J Biol Chem* 282, 23337–47 (2007).

21. Kim, K. *et al.* Alveolar epithelial cell mesenchymal transition develops in vivo during pulmonary fibrosis and is regulated by the extracellular matrix. *Proc Natl Acad Sci USA* 103, 13180–5 (2006).

22. Lee, J. M., Dedhar, S., Kalluri, R. & Thompson, E. W. The epithelial-mesenchymal transition: new insights in signaling, development, and disease. *J Cell Biol* 172, 973–81 (2006).

23. Voulgari, A. & Pintzas, A. Epithelial–mesenchymal transition in cancer metastasis: mechanisms, markers and strategies to overcome drug resistance in the clinic. *Biochim Biophys Acta* 1796, 75–90 (2009).

24. Kalluri, R. EMT: when epithelial cells decide to become mesenchymal-like cells. *J Clin Invest* 119, 1417–9 (2009).

25. Principe, D. R. *et al.* TGF-β: duality of function between tumor prevention and carcinogenesis. *J Natl Cancer Inst* 106, djt369 (2014).

26. Zarzynska, J. M. Two Faces of TGF-Beta1 in Breast Cancer. *Mediat. Inflamm* 2014, 141747 (2014).

27. Morrison, C. D., Parvani, J. G. & Schiemann, W. P. The relevance of the TGF-β Paradox to EMT-MET programs. *Cancer Lett* 341, 30–40 (2013).

28. Wendt, M., Tian, M. & Schiemann, W. Deconstructing the mechanisms and consequences of TGF-β-induced EMT during cancer progression. *Cell Tissue Res* 347, 85–101 (2012).

29. Wendt, M., Allington, T. & Schiemann, W. Mechanisms of the epithelial-mesenchymal transition by TGF-β. *Futur. Oncol* 5, 1145–68 (2009).

30. Gordon, K. J. & Blobe, G. C. Role of transforming growth factor-beta superfamily signaling pathways in human disease. *Biochim Biophys Acta* 1782, 197–228 (2008).

31. Zavadil, J. *et al.* Integration of TGF-β/Smad and Jagged1/Notch signalling in epithelial-to-mesenchymal transition. *EMBO J* 23, 1155–65 (2004).

32. Timmerman, L. *et al.* Notch promotes epithelial-mesenchymal transition during cardiac development and oncogenic transformation. *Genes Dev* 18, 99–115 (2004).

33. Saad, S. *et al.* Notch mediated epithelial to mesenchymal transformation is associated with increased expression of the Snail transcription factor. *Int J Biochem Cell Biol* 42, 1115–22 (2010).

34. Maier, H. J. *et al.* NF-kappaB promotes epithelial-mesenchymal transition, migration and invasion of pancreatic carcinoma cells. *Cancer Lett* 295, 214–28 (2010).

35. Mu, Y., Gudey, S. K. & Landström, M. Non-Smad signaling pathways. *Cell Tissue Res* 347, 11–20 (2012).

36. Mongroo, P. & Rustgi, A. The role of the miR-200 family in epithelial-mesenchymal transition. *Cancer Biol Ther* 10, 219–22 (2010).

37. Moustakas, A. & Heldin, C.-H. Induction of epithelial-mesenchymal transition by transforming growth factor β. *Semin Cancer Biol* 22, 446–54 (2012).

38. Medici, D. & Nawshad, A. Type I collagen promotes epithelial-mesenchymal transition through ILK-dependent activation of NF-kappaB and LEF-1. *Matrix Biol* 29, 161–5 (2010).

39. Kim, K., Lu, Z. & Hay, E. Direct evidence for a role of beta-catenin/LEF-1 signaling pathway in induction of EMT. *Cell Biol Int* 26, 463–76 (2002).

40. Kobayashi, W. & Ozawa, M. The transcription factor LEF-1 induces an epithelial-mesenchymal transition in MDCK cells independent of β-catenin. *Biochem Biophys Res Commun* 442, 133–8 (2013).

41. Ha, G.-H., Kim, J.-L. & Breuer, E.-K. Y. TACC3 is essential for EGF-mediated EMT in cervical cancer. *PLoS One* 8, e70353 (2013).

42. Lamouille, S., Xu, J. & Derynck, R. Molecular mechanisms of epithelial-mesenchymal transition. *Nat Rev Mol Cell Biol* 15, 178–96 (2014).

43. Vincent-Salomon, A. & Thiery, J. Epithelial-mesenchymal transition in breast cancer development. *Breast Cancer Res* 5, 101–6 (2003).

44. Peinado, H., Portillo, F. & Cano, A. Transcriptional regulation of cadherins during development and carcinogenesis. *Int J Dev Biol* 48, 365–75 (2004).

45. Gheldof, A. & Berx, G. Cadherins and epithelial-to-mesenchymal transition. *Prog Mol Biol Transl Sci* 116, 317–36 (2013).

46. Berx, G. *et al.* Mutations of the human E-cadherin (CDH1) gene. *Hum Mutat* 12, 226–37 (1998).

47. Saito, T. *et al.* E-cadherin mutation and Snail overexpression as alternative mechanisms of E-cadherin inactivation in synovial sarcoma. *Oncogene* 23, 8629–38 (2004).

48. Lombaerts, M. *et al.* E-cadherin transcriptional downregulation by promoter methylation but not mutation is related to epithelial-to-mesenchymal transition in breast cancer cell lines. *Br J Cancer* 94, 661–71 (2006).

49. Ling, Z. Q. *et al.* Hypermethylation-modulated down-regulation of CDH1 expression contributes to the progression of esophageal cancer. *Int J Mol Med* 27, 625–35 (2011).

50. Zhao, C. & Bu, X. Promoter methylation of tumor-related genes in gastric carcinogenesis. *Histol Histopathol* 27, 1271–82 (2012).

51. Moghbeli, M. *et al.* Role of hMLH1 and E-cadherin promoter methylation in gastric cancer progression. *J Gastrointest Cancer* 45, 40–7 (2014).

52. Cano, A. *et al.* The transcription factor snail controls epithelial-mesenchymal transitions by repressing E-cadherin expression. *Nat Cell Biol* 2, 76–83 (2000).

53. Peinado, H., Olmeda, D. & Cano, A. Snail, Zeb and bHLH factors in tumour progression: an alliance against the epithelial phenotype? *Nat Rev Cancer* 7, 415–28 (2007).

54. Lilien, J. & Balsamo, J. The regulation of cadherin-mediated adhesion by tyrosine phosphorylation/dephosphorylation of beta-catenin. *Curr Opin Cell Biol* 17, 459–65 (2005).

55. Pinho, S. S. *et al.* Loss and recovery of Mgat3 and GnT-III Mediated E-cadherin N-glycosylation is a mechanism involved in epithelial-mesenchymal-epithelial transitions. *PLoS One* 7, e33191 (2012).

56. Hazan, R. B. *et al.* Exogenous expression of N-cadherin in breast cancer cells induces cell migration, invasion, and metastasis. *J Cell Biol* 148, 779–90 (2000).

57. Paredes, J. *et al.* P-cadherin overexpression is an indicator of clinical outcome in invasive breast carcinomas and is associated with CDH3 promoter hypomethylation. *Clin Cancer Res* 11, 5869–77 (2005).

58. Hanahan, D. & Weinberg, R. Hallmarks of Cancer: The Next Generation. *Cell* 144, 646–74 (2011).

59. Catalano, V. *et al.* Tumor and its microenvironment: A synergistic interplay. *Semin Cancer Biol* 23, 522–32 (2013).

60. Iwatsuki, M. *et al.* Epithelial-mesenchymal transition in cancer development and its clinical significance. *Cancer Sci* 101, 293–9 (2010).

61. Cannito, S. *et al.* Redox mechanisms switch on hypoxia-dependent epithelial-mesenchymal transition in cancer cells. *Carcinogenesis* 29, 2267–78 (2008).

62. Yang, M. *et al.* Direct regulation of TWIST by HIF-1alpha promotes metastasis. *Nat Cell Biol* 10, 295–305 (2008).

63. Lu, X. & Kang, Y. Hypoxia and hypoxia-inducible factors: master regulators of metastasis. *Clin Cancer Res* 16, 5928–35 (2010).

64. Imamichi, Y. & Menke, A. Signaling pathways involved in collagen-induced disruption of the E-cadherin complex during epithelial– mesenchymal transition. *Cells Tissues Organs* 185, 180–90 (2007).

65. Cheng, J.-C. & Leung, P. C. K. Type I collagen down-regulates E-cadherin expression by increasing PI3KCA in cancer cells. *Cancer Lett* 304, 107–16 (2011).

66. Prevarskaya, N., Skryma, R. & Shuba, Y. Calcium in tumour metastasis: new roles for known actors. *Nat Rev Cancer* 11, 609–18 (2011).

67. Davis, F. M. *et al.* Induction of epithelial-mesenchymal transition (EMT) in breast cancer cells is calcium signal dependent. *Oncogene* 1–10 (2013).

68. Sánchez-Tilló, E. *et al.* EMT-activating transcription factors in cancer: beyond EMT and tumor invasiveness. *Cell Mol Life Sci* 69, 3429–56 (2012).

69. Al-Hajj, M. *et al.* Prospective identification of tumorigenic breast cancer cells. *Proc Natl Acad Sci USA* 100, 3983–8 (2003).

70. Li, C. *et al.* Identification of pancreatic cancer stem cells. *Cancer Res* 67, 1030–7 (2007).

71. O'Brien, C. *et al.* A human colon cancer cell capable of initiating tumour growth in immunodeficient mice. *Nature* 445, 106–10 (2007).

72. Geng, S. *et al.* Cancer stem-like cells enriched with CD29 and CD44 markers exhibit molecular characteristics with epithelial-mesenchymal transition in squamous cell carcinoma. *Arch Dermatol Res* 305, 35–47 (2013).

73. Mani, S. A. *et al.* The epithelial-mesenchymal transition generates cells with properties of stem cells. *Cell* 133, 704–15 (2008).

74. Radisky, D. C. & LaBarge, M. A. Epithelial-mesenchymal transition and the stem cell phenotype. *Cell Stem Cell* 2, 511–2 (2008).

75. Tsuji, T., Ibaragi, S. & Hu, G. Epithelial-mesenchymal transition and cell cooperativity in metastasis. *Cancer Res* 69, 7135–9 (2009).

76. Sleeman, J. P. The metastatic niche and stromal progression. *Cancer Metastasis Rev* 31, 429–40 (2012).

77. Chang, C.-J. *et al.* p53 regulates epithelial-mesenchymal transition and stem cell properties through modulating miRNAs. *Nat Cell Biol* 13, 317–23 (2011).

78. Taube, J. H. *et al.* Epigenetic silencing of microRNA-203 is required for EMT and cancer stem cell properties. *Sci Rep* 3, 2687 (2013).

79. Xia, H. & Hui, K. M. MicroRNAs involved in regulating epithelial-mesenchymal transition and cancer stem cells as molecular targets for cancer therapeutics. *Cancer Gene Ther* 19, 723–30 (2012).

80. Dave, B. *et al.* Epithelial-mesenchymal transition, cancer stem cells and treatment resistance. *Breast Cancer Res* 14, 202 (2012).

81. Hindriksen, S. & Bijlsma, M. F. Cancer Stem Cells, EMT, and Developmental Pathway Activation in Pancreatic Tumors. *Cancers (Basel).* 4, 989–1035 (2012).

82. Chen, X. *et al.* Cancer stem cells, epithelial-mesenchymal transition, and drug resistance in high-grade ovarian serous carcinoma. *Hum Pathol* 44, 2373–84 (2013).

83. Gunasinghe, N. P. *et al.* Mesenchymal-epithelial transition (MET) as a mechanism for metastatic colonisation in breast cancer. *Cancer Metastasis Rev* 31, 469–78 (2012).

84. Krebs, M. G. *et al.* Molecular analysis of circulating tumour cells—biology and biomarkers. *Nat Rev Clin Oncol* 11, 129–44 (2014).

85. Aggarwal, B. B., Danda, D., Gupta, S. & Gehlot, P. Models for prevention and treatment of cancer: problems vs promises. *Biochem Pharmacol* 78, 1083–94 (2009).

86. Hait, W. N. Anticancer drug development: the grand challenges. *Nat Rev Drug Discov* 9, 253–4 (2010).

87. Van der Worp, H. B. *et al.* Can animal models of disease reliably inform human studies? *PloS Med* 7, e1000245 (2010).

88. Francia, G. & Kerbel, R. S. Raising the bar for cancer therapy models. *Nat Biotechnol* 28, 561–2 (2010).

89. Steele, V. E. & Lubet, R. A. The use of animal models for cancer chemoprevention drug development. *Semin Oncol* 37, 328–38 (2010).

90. Hutmacher, D. W. *et al.* Can tissue engineering concepts advance tumor biology research? *Trends Biotechnol* 28, 125–33 (2010).

91. Weigelt, B. & Bissell, M. J. The need for complex 3D culture models to unravel novel pathways and identify accurate biomarkers in breast cancer. *Adv Drug Deliv. Rev* 1–10 (2014).

92. Lutolf, M. P., Gilbert, P. M. & Blau, H. M. Designing materials to direct stem-cell fate. *Nature* 462, 433–41 (2009).

93. Santos, E. *et al.* Novel advances in the design of three-dimensional bio-scaffolds to control cell fate: translation from 2D to 3D. *Trends Biotechnol* 30, 331–41 (2012).

94. Chitcholtan, K. *et al.* Differences in growth properties of endometrial cancer in three dimensional (3D) culture and 2D cell monolayer. *Exp Cell Res* 319, 75–87 (2013).

95. Kim, J., Stein, R. & O'Hare, M. Three-dimensional in vitro tissue culture models of breast cancer—a review. *Breast Cancer Res Treat* 85, 281–91 (2004).

96. Harrison, R. G. The reaction of embryonic cells to solid structures. *J Exp Zool* 17, 521–544 (1914).

97. McLimans, W. *et al.* The submerged culture of mammalian cells; the spinner culture. *J Immunol* 79, 428–33 (1957).

98. Wichterle, O. & Lim, D. Hydrophilic gels in biologic use. *Nature* 185, 117 (1960).

99. Lim, F. & Sun, A. M. Microencapsulated islets as bioartificial endocrine pancreas. *Science (80-. ).* 210, 908–10 (1980).

100. Miller, B. E., Miller, F. R. & Heppner, G. H. Factors affecting growth and drug sensitivity of mouse mammary tumor lines in collagen gel cultures. *Cancer Res* 45, 4200–5 (1985).

101. Lochter, A. *et al.* Matrix metalloproteinase stromelysin-1 triggers a cascade of molecular alterations that leads to stable epithelial-to-mesenchymal conversion and a premalignant phenotype in mammary epithelial cells. *J Cell Biol* 139, 1861–72 (1997).

102. Hubbell, J. A. Bioactive biomaterials. *Curr Opin Biotechnol* 10, 123–9 (1999).

103. West, J. L. & Hubbell, J. A. Polymeric biomaterials with degradation sites for proteases involved in cell migration. *Macromolecules* 32, 241–4 (1999).

104. Fischbach, C. *et al.* Engineering tumors with 3D scaffolds. *Nat Methods* 4, 855–60 (2007).

105. Tibbitt, M. W. & Anseth, K. S. Hydrogels as extracellular matrix mimics for 3D cell culture. *Biotechnol Bioeng* 103, 655–63 (2009).

106. Barralet, J. *et al.* Comparison of bone marrow cell growth on 2D and 3D alginate hydrogels. *J Mater Sci Mater Med* 16, 515–9 (2005).

107. Azab, A. *et al.* Crosslinked chitosan implants as potential degradable devices for brachytherapy: In vitro and in vivo analysis. *J Control Release* 111, 281–9 (2006).

108. Bidarra, S. *et al.* Injectable in situ crosslinkable RGD-modified alginate matrix for endothelial cells delivery. *Biomaterials* 32, 7898–904 (2011).

109. Godugu, C. *et al.* AlgiMatrix™ based 3D cell culture system as an in-vitro tumor model for anticancer studies. *PLoS One* 8, e53708 (2013).

110. Aizawa, Y., Owen, S. C. & Shoichet, M. S. Polymers used to influence cell fate in 3D geometry: New trends. *Prog Polym Sci* 37, 645–58 (2012).

111. Boontheekul, T., Kong, H. J. & Mooney, D. J. Controlling alginalte gel degradation utilizing partial oxidation and bimodal molecular weight distribution. *Biomaterials* 26, 2455–65 (2005).

112. Fonseca, K. B. *et al.* Injectable MMP-sensitive alginate hydrogels as hMSC delivery systems. *Biomacromolecules* 15, 380–90 (2014).

113. Loessner, D. *et al.* Bioengineered 3D platform to explore cell–ECM interactions and drug resistance of epithelial ovarian cancer cells. *Biomaterials* 31, 8494–506 (2010).

114. Greiner, A. M., Richter, B. & Bastmeyer, M. Micro-engineered 3D scaffolds for cell culture studies. *Macromol Biosci* 12, 1301–14 (2012).

115. Sawhney, A., Pathak, C. & Hubbell, J. Bioerodible hydrogels based on photopolymerized poly(ethylene glycol)-co-poly(a-hydroxy acid) diacrylate macromers. *Macromolecules* 26, 581–7 (1993).

116. Drury, J. & Mooney, D. Hydrogels for tissue engineering: scaffold design variables and applications. *Biomaterials* 24, 4337–51 (2003).

117. Wang, Y. L. & Pelham, R. J. J. Preparation of a flexible, porous polyacrylamide substrate for mechanical studies of cultured cells. *Methods Enzym.* 298, 489–96 (1998).

118. Gill, B. *et al.* A synthetic matrix with independently tunable biochemistry and mechanical properties to study epithelial morphogenesis and EMT in a lung adenocarcinoma model. *Cancer Res* 72, 6013–23 (2012).

119. Zhu, J. Bioactive modification of poly(ethylene glycol) hydrogels for tissue engineering. *Biomaterials* 31, 4639–56 (2010).

120. Kraning-Rush, C. M., Califano, J. P. & Reinhart-King, C. A. Cellular traction stresses increase with increasing metastatic potential. *PLoS One* 7, e32572 (2012).

121. Infanger, D. W., Lynch, M. E. & Fischbach, C. Engineered culture models for studies of tumor-microenvironment interactions. *Annu Rev. Biomed Eng* 15, 29–53 (2013).

122. Achilli, T.-M., Meyer, J. & Morgan, J. R. Advances in the formation, use and understanding of multi-cellular spheroids. *Expert Opin Biol Ther* 12, 1347–60 (2012).

123. Kim, J. Bin. Three-dimensional tissue culture models in cancer biology. *Semin Cancer Biol* 15, 365–77 (2005).

124. Breslin, S. & O'Driscoll, L. Three-dimensional cell culture: the missing link in drug discovery. *Drug Discov Today* 18, 240–9 (2013).

125. Goodwin, T. *et al.* Reduced shear stress: a major component in the ability of mammalian tissues to form three-dimensional assemblies in simulated microgravity. *J Cell Biochem* 51, 301–11 (1993).

126. Kelm, J. *et al.* Method for generation of homogeneous multicellular tumor spheroids applicable to a wide variety of cell types. *Biotechnol Bioeng* 83, 173–80 (2003).

127. Timmins, N. & Nielsen, L. Generation of multicellular tumor spheroids by the hanging-drop method. *Methods Mol Med* 140, 141–51 (2007).

128. Tung, Y. *et al.* High-throughput 3D spheroid culture and drug testing using a 384 hanging drop array. *Analyst* 136, 473–8 (2011).

129. Griffith, L. & Swartz, M. Capturing complex 3D tissue physiology in vitro. *Nat Rev Mol Cell Biol* 73, 211–24 (2006).

130. Baker, B. M. & Chen, C. S. Deconstructing the third dimension: how 3D culture microenvironments alter cellular cues. *J Cell Sci* 125, 3015–24 (2012).

131. Gal, A. *et al.* Sustained TGF beta exposure suppresses Smad and non-Smad signalling in mammary epithelial cells, leading to EMT and inhibition of growth arrest and apoptosis. *Oncogene* 27, 1218–30 (2008).

132. Gibbons, D. L. *et al.* Contextual extracellular cues promote tumor cell EMT and metastasis by regulating miR-200 family expression. *Genes Dev* 23, 2140–51 (2009).

133. Wendt, M., Smith, J. & Schiemann, W. Transforming growth factor-β-induced epithelial-mesenchymal transition facilitates epidermal growth factor-dependent breast cancer progression. *Oncogene* 29, 6485–98 (2010).

134. Cieślik, M. *et al.* Epigenetic coordination of signaling pathways during the epithelial-mesenchymal transition. *Epigenetics Chromatin* 6, 28 (2013).

135. Oyanagi, J. *et al.* Epithelial-mesenchymal transition stimulates human cancer cells to extend microtubule-based invasive protrusions and suppresses cell growth in collagen gel. *PLoS One* 7, e53209 (2012).

136. Chu, J. H. *et al.* Development of a three-dimensional culture model of prostatic epithelial cells and its use for the study of epithelial-mesenchymal transition and inhibition of PI3K pathway in prostate cancer. *Prostate* 69, 428–42 (2009).

137. Lim, M., Chuong, C.-M. & Roy-Burman, P. PI3K, Erk signaling in BMP7-induced epithelial-mesenchymal transition (EMT) of PC-3 prostate cancer cells in 2- and 3-dimensional cultures. *Horm Cancer* 2, 298–309 (2011).

138. Shih, W. & Yamada, S. N-cadherin-mediated cell-cell adhesion promotes cell migration in a three-dimensional matrix. *J Cell Sci* 125, 3661–70 (2012).

139. Chen, L. *et al.* The enhancement of cancer stem cell properties of MCF-7 cells in 3D collagen scaffolds for modeling of cancer and anti-cancer drugs. *Biomaterials* 33, 1437–44 (2012).

140. Liu, L.-J. *et al.* Three-dimensional collagen scaffold enhances the human adenoid cystic carcinoma cancer stem cell and epithelial-mesenchymal transition properties. *J Biomed Mater Res B Appl Biomater* 1–9 (2013).

141. Sieh, S., Lubik, A., Clements, J., Nelson, C. & Hutmacher, D. Interactions between human osteoblasts and prostate cancer cells in a novel 3D in vitro model. *Organogenesis* 6, 181–8 (2010).

142. Lee, K. *et al.* Matrix compliance regulates Rac1b localization, NADPH oxidase assembly, and epithelial-mesenchymal transition. *Mol Biol Cell* 23, 4097–108 (2012).

143. Chen, Q. K. *et al.* Extracellular matrix proteins regulate epithelial-mesenchymal transition in mammary epithelial cells. *Differentiation* 86, 126–32 (2013).

144. Sigurdsson, V. *et al.* Endothelial induced EMT in breast epithelial cells with stem cell properties. *PLoS One* 6, e23833 (2011).

145. Maschler, S. *et al.* Enhanced tenascin-C expression and matrix deposition during Ras/TGF-beta-induced progression of mammary tumor cells. *Oncogene* 23, 3622–33 (2004).

146. Jones, F. S. & Jones, P. L. The tenascin family of ECM glycoproteins: structure, function, and regulation during embryonic development and tissue remodeling. *Dev Dyn* 218, 235–59 (2000).

147. Maschler, S. *et al.* Tumor cell invasiveness correlates with changes in integrin expression and localization. *Oncogene* 24, 2032–41 (2005).

148. Mussunoor, S. & Murray, G. I. The role of annexins in tumour development and progression. *J Pathol* 216, 131–40 (2008).

149. Maschler, S. *et al.* Annexin A1 attenuates EMT and metastatic potential in breast cancer. *EMBO Mol Med* 2, 401–14 (2010).

150. Markowski, M. C., Brown, A. C. & Barker, T. H. Directing epithelial to mesenchymal transition through engineered microenvironments displaying orthogonal adhesive and mechanical cues. *J Biomed Mater Res A* 100, 2119–27 (2012).

151. Chaudhuri, O. *et al.* Extracellular matrix stiffness and composition jointly regulate the induction of malignant phenotypes in mammary epithelium. *Nat Mater* (2014).

152. Foroni, L. *et al.* The role of 3D microenvironmental organization in MCF-7 epithelial-mesenchymal transition after 7 culture days. *Exp Cell Res* 319, 1515–22 (2013).

153. Shibata, S. *et al.* Three-dimensional culture using a radial flow bioreactor induces matrix metalloprotease 7-mediated EMT-like process in tumor cells via TGFß1/Smad pathway. *Int J Oncol* 34, 1433–48 (2009).

154. Chen, M. C. W., Gupta, M. & Cheung, K. C. Alginate-based microfluidic system for tumor spheroid formation and anticancer agent screening. *Biomed Microdevices* 12, 647–54 (2010).

155. Li, Q. *et al.* 3D models of epithelial-mesenchymal transition in breast cancer metastasis: high-throughput screening assay development, validation, and pilot screen. *J Biomol Screen* 16, 141–54 (2011).

156. Kuo, C.-T. *et al.* Configurable 2D and 3D spheroid tissue cultures on bioengineered surfaces with acquisition of epithelial–mesenchymal transition characteristics. *NPG Asia Mater.* 4, e27 (2012).

157. Aref, A. R. *et al.* Screening therapeutic EMT blocking agents in a three-dimensional microenvironment. *Integr Biol* 5, 381–9 (2013).

158. Girard, Y. K. *et al.* A 3D fibrous scaffold inducing tumoroids: a platform for anticancer drug development. *PLoS One* 8, e75345 (2013).

159. Rizvi, I. *et al.* Flow induces epithelial-mesenchymal transition, cellular heterogeneity and biomarker modulation in 3D ovarian cancer nodules. *Proc Natl Acad Sci USA* 110, E1974–83 (2013).

160. Stratmann, A. T. *et al.* Establishment of a human 3D lung cancer model based on a biological tissue matrix combined with a Boolean in silico model. *Mol Oncol* 8, 351–65 (2014).

161. Kim, Y. J. *et al.* A microchip filter device incorporating slit arrays and 3-D flow for detection of circulating tumor cells using CAV1-EpCAM conjugated microbeads. *Biomaterials* 35, 7501–10 (2014).

162. Moreno-Bueno, G. *et al.* The morphological and molecular features of the epithelial-to-mesenchymal transition. *Nat Protoc* 4, 1591–613 (2009).

163. Montesano, R. *et al.* Isolation of EpH4 mammary epithelial cell subpopulations which differ in their morphogenetic properties. *Vitr. Cell Dev Biol* 34, 468–77 (1998).

164. Fonseca, K. *et al.* Molecularly designed alginate hydrogels susceptible to local proteolysis as three-dimensional cellular microenvironments. *Acta Biomater* 7, 1674–82 (2011).

165. Rowley, J. A., Madlambayan, G. & Mooney, D. J. Alginate hydrogels as synthetic extracellular matrix materials. *Biomaterials* 20, 45–53 (1999).

166. Gacesa, P. Alginates. *Carbohydr Polym* 8, 161–82 (1988).

167. Folkman, J. & Moscona, A. Role of cell shape in growth control. *Nature* 273, 345–9 (1978).

168. Livak, K. J. & Schmittgen, T. D. Analysis of relative gene expression data using real-time quantitative PCR and the 2(-Delta Delta C(T)) Method. *Methods* 25, 402–8 (2001).

169. Dumitriu, S. & Popa, V. I. *Polymeric Biomaterials*. 920 (CRC Press/Taylor &Francis, 2013).

170. Eger, A. *et al.* beta-Catenin and TGFbeta signalling cooperate to maintain a mesenchymal phenotype after FosER-induced epithelial to mesenchymal transition. *Oncogene* 23, 2672–80 (2004).

171. Waerner, T. *et al.* ILEI: a cytokine essential for EMT, tumor formation, and late events in metastasis in epithelial cells. *Cancer Cell* 10, 227–39 (2006).

172. Lee, E. K. *et al.* Decreased expression of glutaredoxin 1 is required for transforming growth factor-beta1-mediated epithelial-mesenchymal transition of EpRas mammary epithelial cells. *Biochem Biophys Res Commun* 391, 1021–7 (2010).

173. Janda, E. *et al.* Raf plus TGFbeta-dependent EMT is initiated by endocytosis and lysosomal degradation of E-cadherin. *Oncogene* 25, 7117–30 (2006).

174. Allegra, M. *et al.* Semaphorin-7a reverses the ERF-induced inhibition of EMT in Ras-dependent mouse mammary epithelial cells. *Mol Biol Cell* 23, 3873–81 (2012).

175. Ell, B. & Kang, Y. Transcriptional control of cancer metastasis. *Trends Cell Biol* 23, 603–11 (2013).

176. Zavadil, J. & Bottinger, E. TGF-beta and epithelial-to-mesenchymal transitions. *Oncogene* 24, 5764–74 (2005).

177. Mori, M. *et al.* Zyxin mediates actin fiber reorganization in epithelial-mesenchymal transition and contributes to endocardial morphogenesis. *Mol Biol Cell* 20, 3115–24 (2009).

178. Beach, J. R. *et al.* Myosin II isoform switching mediates invasiveness after TGF-β-induced epithelial-mesenchymal transition. *Proc Natl Acad Sci USA* 108, 17991–6 (2011).

179. Lee, K. Y. & Mooney, D. J. Alginate: properties and biomedical applications. *Prog Polym Sci* 37, 106–26 (2012).

180. Ganguly, K. K., Pal, S., Moulik, S. & Chatterjee, A. Integrins and metastasis. *Cell Adh Migr* 7, 251–61 (2013).

181. Discher, D. E., Janmey, P. & Wang, Y. L. Tissue cells feel and respond to the stiffness of their substrate. *Science (80-. ).* 310, 1139–43 (2005).

182. Wan, L. Q. *et al.* Matrix deposition modulates the viscoelastic shear properties of hydrogel-based cartilage grafts. *Tissue Eng Part A* 17, 1111–22 (2011).

183. Ahearne, M. Introduction to cell–hydrogel mechanosensing. *Interface Focus* 4, 20130038 (2014).

184. Wu, T. H. *et al.* The F-actin and adherence-dependent mechanical differentiation of normal epithelial cells after TGF-β1-induced EMT (tEMT) using a microplate measurement system. *Biomed Microdevices* 16, 465–78 (2014).

185. Campbell, J. J. & Watson, C. J. Three-dimensional culture models of mammary gland. *Organogenesis* 5, 43–9 (2009).

186. Mroue, R. & Bissell, M. J. Three-dimensional cultures of mouse mammary epithelial cells. *Methods Mol Biol* 945, 221–50 (2013).

187. Vega-avila, E. & Pugsley, M. K. An overview of colorimetric assay methods used to assess survival or proliferation of mammalian cells. *Proc West Pharmacol Soc* 54, 10–4 (2011).

188. Abu-Amero, K. & Bosley, T. Detection of mitochondrial respiratory dysfunction in circulating lymphocytes using resazurin. *Arch Pathol Lab Med* 129, 1295–8 (2005).

189. Gomes, L. R. *et al.* TGF-β1 modulates the homeostasis between MMPs and MMP inhibitors through p38 MAPK and ERK1/2 in highly invasive breast cancer cells. *BMC Cancer* 12, 26 (2012).

190. Orlichenko, L. S. & Radisky, D. C. Matrix metalloproteinases stimulate epithelial-mesenchymal transition during tumor development. *Clin Exp Metastasis* 25, 593–600 (2008).

191. Hao, J. *et al.* MicroRNA control of epithelial-mesenchymal transition in cancer stem cells. *Int J Cancer* 135, 1019–27 (2014).